DØ note 6368 [Version 0.99]

Correction For the MC-Data Difference in the Jet Response at DØ for Run IIB

Kamil Augsten, Zhenyu Ye

February 6, 2013

Abstract

Jet responses are different between Monte Carlo (MC) simulation and data for the DØ experiment. Such a difference not only changes with the jet kinematics, but also with the flavor of the partons that initiate the jets. In a previous notes 6143 (RunIIA) and 6144 (RunIIB), a method was described to correct for this MC-data difference. This note presents the updated results for RunIIB MC and data JCCB jets (cone size = 0.5) using up-to-date MC (RunII B1-B3) and data (RunII B1-B4). Processor FMCData for usage in analyses is introduced.

Contents

1 Introduction

In [1] and [2], the method to correct for the MC-data difference in the jet response was described. The method is taking into account both the kinematic and flavor dependence. For each calorimeter jet in the MC, we look for a spatially matched particle jet to calculate the correction factor F

$$F = \frac{\sum_i E_i \cdot R_i^{data}}{\sum_i E_i \cdot R_i^{MC}}, \tag{1}$$

where the subscript i runs over the particles in the particle jet, E_i are the energies of the particles and R_i the single particle responses in MC or data. However, this factor implies new MC Jet Energy Scale. In order to preserve standard JES, we need instead the ratio of this correction factor and average F in γ+jet sample

$$F_{corr} = \frac{\frac{\sum_i E_i \cdot R_i^{data}}{\sum_i E_i \cdot R_i^{MC}}}{\langle F \rangle_{\gamma+jet}}. \tag{2}$$

The average correction factor F from the γ+jet sample is parameterized without any JES correction applied. Factor F_{corr} corrects for the MC-data difference in the jet response and should be applied to the jet energy after the offset correction [3], i.e.,

$$(E_{jet}^{raw} - E_O) \cdot F_{corr} = (E_{jet}^{raw} - E_O) \cdot \frac{\frac{\sum_i E_i \cdot R_i^{data}}{\sum_i E_i \cdot R_i^{MC}}}{\langle F \rangle_{\gamma+jet}}, \tag{3}$$

where E_{jet}^{raw} is the raw jet energy, E_O the offset correction for noise, pile-up and multiple interactions. The correction factor is independent of other JES corrections (response, showering, etc) and they should be applied as usual [3].

In this note, we present the final results for Sample Dependent Correction in all RunIIB samples (MC - B1-B3 and data - B1-B4) of JCCB jets (cone size = 0.5). The note is organized as the following. Section 2 describes the extraction of MC single particle responses and the closure test for the extracted MC responses. Section 3 describes the extraction of data single particle responses and the closure test for the extracted data responses. Section 4 presents the MC-data correction factor averaged for different flavor of jets. Section 5 presents an estimation for the uncertainty of the MC-data correction factor. Section 6 introduces processor written for usage of this correction in analyses.

2 Extracting MC Single Particle Responses

The MC single particle responses are measured for γ, $e^{\pm}$, $\mu^{\pm}$, $\pi^{\pm}$, $K^{\pm}$, K_0^S, K_0^L, $p^{\pm}$, n and Λ from Run IIB single particle MC samples, with all the zero suppression (ZS)[1], calorimeter noise and zero bias (ZB) overlay turned off. Note, that that in this note we used different MC samples than in [2] with additional energy points. For each single particle, the energy of the calorimeter cells contained in the $R = 0.5$ cone around the particle are summed over to give the MC single particle response, defined as the measured energy divided by the MC truth energy. The results are shown in Fig. 44-53. The are no significant differences to the previous result as can be seen by comparing with respective plots in [2]. The parameterizations of the fitting functions, which are found to best describe the MC responses with the minimal number of parameters, are:

$$R_{\gamma}^{MC} = 0.25 \cdot p_{\gamma}^0 \cdot \left[1 + Erf\left(\frac{E + p_{\gamma}^1}{\sqrt{2 \cdot p_{\gamma}^2}}\right)\right]\left[1 + Erf\left(\frac{E + p_{\gamma}^3}{\sqrt{2 \cdot p_{\gamma}^4}}\right)\right] + p_{\gamma}^5, \tag{4}$$

$$R_{e^{\pm}}^{MC} = 0.25 \cdot p_{e^{\pm}}^0 \cdot \left[1 + Erf\left(\frac{E + p_{e^{\pm}}^1}{\sqrt{2 \cdot p_{e^{\pm}}^2}}\right)\right]\left[1 + Erf\left(\frac{E + p_{e^{\pm}}^3}{\sqrt{2 \cdot p_{e^{\pm}}^4}}\right)\right] \text{ if } p_T > 0.3;\ 0 \text{ if } p_T < 0.3, \tag{5}$$

$$R_{\mu^{\pm}}^{MC} = (p_{\mu^{\pm}}^0 + p_{\mu^{\pm}}^1 \cdot E) \cdot \text{TMath :: Landau}(E, p_{\mu^{\pm}}^2, p_{\mu^{\pm}}^3) \text{ if } p_T > 0.3;\ 0 \text{ if } p_T < 0.3, \tag{6}$$

$$R_h^{MC} = p_h^0 \cdot \left[1 - p_h^1 \cdot (E/0.75)^{p_h^2 - 1}\right] \text{ if } p_T > m_h;\ 0 \text{ if } p_T < m_h, \tag{7}$$

$$\tag{8}$$

where $h = \pi$, $K^{\pm}$, K_0^S, K_0^L, $p^{\pm}$, n or Λ. The fitted results can be found in Fig. 44-53.

We check how well the denominator in Eq. 3, $\sum_i E_i \cdot R_i^{MC}$, describes the MC raw jet energy after the offset correction $(E_{jet}^{raw} - E_O) \cdot k_O$, where k_O is the correction for the ZS bias for the offset correction. We refer to the above check as the MC closure test in the following. We use E_O and k_O measured for the standard JES correction. Note that k_O is needed to perform the MC closure test, but not for estimating F in Eq. 1 and Eq. 2.

The MC closure test results for jets in γ+jet MC samples are shown in Fig. 1-5. In [2] has been shown how well the E_O and k_O results works by comparing with results for γ+jet MC samples produced without ZB overlay. We note that the ratio between $(E_{jet}^{raw} - E_O) \cdot k_O$ and $\sum_i E_i \cdot R_i^{MC}$ is not perfectly at one. We consider this residual of the closure test as a systematic uncertainty for the MC-data correction factor F_{corr}, as described in section 5.1.

3 Extracting Data Single Particle Responses

The extraction of data single particle responses is similar to what was done in Run IIA [1] and RunIIB [2] notes. Note that due to the change in the calorimeter calibration for Run IIB data compared to the one for Run IIA data, especially the use of W-mass style (DØ default) MC to estimate the energy loss correction for the EM layers for Run IIB (Run IIA) data[4], the assumption that the default MC has the same photon, electron and muon responses as those in Run IIB data does not hold anymore. The differences between the W-mass style MC and the DØ default MC include the improvements in the GEANT simulation and DØ detector material distribution [4]. The energy loss correction, which is needed to correct the raw EM calorimeter cell energy for an electron to its true energy deposition, is found to be smaller for the one from

[1]Hereafter we refer zero suppression to both online readout and offline reconstruction thresholds as well as the T42 algorithm.

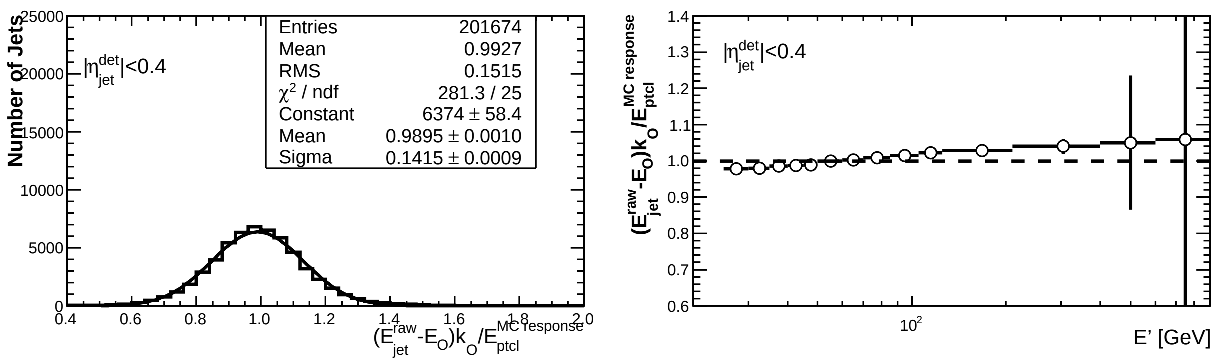

Figure 1: MC closure test for jets in p20 γ+jet MC sample for $|\eta_{det}^{jet}| < 0.4$. The single particle MC responses are derived with ZS turned off. The x-axis E' is given by $p_T^{\gamma} \cdot cosh(\eta^{jet})$. The error bars on y corresponds to the standard deviation of $y = (E_{jet}^{raw} - E_O) \cdot k_O / \sum_i E_i \cdot R_i^{MC}$ in each bin.

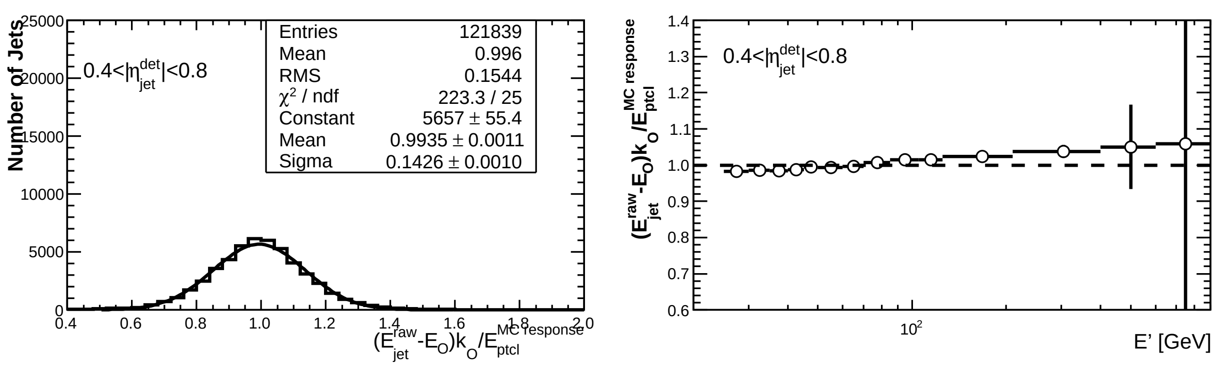

Figure 2: MC closure test for jets in p20 γ+jet MC sample for $0.4 < |\eta_{det}^{jet}| < 0.8$. The single particle MC responses are derived with ZS turned off. The x-axis E' is given by $p_T^{\gamma} \cdot cosh(\eta^{jet})$. The error bars on y corresponds to the standard deviation of $y = (E_{jet}^{raw} - E_O) \cdot k_O / \sum_i E_i \cdot R_i^{MC}$ in each bin.

the W-mass style MC than the one from the default DØ MC. Therefore the raw calorimeter jet energy in Run IIB data is higher than the raw calorimeter jet energy in Run IIA data. The difference between the two can be approximated by the ratios shown in Fig. 6. These ratios are made from the information encoded in the jetcorr processor JetP20ToP17, which was designed to bring the jet raw energy of Run IIB data on average back to the Run IIA data level.

In previous result [2], the correction for the difference was done using the ratio in Fig. 6, namely for

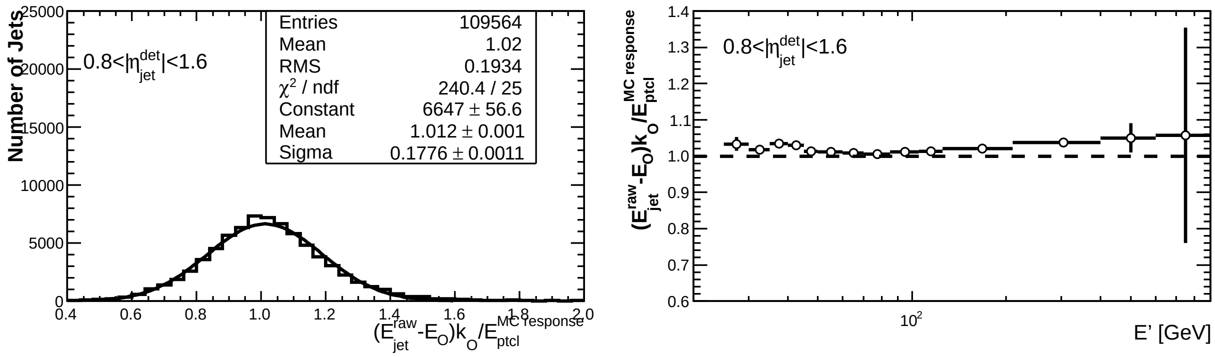

Figure 3: MC closure test for jets in p20 γ+jet MC sample for $0.8 < |\eta_{det}^{jet}| < 1.6$. The single particle MC responses are derived with ZS turned off. The x-axis E' is given by $p_T^{\gamma} \cdot cosh(\eta^{jet})$. The error bars on y corresponds to the standard deviation of $y = (E_{jet}^{raw} - E_O) \cdot k_O / \sum_i E_i \cdot R_i^{MC}$ in each bin.

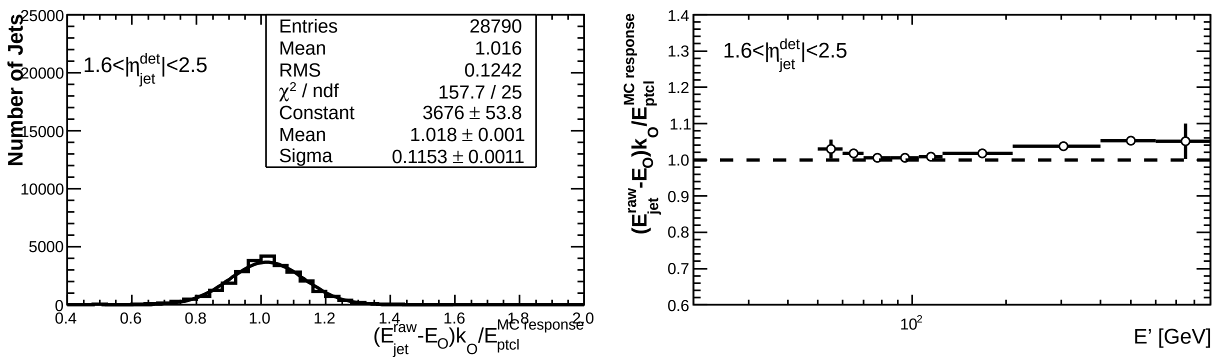

Figure 4: MC closure test for jets in p20 γ+jet MC sample for $1.6 < |\eta_{det}^{jet}| < 2.5$. The single particle MC responses are derived with ZS turned off. The x-axis E' is given by $p_T^{\gamma} \cdot cosh(\eta^{jet})$. The error bars on y corresponds to the standard deviation of $y = (E_{jet}^{raw} - E_O) \cdot k_O / \sum_i E_i \cdot R_i^{MC}$ in each bin.

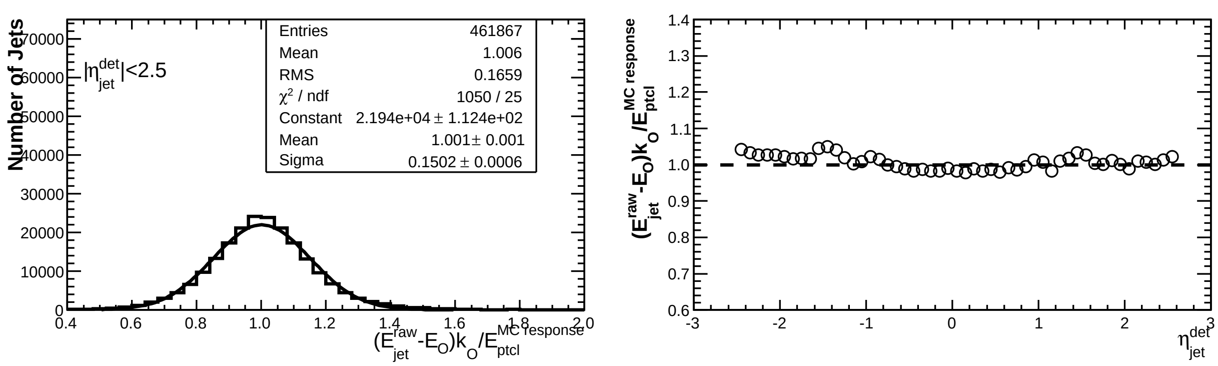

Figure 5: MC closure test for jets in p20 γ+jet MC sample for $|\eta_{det}^{jet}| < 2.5$. The single particle MC responses are derived with ZS turned off. The x-axis E' is given by $p_T^{\gamma} \cdot cosh(\eta^{jet})$. The error bars on y corresponds to the standard deviation of $y = (E_{jet}^{raw} - E_O) \cdot k_O / \sum_i E_i \cdot R_i^{MC}$ in each bin.

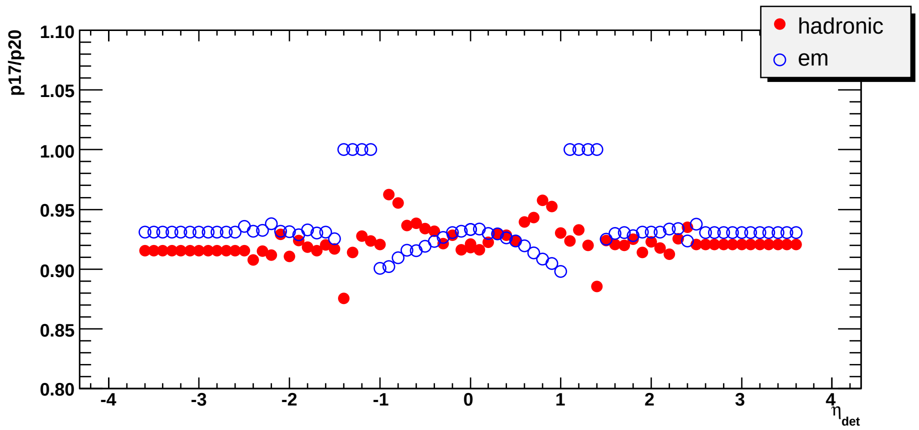

Figure 6: The difference between the Run IIA and Run IIB data in the raw calorimeter jet energy for EM and hadronic components.

each calorimeter cell in these MC samples, its energy was divided by the ratio. This correction only took into account the η_{det} dependence of the difference between Run IIA and Run IIB data, but not the energy dependence. In this note, we measure the corrected single particle responses directly from W-mass style single particle MC samples, that were newly generated. We refer to such W-mass style Run IIB single particle MC responses as $R^{MC'}$. The results for W-mass style single particle MC sample are shown in Fig. 59-68.

We make the assumption that the W-mass style single particle MC does a good job in simulating the EM component of the calorimeter, as well as the muon interaction within the detector in Run IIB data. Therefore the corrected single particle MC has the same photon, electron and muon responses as those in Run IIB data:

$$R_{\gamma}^{data} = R_{\gamma}^{MC'}, \tag{9}$$
$$R_{e^{\pm}}^{data} = R_{e^{\pm}}^{MC'}, \tag{10}$$
$$R_{\mu^{\pm}}^{data} = R_{\mu^{\pm}}^{MC'}. \tag{11}$$

For the hadrons, we introduce three additional parameters A, B, and C into Eq. 7 to parametrize the difference between the corrected MC responses and the Run IIB data ones:

$$R_h^{data} = C \cdot p_h^0 \cdot \left[1 - A \cdot p_h^1 \cdot (E/0.75)^{p_h^2 + B - 1}\right] \text{ if } p_T > m_h;\ 0 \text{ if } p_T < m_h, \tag{12}$$

where $R_h^{data} = R_h^{MC'}$ when $A = C = 1$ and $B = 0$. Thus the correction factor F defined in Eq. 1 depends on A, B and C through Eq. 12.

The tuning of the MC jet responses is made by changing A, B and C in Eq. 12 which enters into Eq. 3. We tune the parameters A, B and C so that the ratio $p_{T,\ corr}^{jet}/p_T^{\gamma}$ from MC is consistent to that from data.

The tuning is performed for two different event selections: tight photon selection in which we apply tight photon isolation cuts to select γ+jet events, and reversed isolation selection, where we apply the same photon selection cuts except a reversed track isolation requirement and select mainly di-jets events. The simultaneous tuning in the two event selections is performed and when the both selection tuning converge, we obtain the tuned parameters A, B, and C. We present results for RunIIB1 MC and data, RunIIB2 MC and data and RunIIB3 MC with merged RunIIB3 and B4 data as shown in Fig. 7-12.

We perform a closure test for the above MC tuning procedure. The results are shown in Fig. 13-36. As can be seen, the jet responses from the corrected MC are consistent with those in data, for both tight photon and reversed photon selections, which have different jet flavor composition.

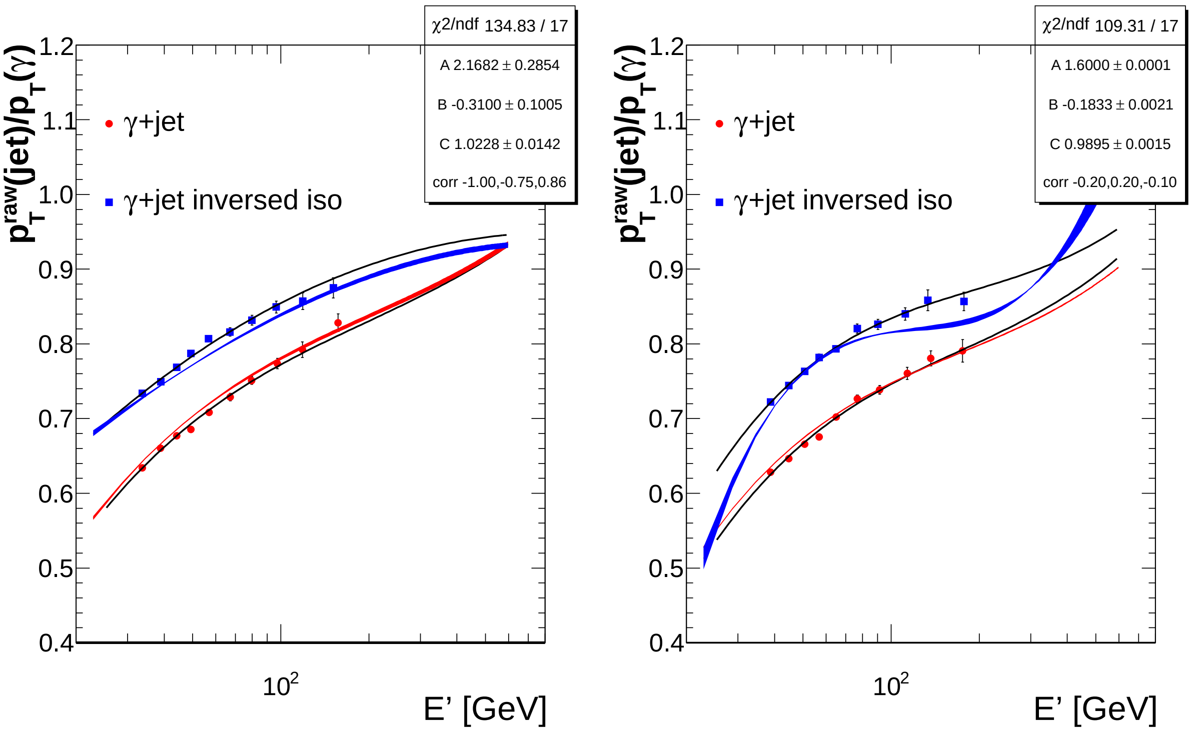

Figure 7: RunIIB1 MC tuning for $|\eta_{det}^{jet}| < 0.4$ (left) and for $0.4 < |\eta_{det}^{jet}| < 0.8$ (right) with simultaneous tuning of tight photon selection and reversed isolation cut selection. The points are data. The bands are MC tuning with the smallest χ^2 as described in the text.

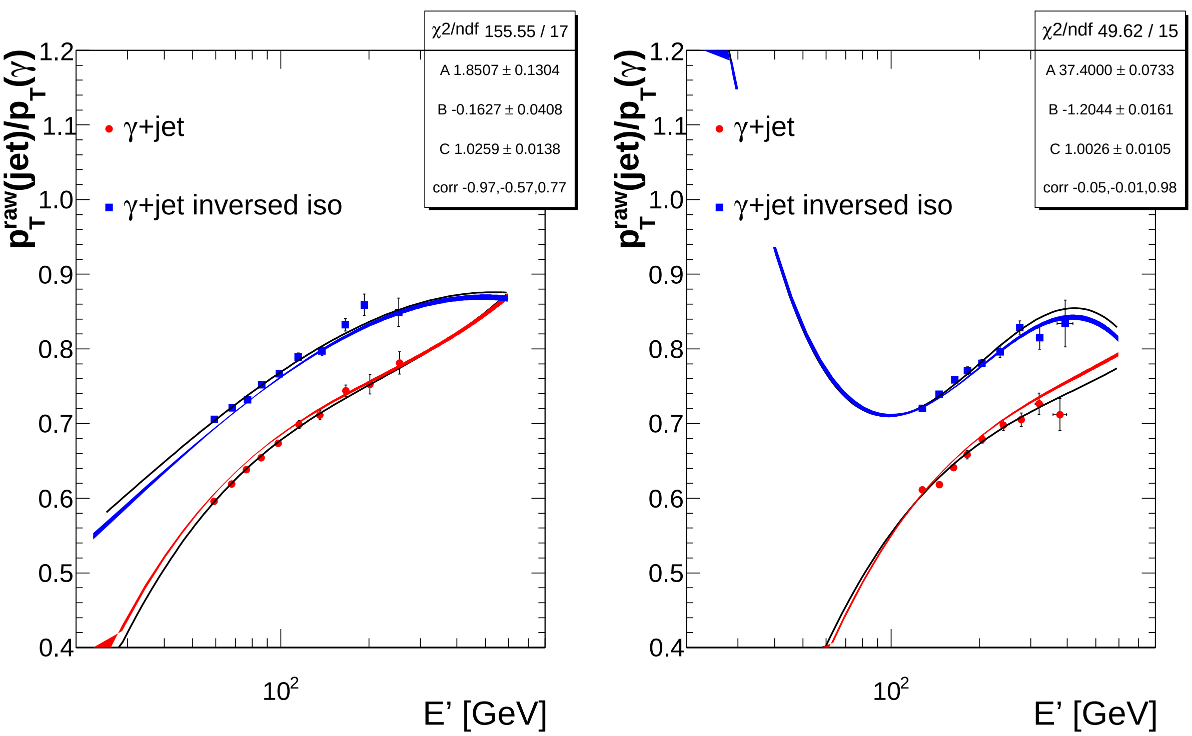

Figure 8: RunIIB1 MC tuning for $0.8 < |\eta_{det}^{jet}| < 1.6$ (left) and for $1.6 < |\eta_{det}^{jet}| < 2.5$ (right) with simultaneous tuning of tight photon selection and reversed isolation cut selection. The points are data. The bands are MC tuning with the smallest χ^2 as described in the text.

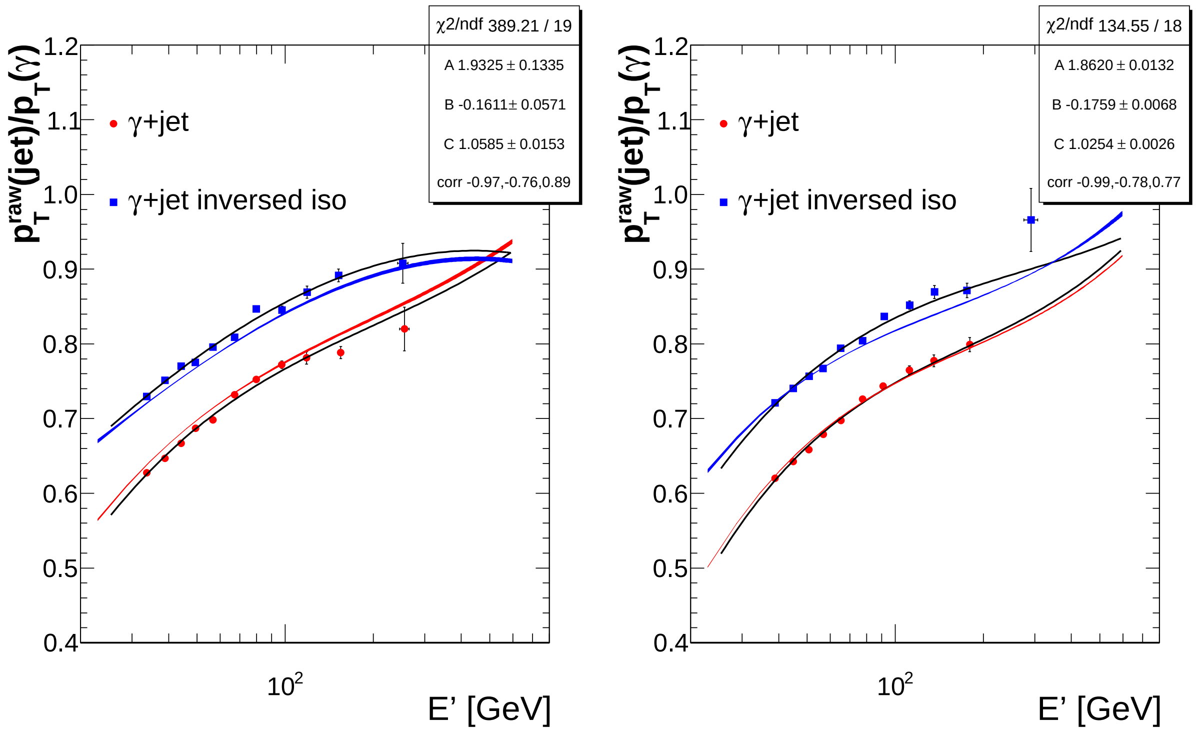

Figure 9: RunIIB2 MC tuning for $|\eta_{det}^{jet}| < 0.4$ (left) and for $0.4 < |\eta_{det}^{jet}| < 0.8$ (right) with simultaneous tuning of tight photon selection and reversed isolation cut selection. The points are data. The bands are MC tuning with the smallest χ^2 as described in the text.

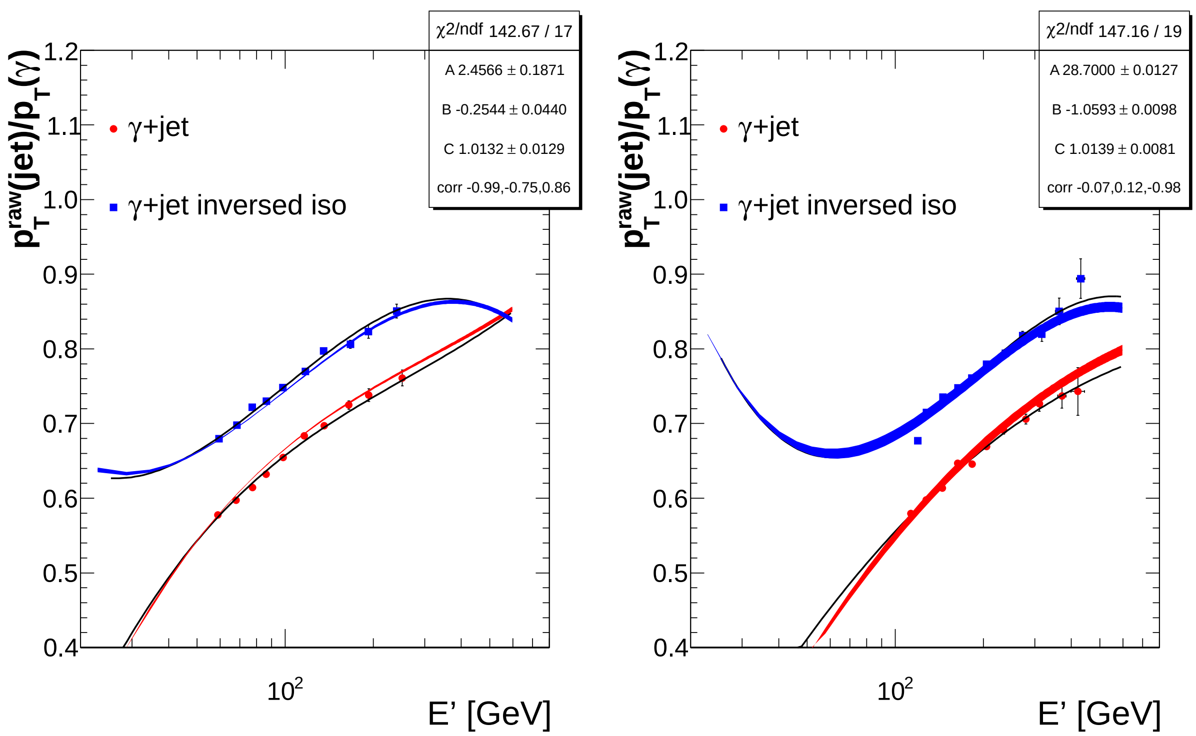

Figure 10: RunIIB2 MC tuning for $0.8 < |\eta_{det}^{jet}| < 1.6$ (left) and for $1.6 < |\eta_{det}^{jet}| < 2.5$ (right) with simultaneous tuning of tight photon selection and reversed isolation cut selection. The points are data. The bands are MC tuning with the smallest χ^2 as described in the text.

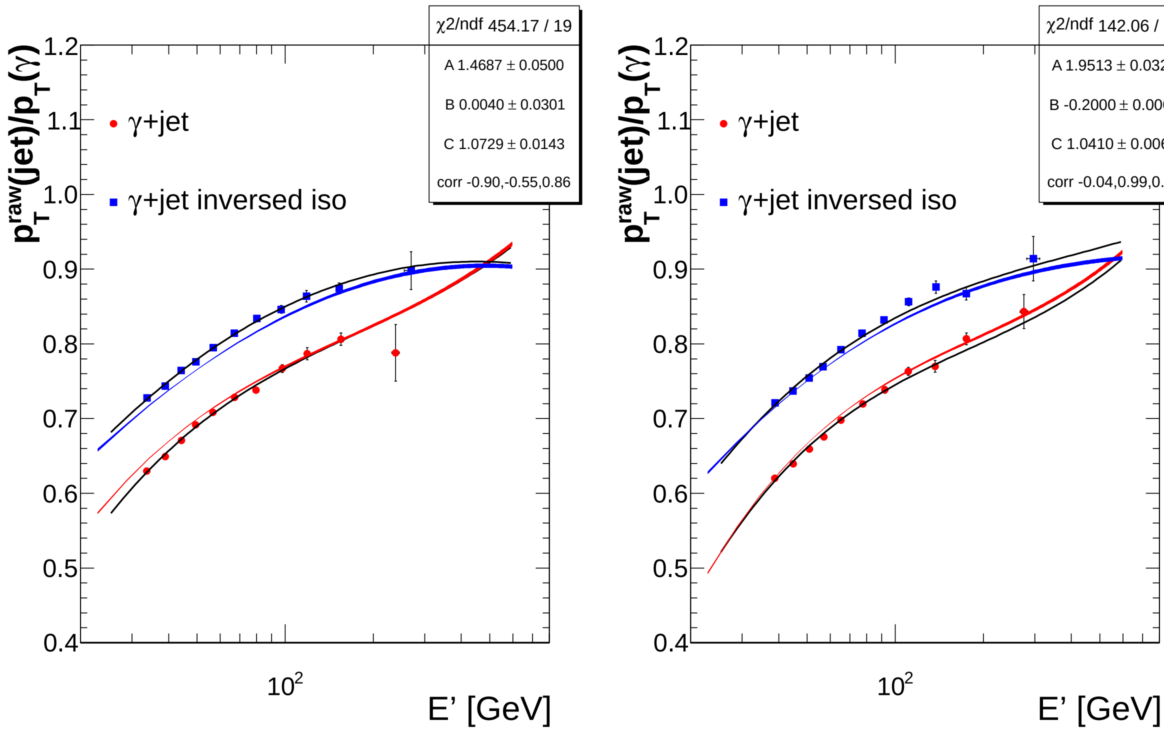

Figure 11: RunIIB34 MC tuning for $|\eta_{det}^{jet}| < 0.4$ (left) and for $0.4 < |\eta_{det}^{jet}| < 0.8$ (right) with simultaneous tuning of tight photon selection and reversed isolation cut selection. The points are data. The bands are MC tuning with the smallest χ^2 as described in the text.

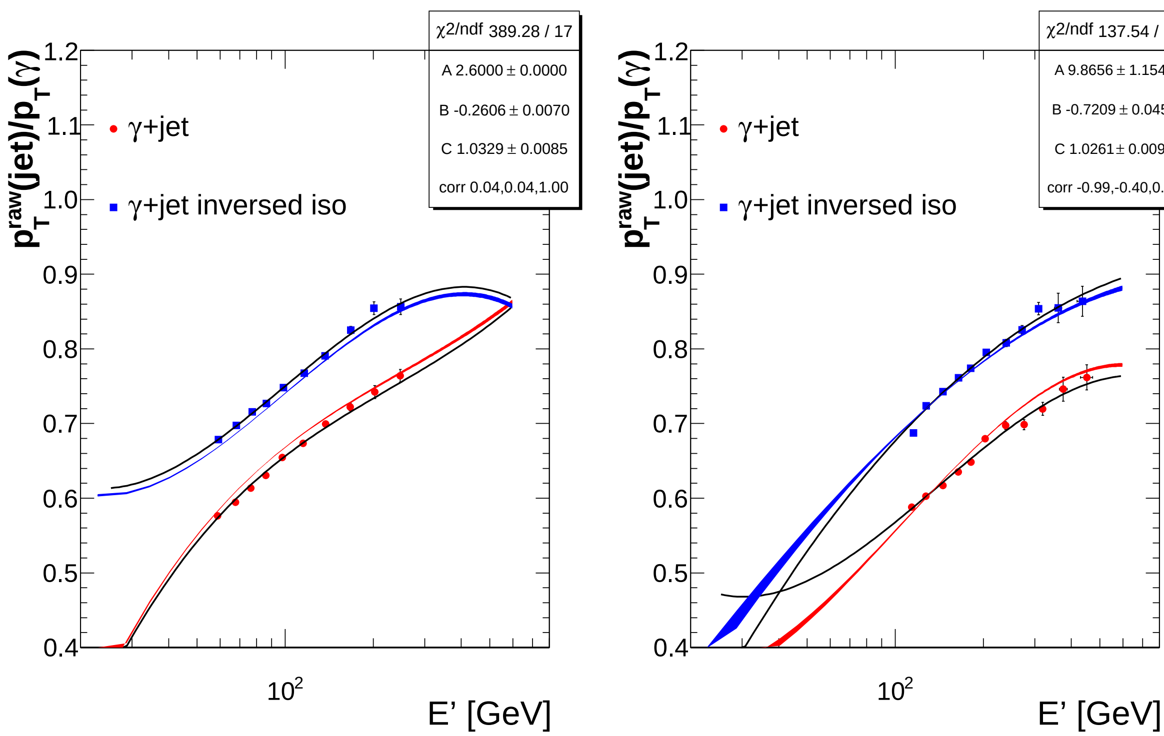

Figure 12: RunIIB34 MC tuning for $0.8 < |\eta_{det}^{jet}| < 1.6$ (left) and for $1.6 < |\eta_{det}^{jet}| < 2.5$ (right) with simultaneous tuning of tight photon selection and reversed isolation cut selection. The points are data. The bands are MC tuning with the smallest χ^2 as described in the text.

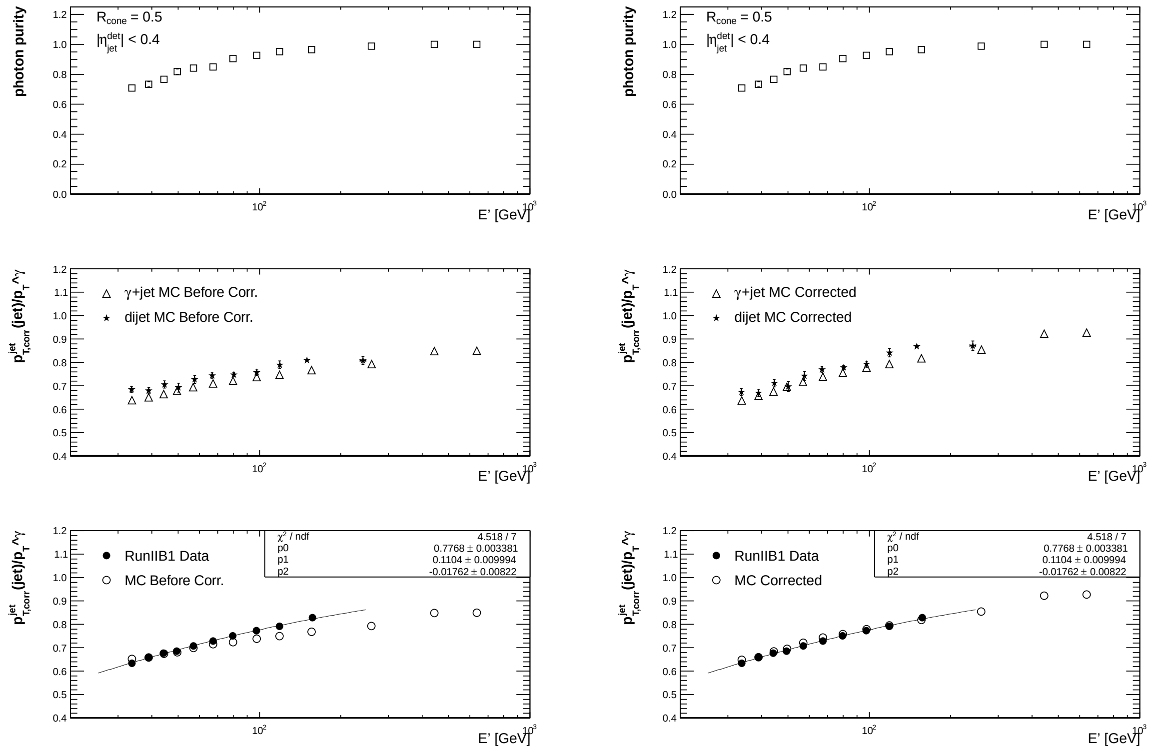

Figure 13: RunIIB1 Closure test for MC tuning to data for tight photon selection with $|\eta_{det}^{jet}| < 0.4$. Photon purity (top), γ+jet and di-jets MC responses (middle) and combined γ+jet and di-jets MC response compared to data (bottom). Left: default MC; right: MC after tuning.

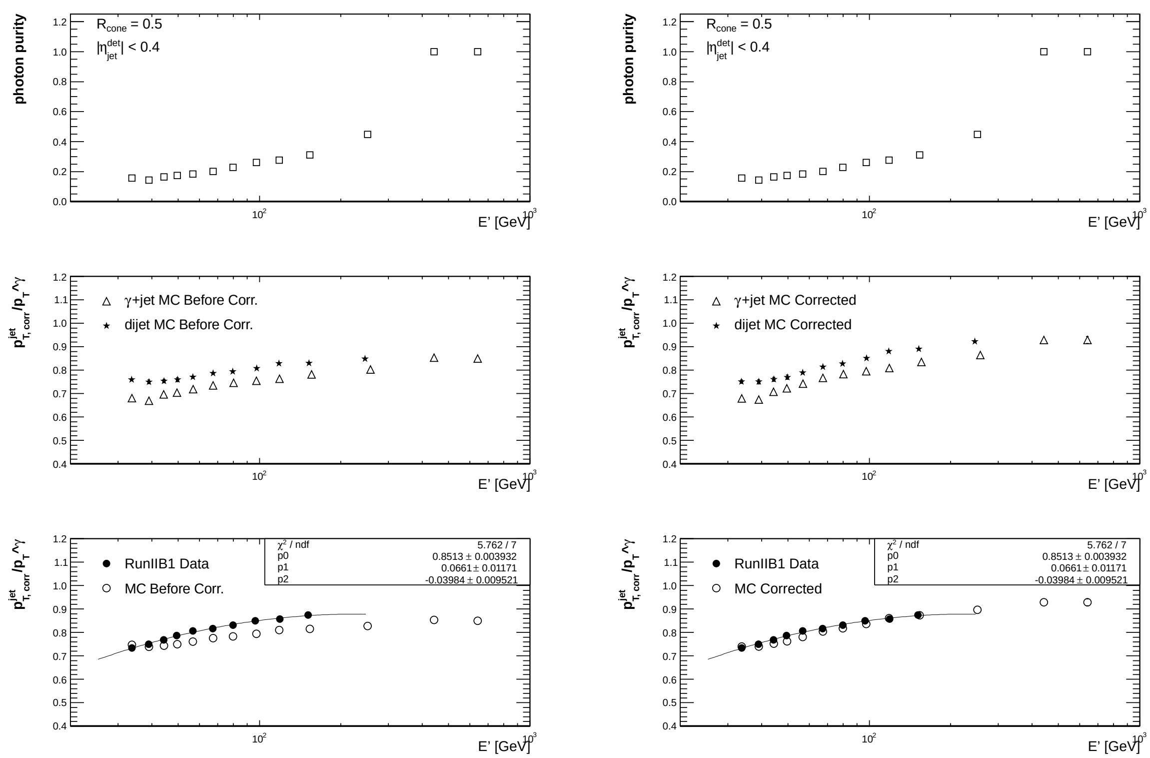

Figure 14: RunIIB1 Closure test for MC tuning to data for reversed photon selection with $|\eta_{det}^{jet}| < 0.4$. Photon purity (top), γ+jet and di-jets MC responses (middle) and combined γ+jet and di-jets MC response compared to data (bottom). Left: default MC; right: MC after tuning.

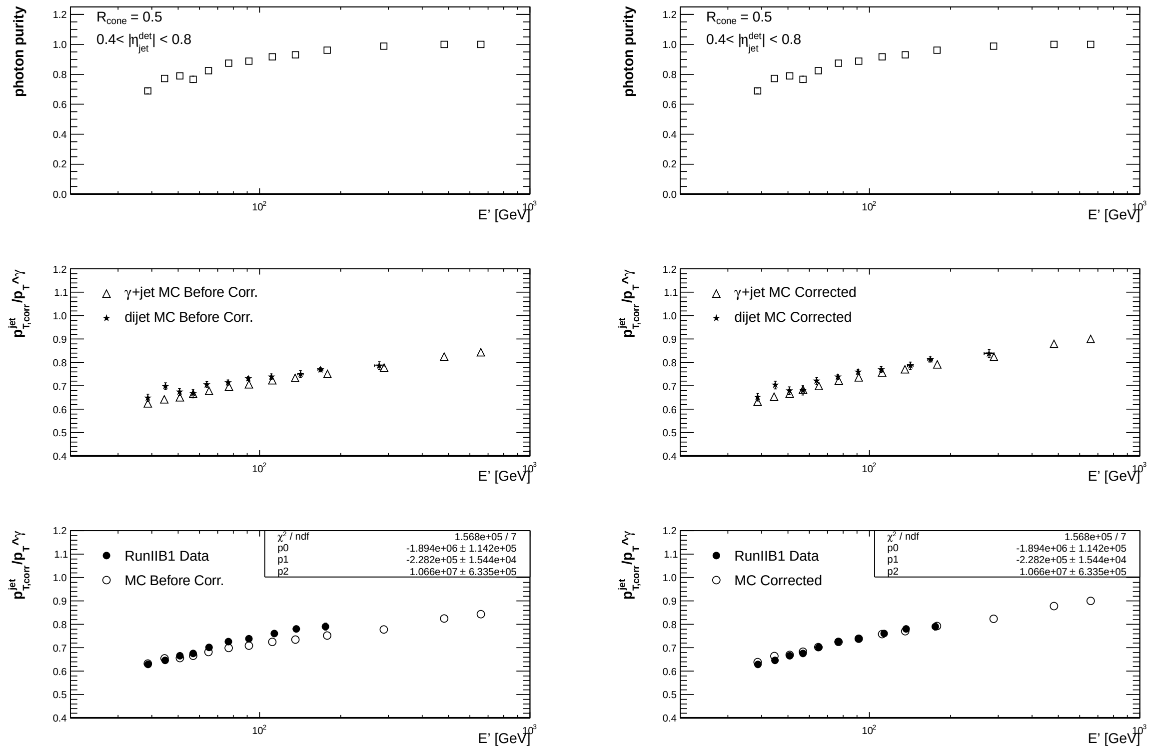

Figure 15: RunIIB1 Closure test for MC tuning to data for tight photon selection with $0.4 < |\eta_{det}^{jet}| < 0.8$. Photon purity (top), γ+jet and di-jets MC responses (middle) and combined γ+jet and di-jets MC response compared to data (bottom). Left: default MC; right: MC after tuning.

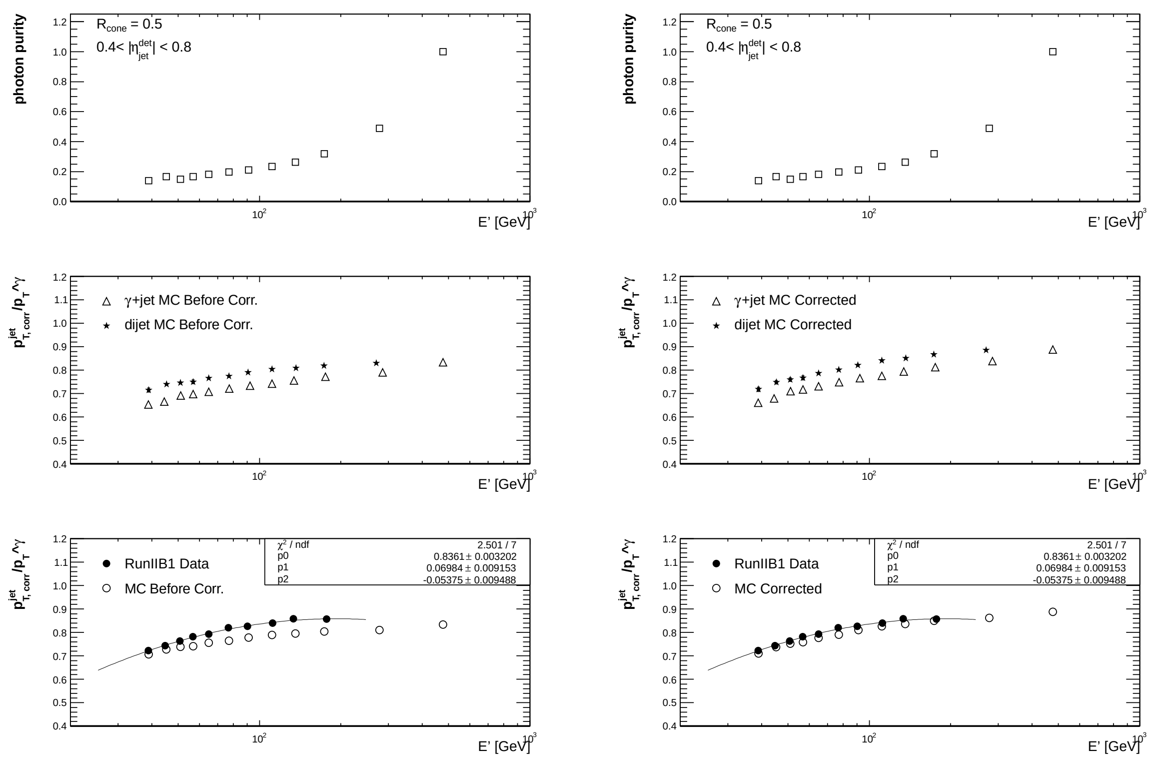

Figure 16: RunIIB1 Closure test for MC tuning to data for reversed photon selection with $0.4 < |\eta_{det}^{jet}| < 0.8$. Photon purity (top), γ+jet and di-jets MC responses (middle) and combined γ+jet and di-jets MC response compared to data (bottom). Left: default MC; right: MC after tuning.

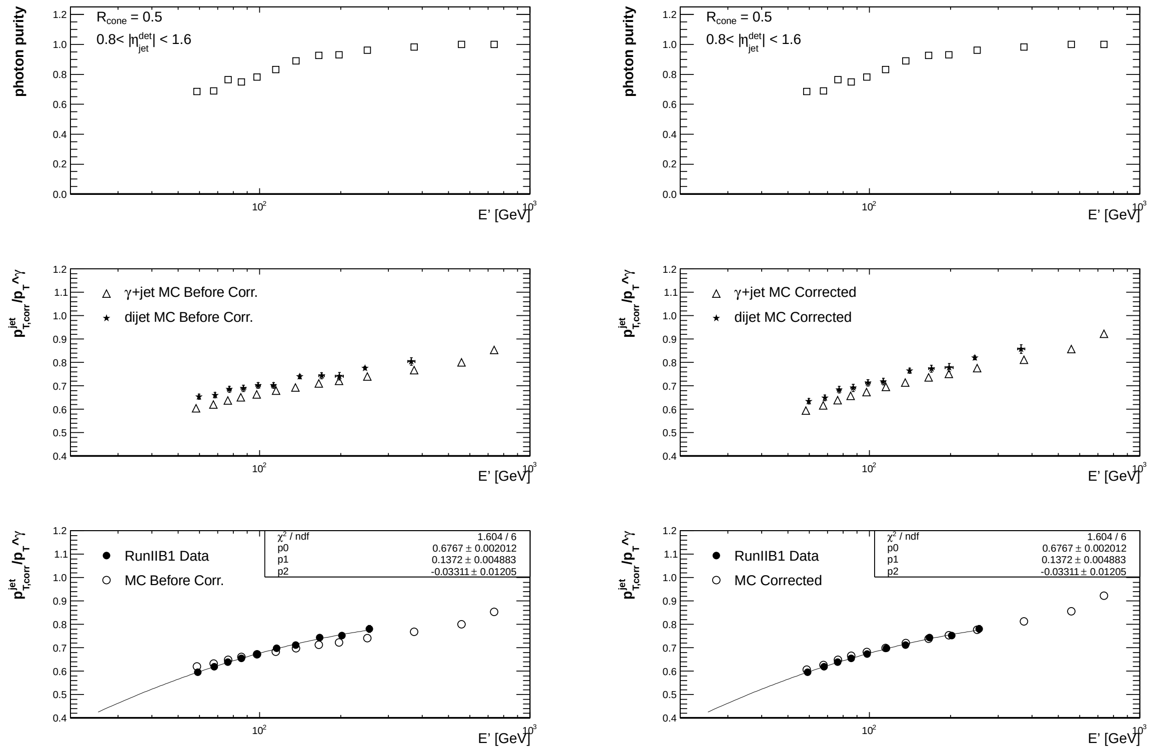

Figure 17: RunIIB1 Closure test for MC tuning to data for tight photon selection with $0.8 < |\eta_{det}^{jet}| < 1.6$. Photon purity (top), γ+jet and di-jets MC responses (middle) and combined γ+jet and di-jets MC response compared to data (bottom). Left: default MC; right: MC after tuning.

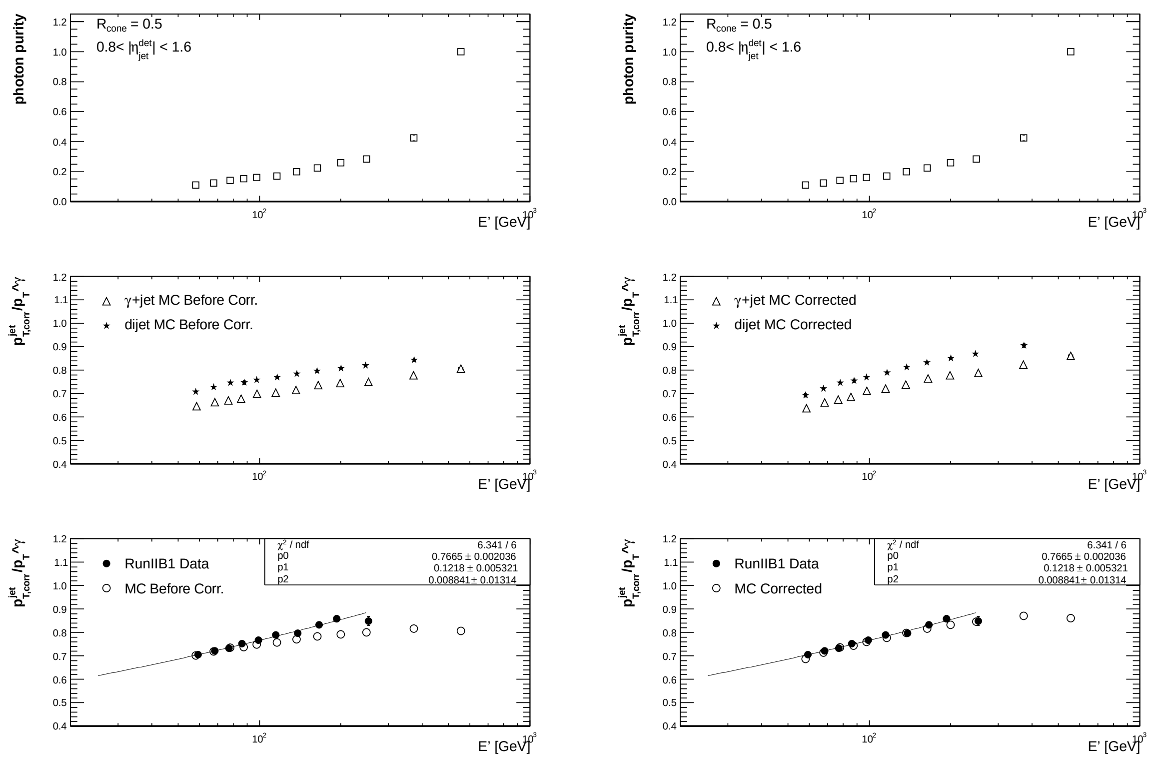

Figure 18: RunIIB1 Closure test for MC tuning to data for reversed photon selection with $0.8 < |\eta_{det}^{jet}| < 1.6$. Photon purity (top), γ+jet and di-jets MC responses (middle) and combined γ+jet and di-jets MC response compared to data (bottom). Left: default MC; right: MC after tuning.

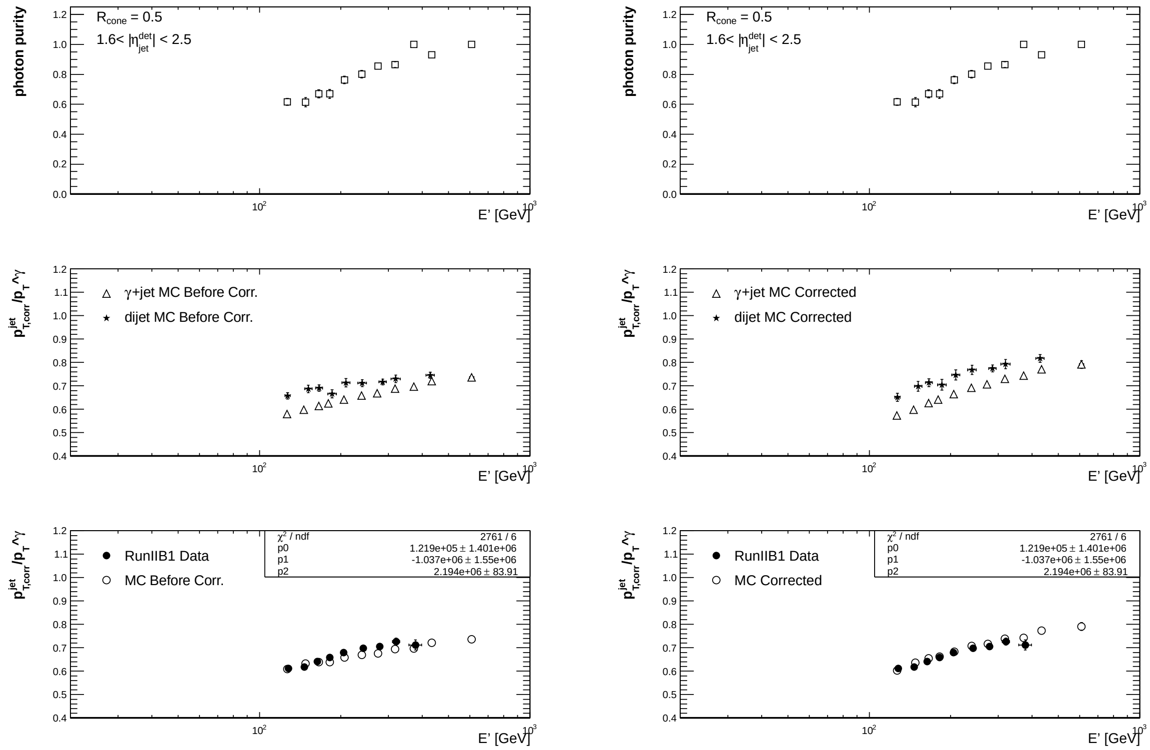

Figure 19: RunIIB1 Closure test for MC tuning to data for tight photon selection with $1.6 < |\eta^{jet}_{det}| < 2.5$. Photon purity (top), γ+jet and di-jets MC responses (middle) and combined γ+jet and di-jets MC response compared to data (bottom). Left: default MC; right: MC after tuning.

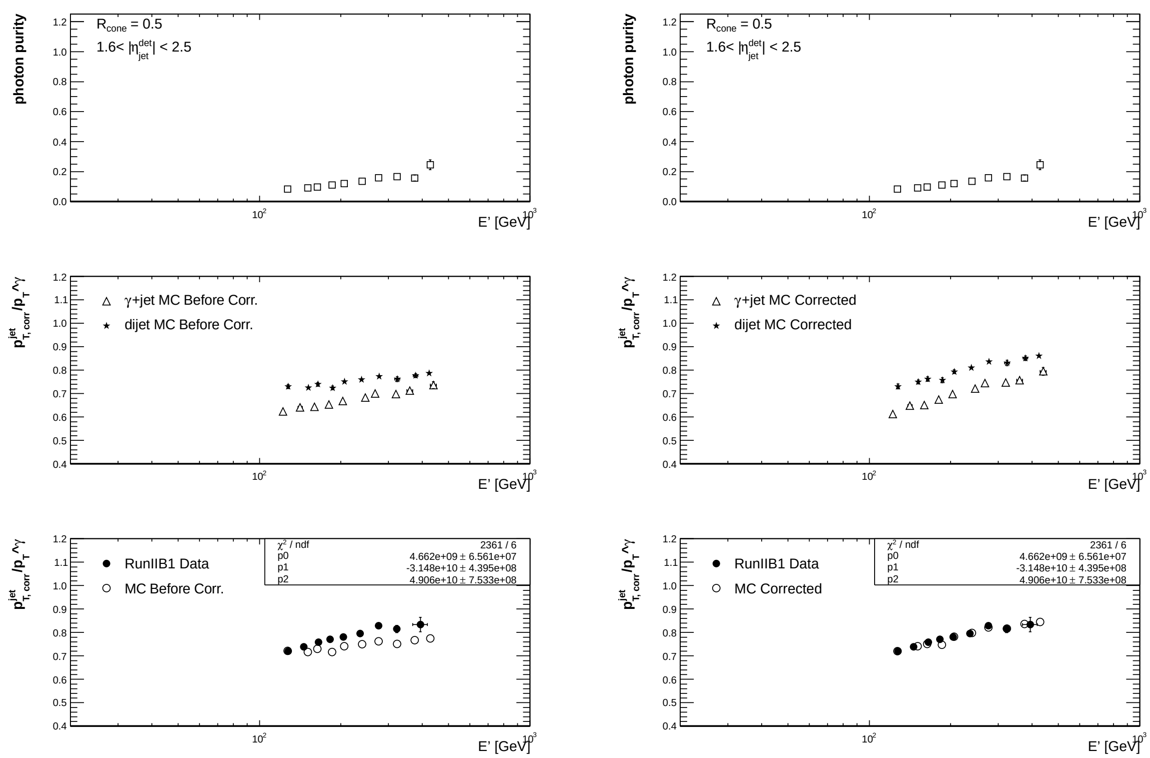

Figure 20: RunIIB1 Closure test for MC tuning to data for reversed photon selection with $1.6 < |\eta^{jet}_{det}| < 2.5$. Photon purity (top), γ+jet and di-jets MC responses (middle) and combined γ+jet and di-jets MC response compared to data (bottom). Left: default MC; right: MC after tuning.

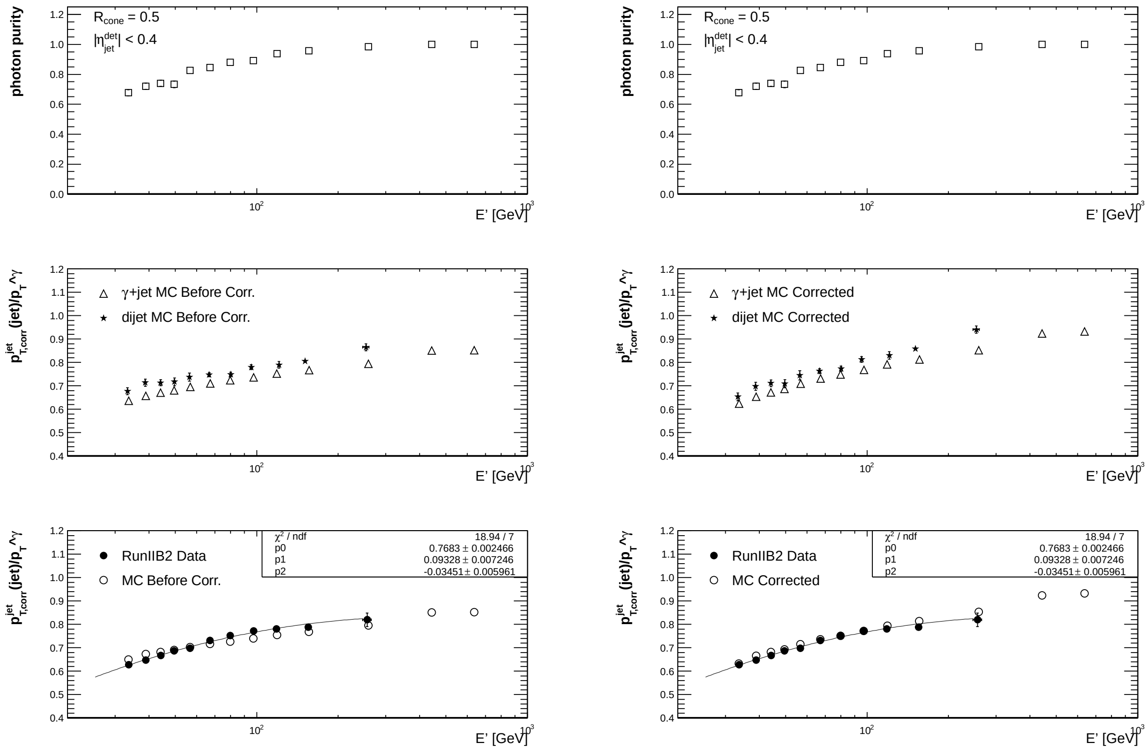

Figure 21: RunIIB2 Closure test for MC tuning to data for tight photon selection with $|\eta^{jet}_{det}| < 0.4$. Photon purity (top), γ+jet and di-jets MC responses (middle) and combined γ+jet and di-jets MC response compared to data (bottom). Left: default MC; right: MC after tuning.

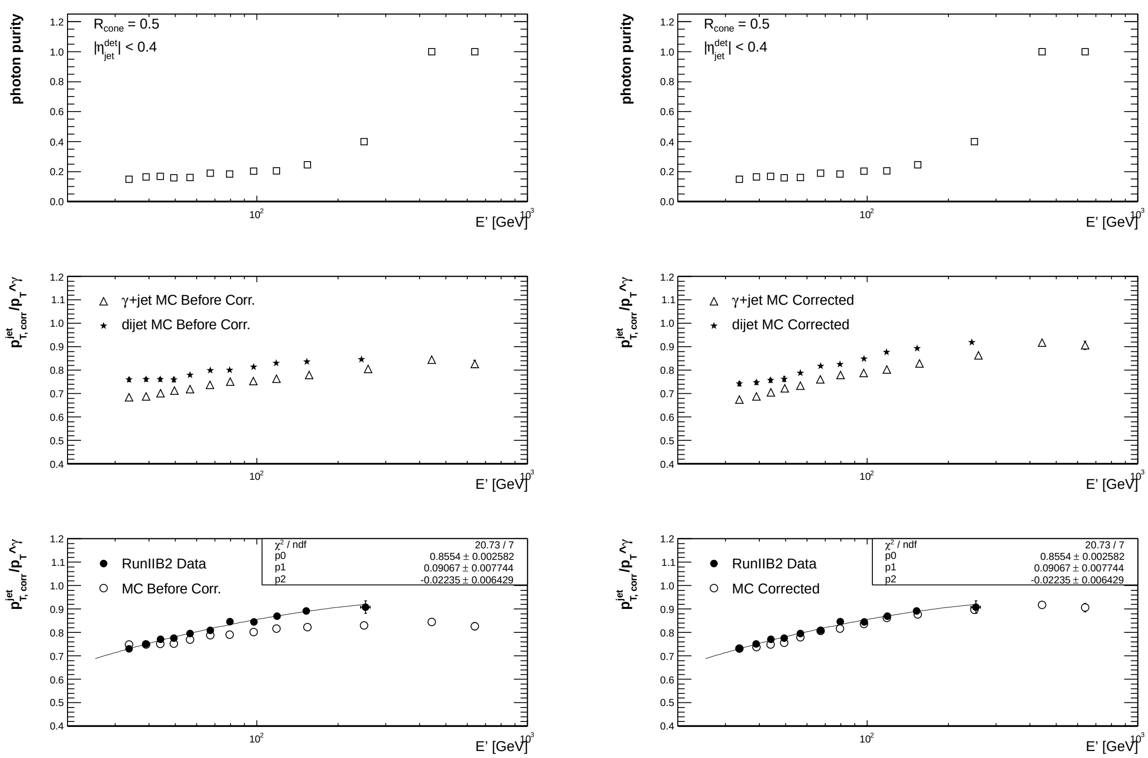

Figure 22: RunIIB2 Closure test for MC tuning to data for reversed photon selection with $|\eta^{jet}_{det}| < 0.4$. Photon purity (top), γ+jet and di-jets MC responses (middle) and combined γ+jet and di-jets MC response compared to data (bottom). Left: default MC; right: MC after tuning.

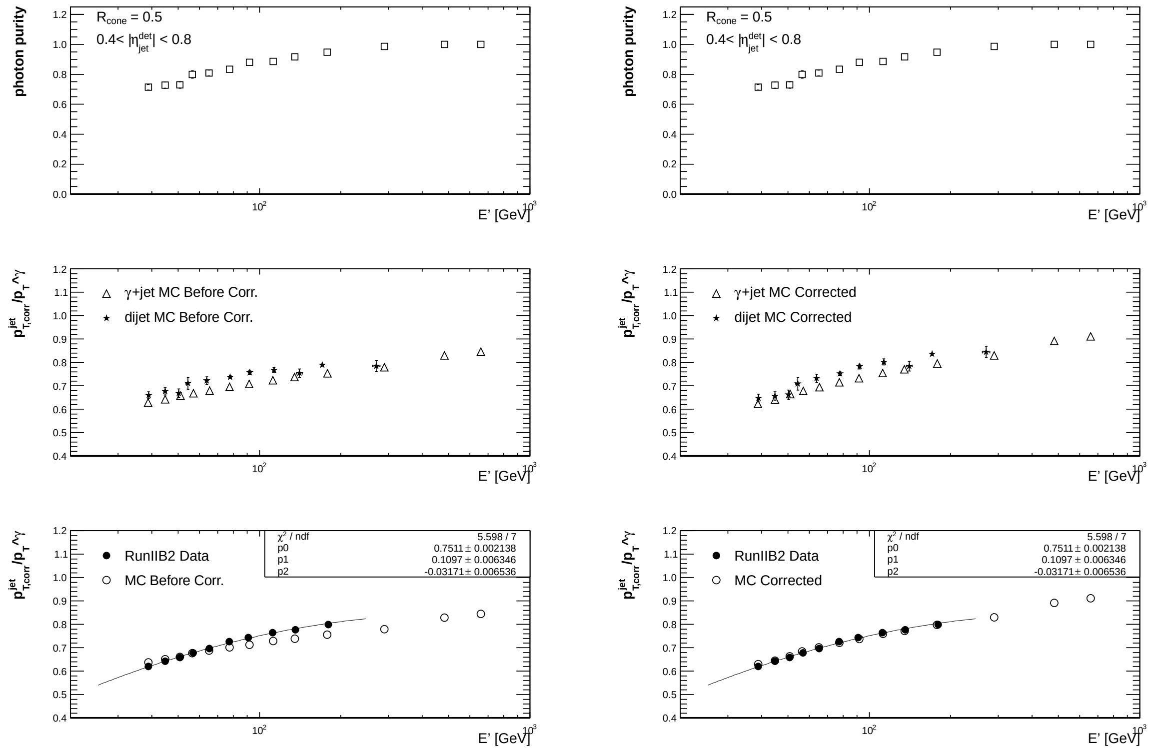

Figure 23: RunIIB2 Closure test for MC tuning to data for tight photon selection with $0.4 < |\eta_{det}^{jet}| < 0.8$. Photon purity (top), γ+jet and di-jets MC responses (middle) and combined γ+jet and di-jets MC response compared to data (bottom). Left: default MC; right: MC after tuning.

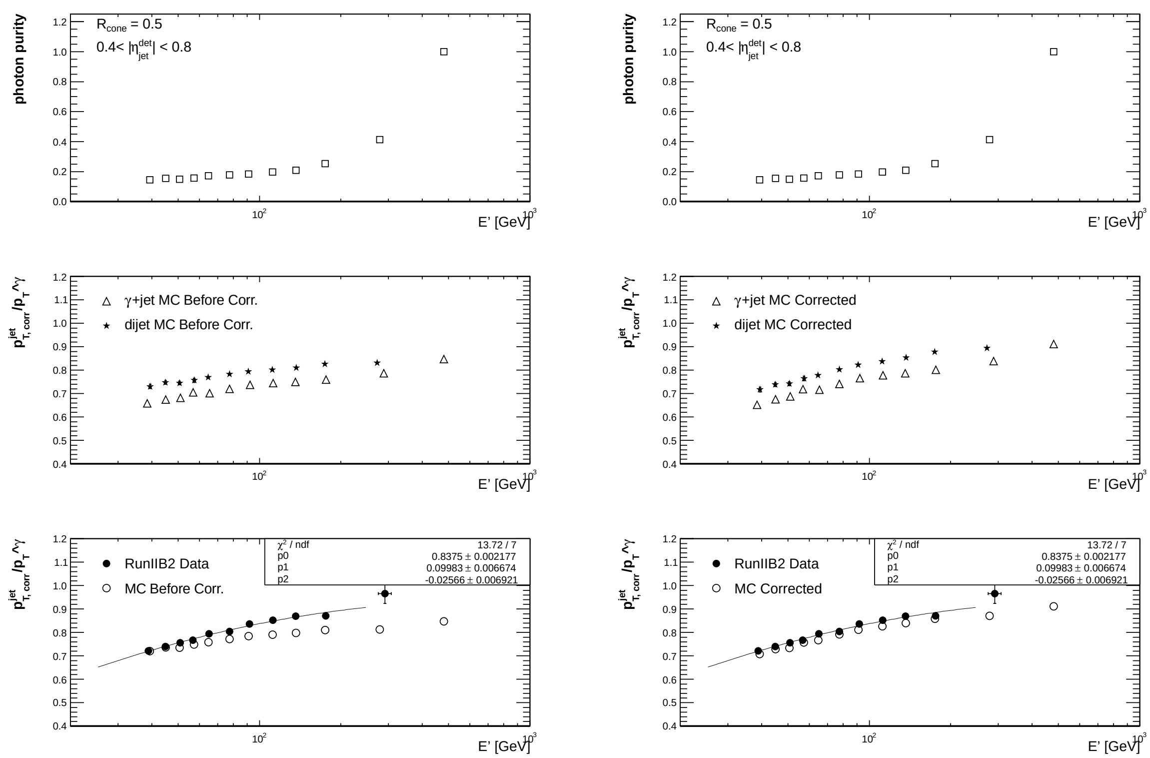

Figure 24: RunIIB2 Closure test for MC tuning to data for reversed photon selection with $0.4 < |\eta_{det}^{jet}| < 0.8$. Photon purity (top), γ+jet and di-jets MC responses (middle) and combined γ+jet and di-jets MC response compared to data (bottom). Left: default MC; right: MC after tuning.

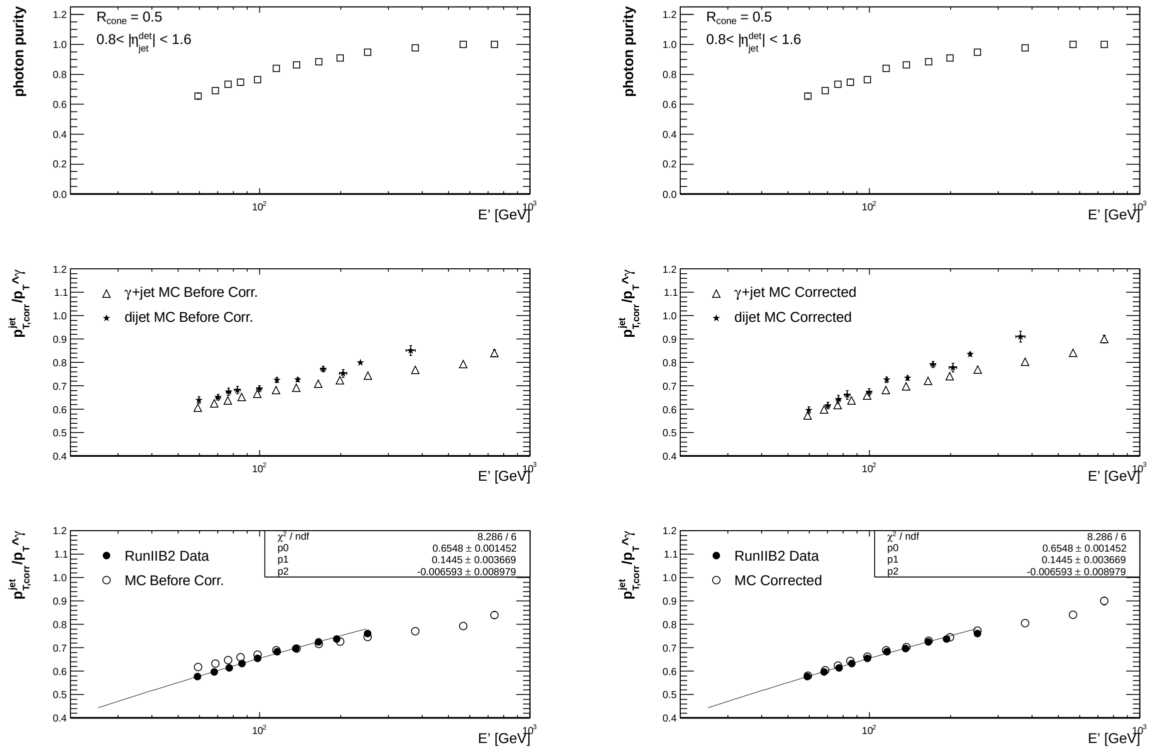

Figure 25: RunIIB2 Closure test for MC tuning to data for tight photon selection with $0.8 < |\eta_{det}^{jet}| < 1.6$. Photon purity (top), γ+jet and di-jets MC responses (middle) and combined γ+jet and di-jets MC response compared to data (bottom). Left: default MC; right: MC after tuning.

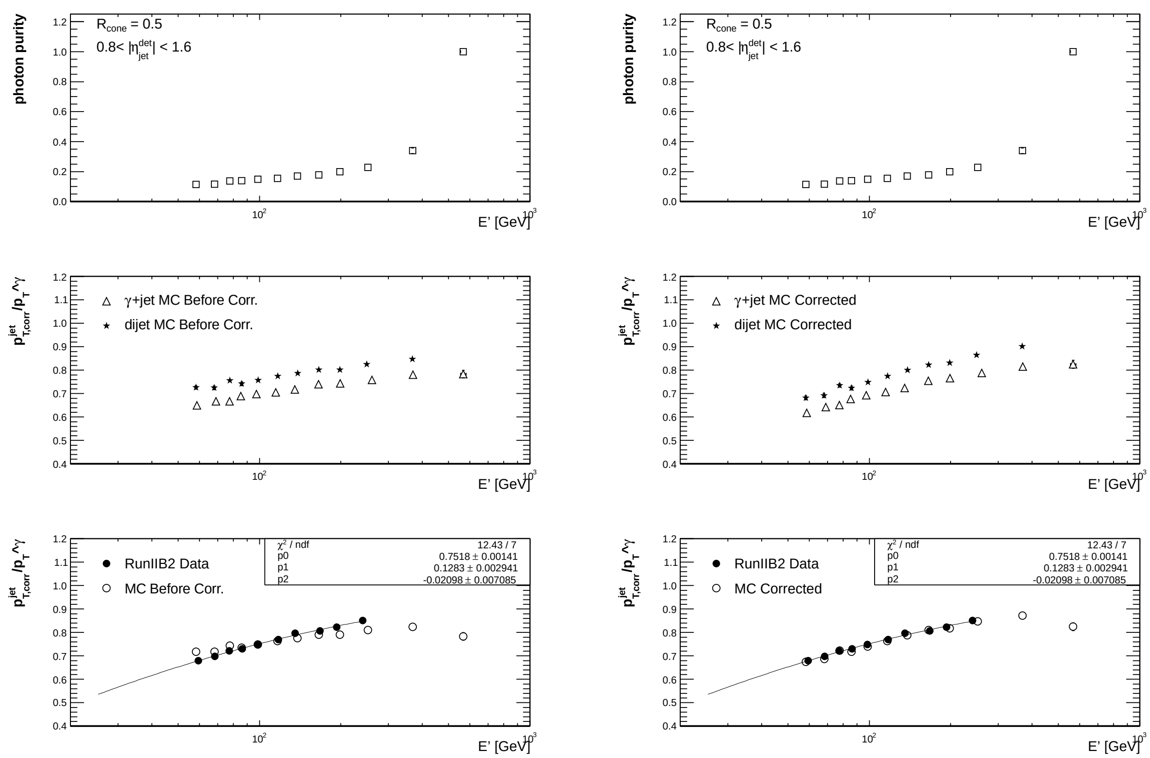

Figure 26: RunIIB2 Closure test for MC tuning to data for reversed photon selection with $0.8 < |\eta_{det}^{jet}| < 1.6$. Photon purity (top), γ+jet and di-jets MC responses (middle) and combined γ+jet and di-jets MC response compared to data (bottom). Left: default MC; right: MC after tuning.

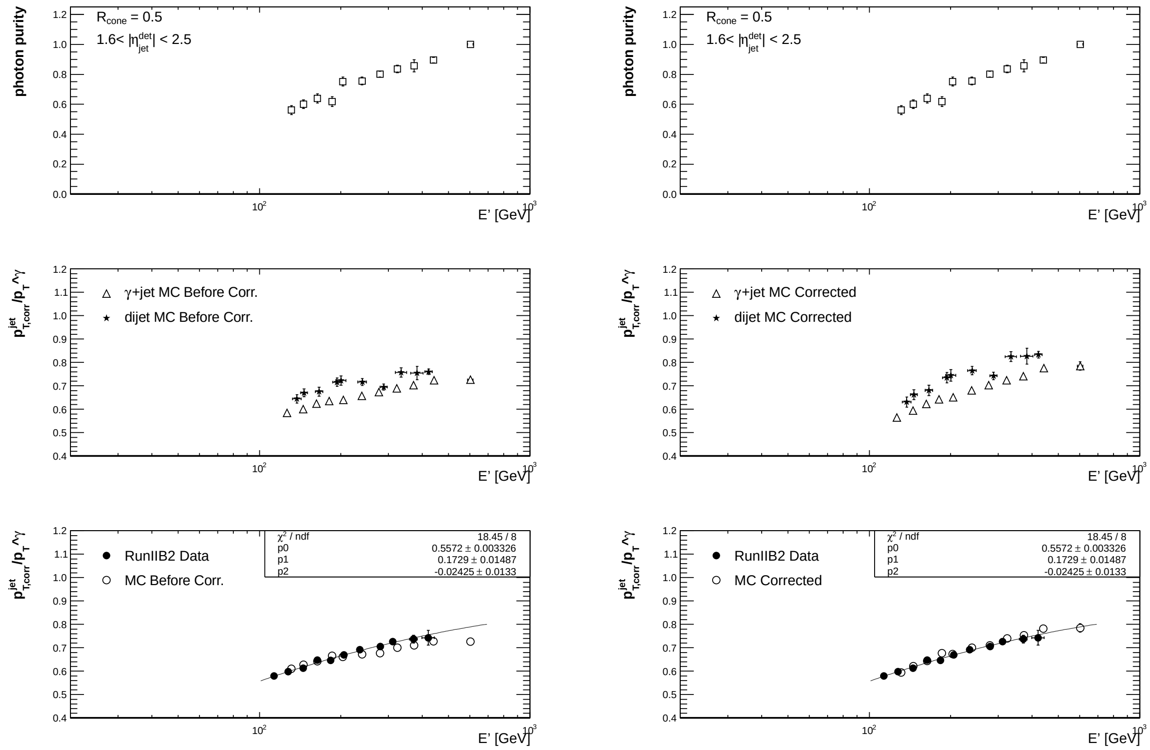

Figure 27: RunIIB2 Closure test for MC tuning to data for tight photon selection with $1.6 < |\eta_{det}^{jet}| < 2.5$. Photon purity (top), γ+jet and di-jets MC responses (middle) and combined γ+jet and di-jets MC response compared to data (bottom). Left: default MC; right: MC after tuning.

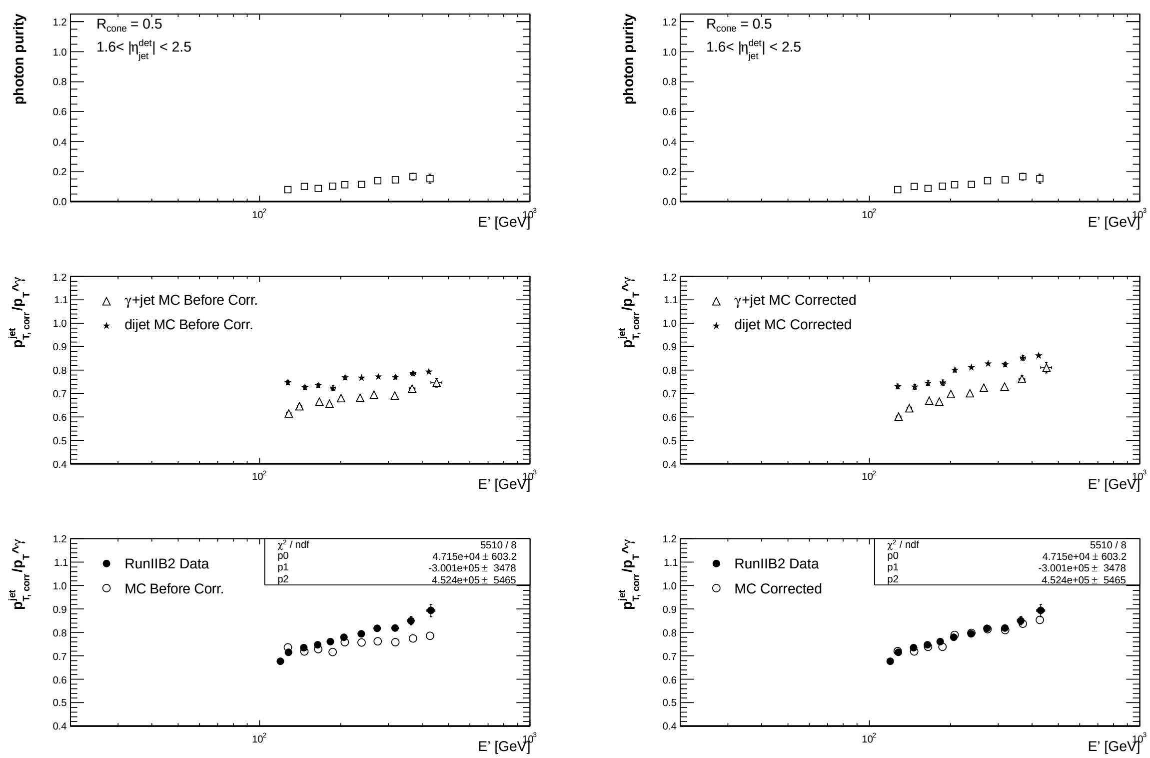

Figure 28: RunIIB2 Closure test for MC tuning to data for reversed photon selection with $1.6 < |\eta_{det}^{jet}| < 2.5$. Photon purity (top), γ+jet and di-jets MC responses (middle) and combined γ+jet and di-jets MC response compared to data (bottom). Left: default MC; right: MC after tuning.

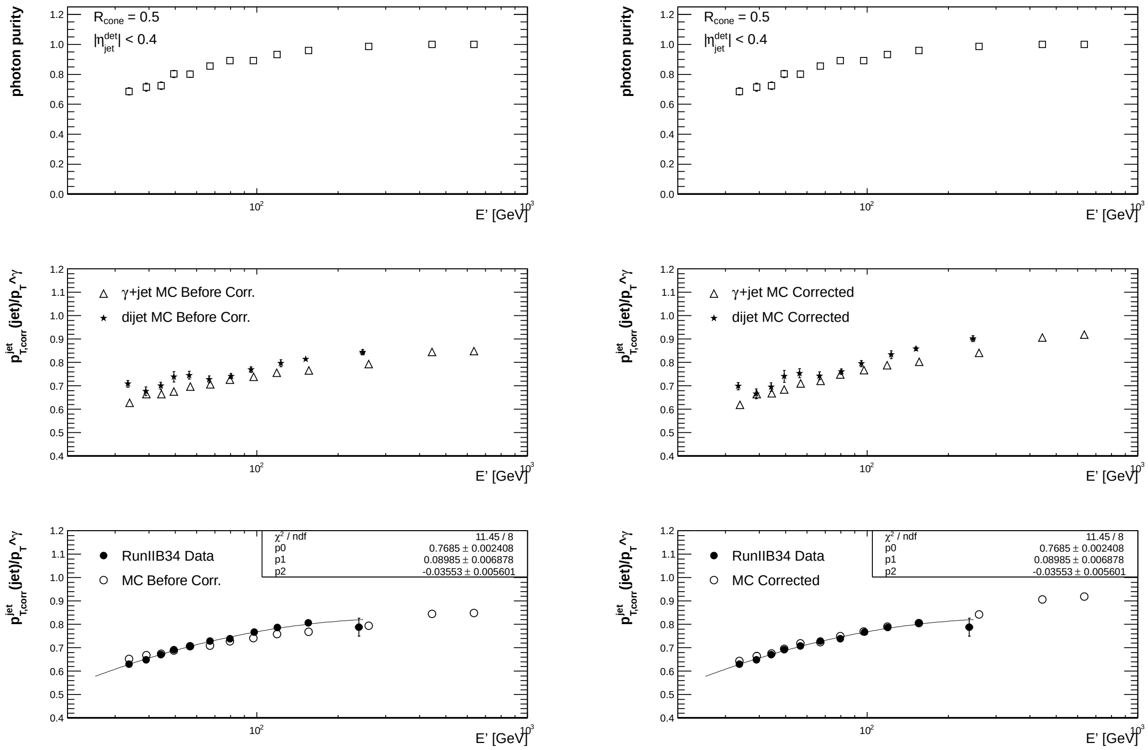

Figure 29: RunIIB34 Closure test for MC tuning to data for tight photon selection with $|\eta_{det}^{jet}| < 0.4$. Photon purity (top), γ+jet and di-jets MC responses (middle) and combined γ+jet and di-jets MC response compared to data (bottom). Left: default MC; right: MC after tuning.

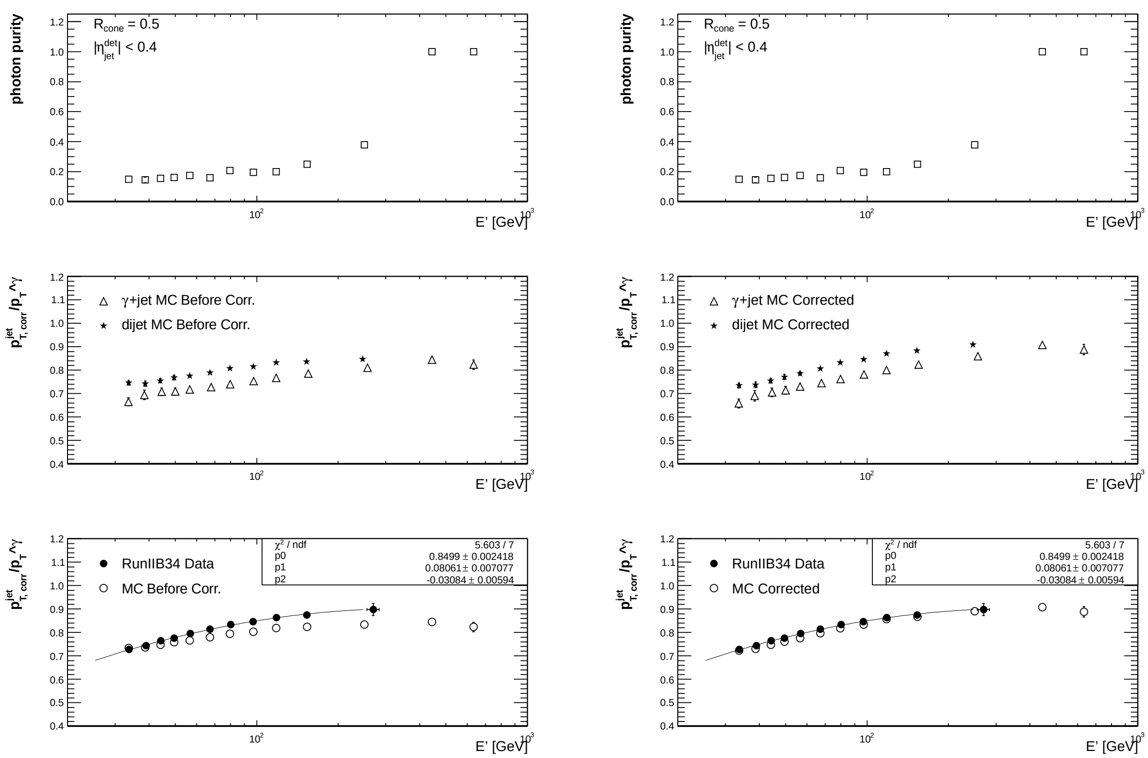

Figure 30: RunIIB34 Closure test for MC tuning to data for reversed photon selection with $|\eta_{det}^{jet}| < 0.4$. Photon purity (top), γ+jet and di-jets MC responses (middle) and combined γ+jet and di-jets MC response compared to data (bottom). Left: default MC; right: MC after tuning.

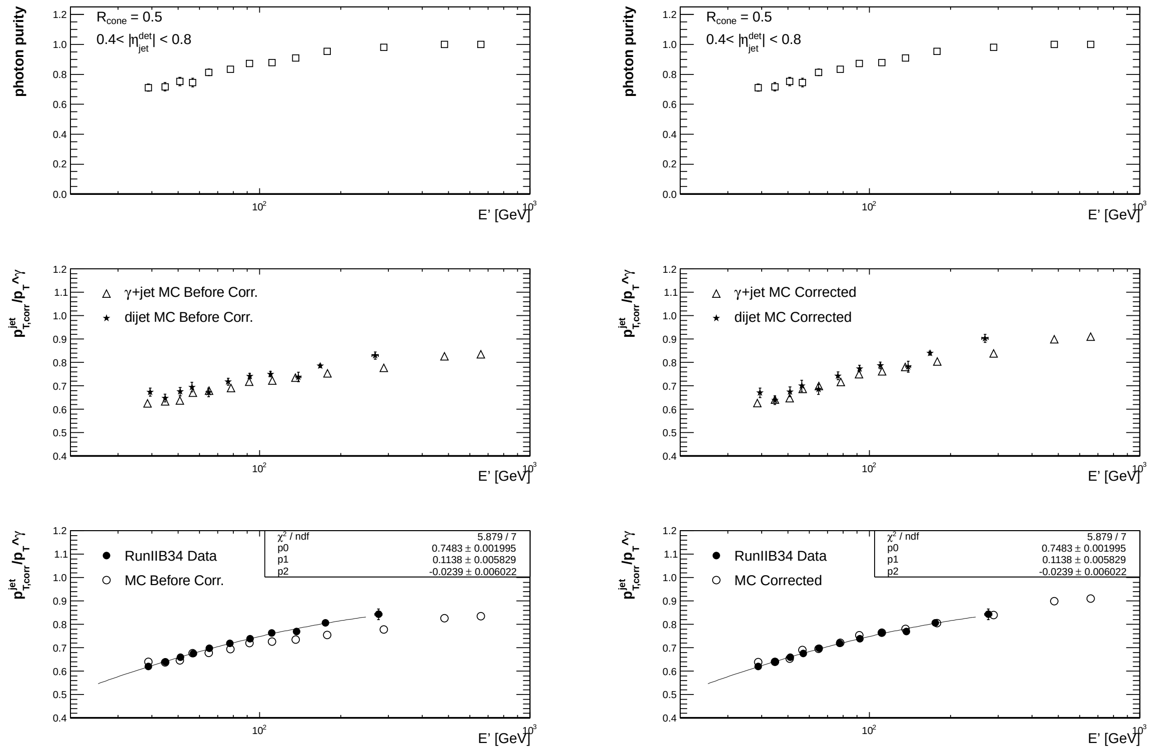

Figure 31: RunIIB34 Closure test for MC tuning to data for tight photon selection with $0.4 < |\eta_{det}^{jet}| < 0.8$. Photon purity (top), γ+jet and di-jets MC responses (middle) and combined γ+jet and di-jets MC response compared to data (bottom). Left: default MC; right: MC after tuning.

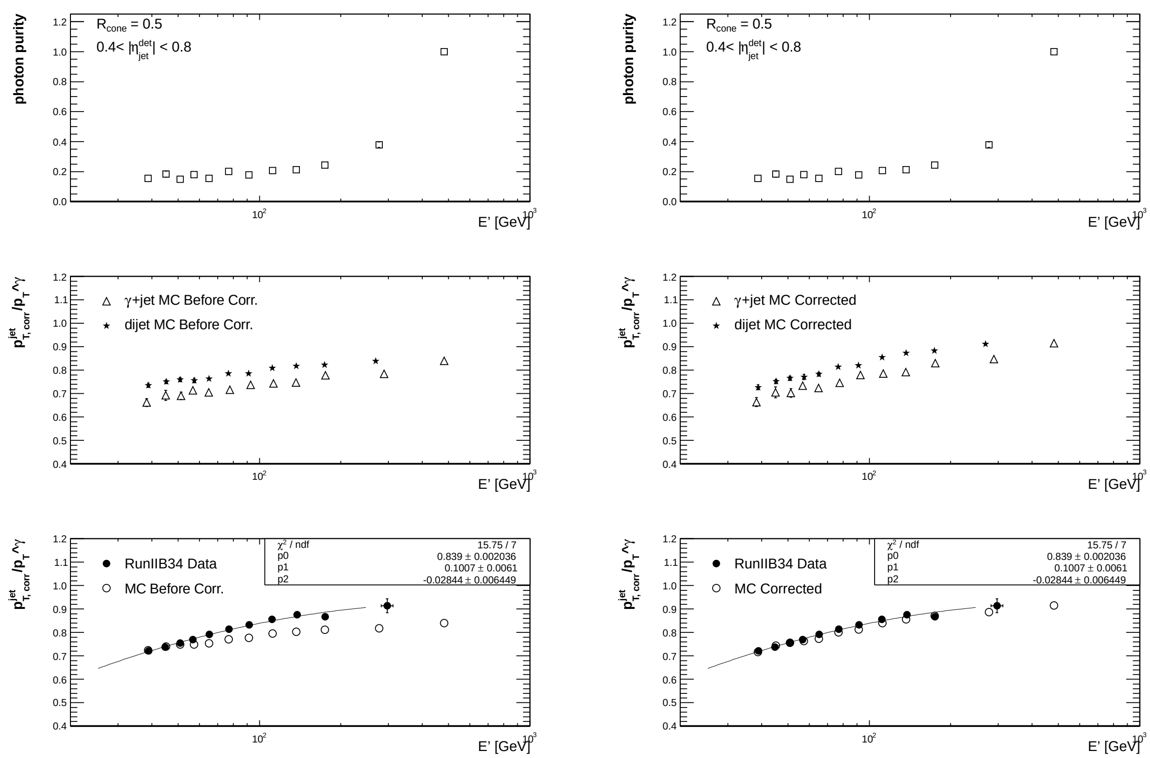

Figure 32: RunIIB34 Closure test for MC tuning to data for reversed photon selection with $0.4 < |\eta_{det}^{jet}| < 0.8$. Photon purity (top), γ+jet and di-jets MC responses (middle) and combined γ+jet and di-jets MC response compared to data (bottom). Left: default MC; right: MC after tuning.

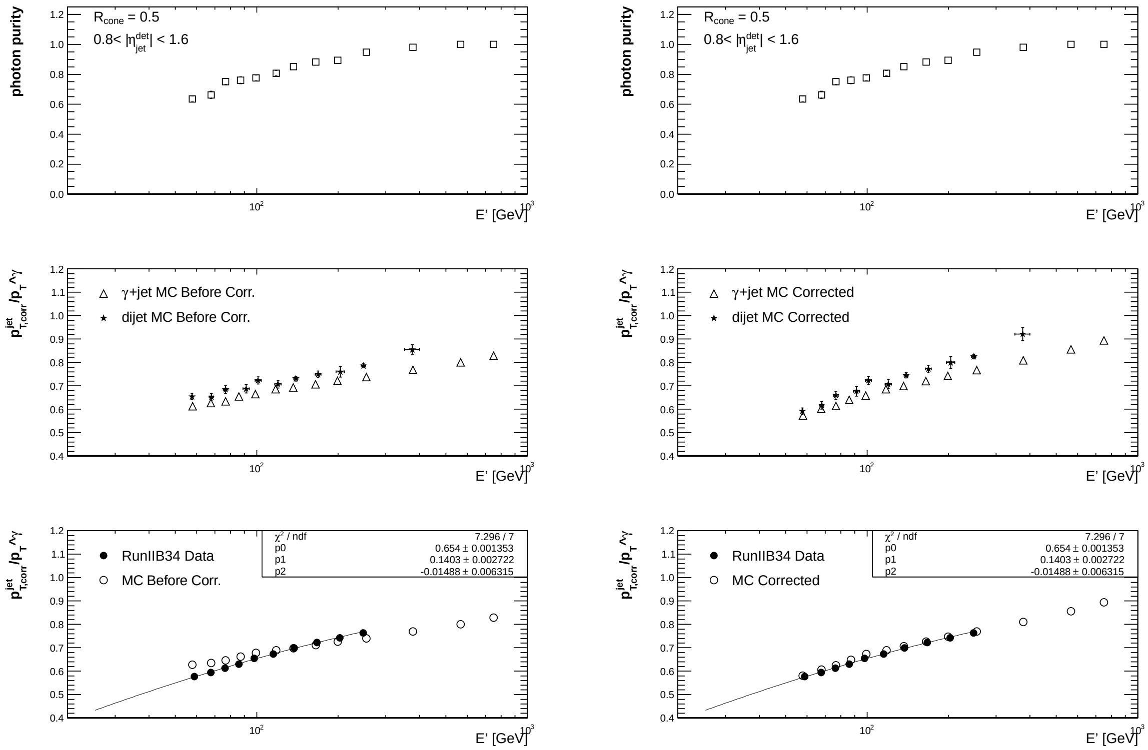

Figure 33: RunIIB34 Closure test for MC tuning to data for tight photon selection with $0.8 < |\eta_{det}^{jet}| < 1.6$. Photon purity (top), γ+jet and di-jets MC responses (middle) and combined γ+jet and di-jets MC response compared to data (bottom). Left: default MC; right: MC after tuning.

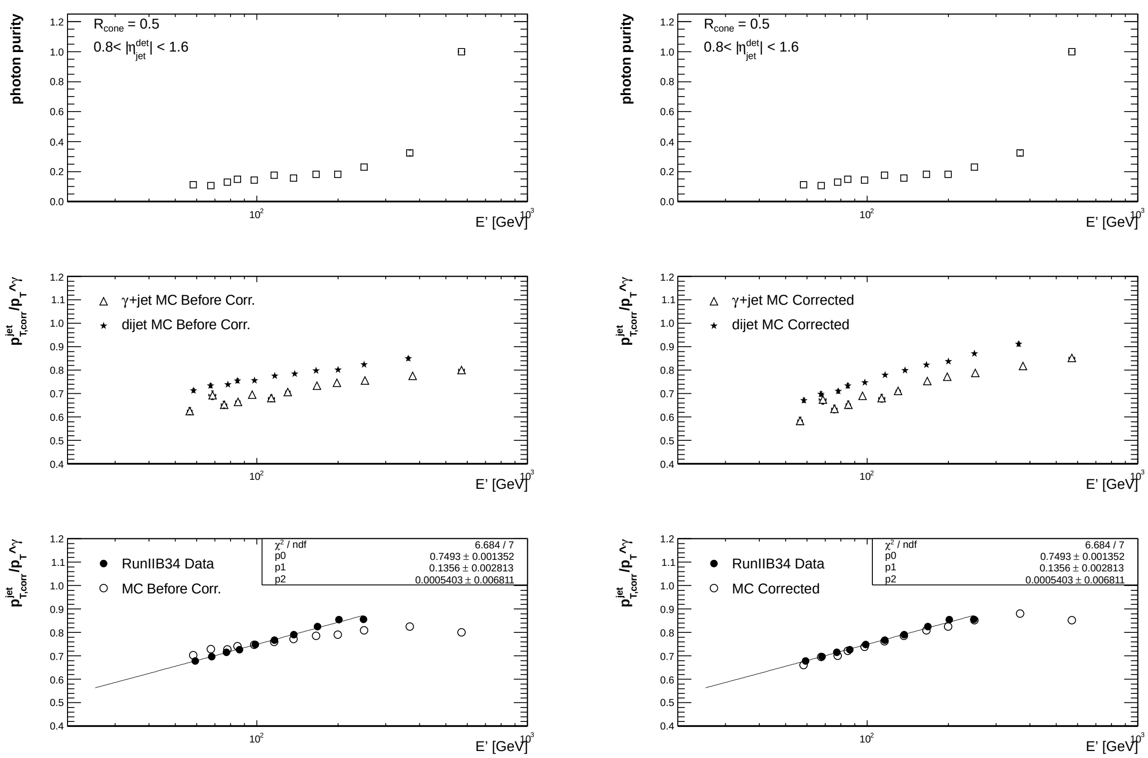

Figure 34: RunIIB34 Closure test for MC tuning to data for reversed photon selection with $0.8 < |\eta_{det}^{jet}| < 1.6$. Photon purity (top), γ+jet and di-jets MC responses (middle) and combined γ+jet and di-jets MC response compared to data (bottom). Left: default MC; right: MC after tuning.

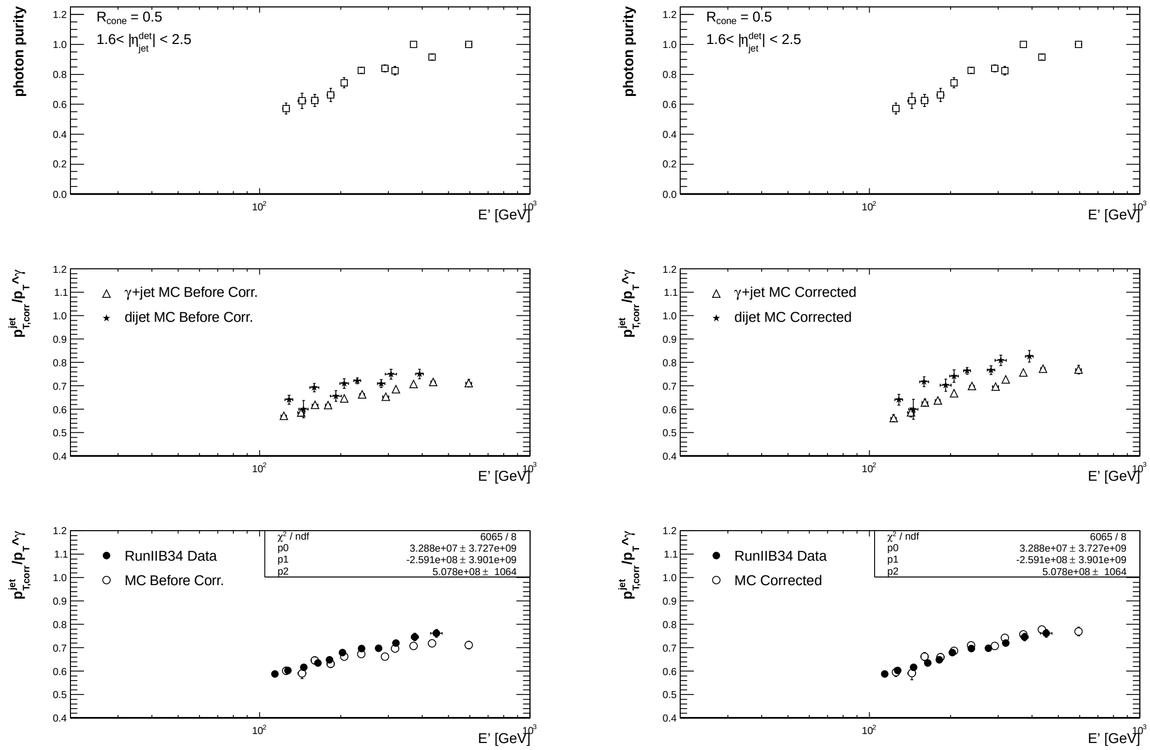

Figure 35: RunIIB34 Closure test for MC tuning to data for tight photon selection with $1.6 < |\eta^{jet}_{det}| < 2.5$. Photon purity (top), γ+jet and di-jets MC responses (middle) and combined γ+jet and di-jets MC response compared to data (bottom). Left: default MC; right: MC after tuning.

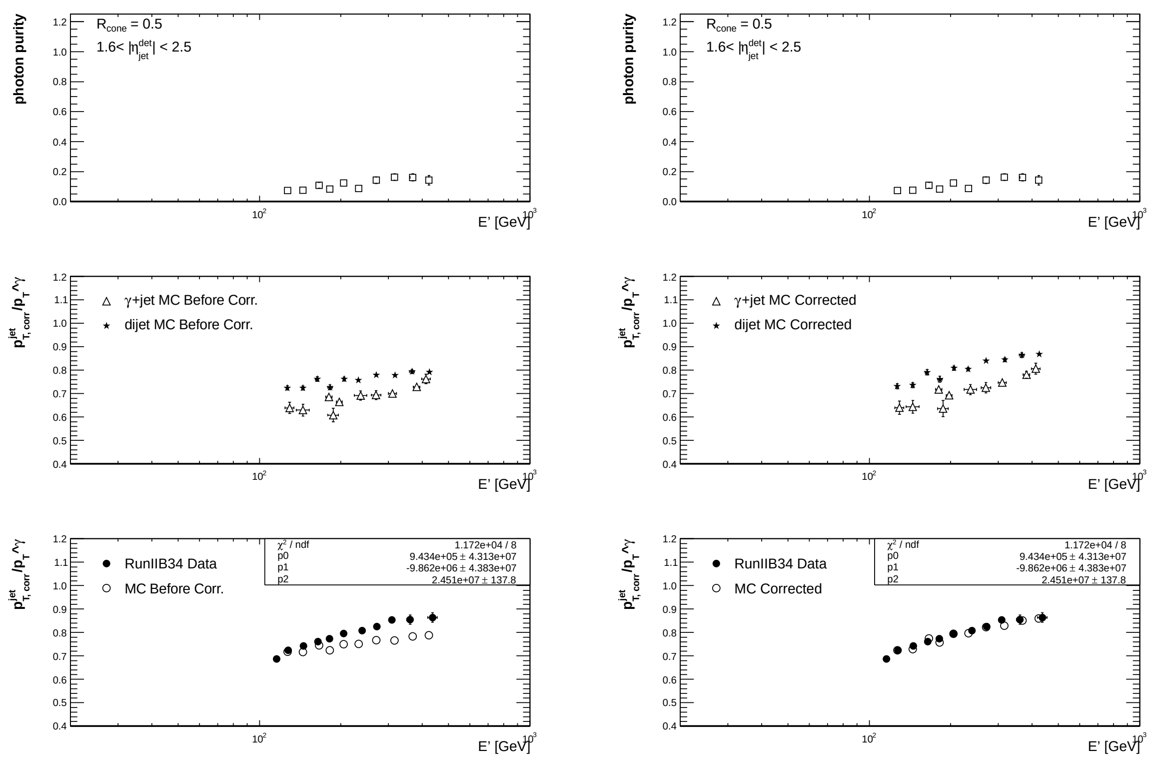

Figure 36: RunIIB34 Closure test for MC tuning to data for reversed photon selection with $1.6 < |\eta^{jet}_{det}| < 2.5$. Photon purity (top), γ+jet and di-jets MC responses (middle) and combined γ+jet and di-jets MC response compared to data (bottom). Left: default MC; right: MC after tuning.

4 MC-Data Correction Factor

Using the results obtained in section 2 and 3, we can calculate the MC-data correction factor F defined in Eq. 1. The results for different run epochs can be seen in Fig. 37-39. The top rows in Fig. 37 and 39 show the correction factor F for different flavors of jets. The 2nd-4th rows show the ratio between F for different flavors of jets and the averaged F for the jets in the γ+jets sample. The ratios presented in the 2nd-4th rows are the same as introduced in Eq. 2 and are used to correct for the MC-data difference in the jet response for different flavors of jets, while at the same time preserves the standard MC JES correction.

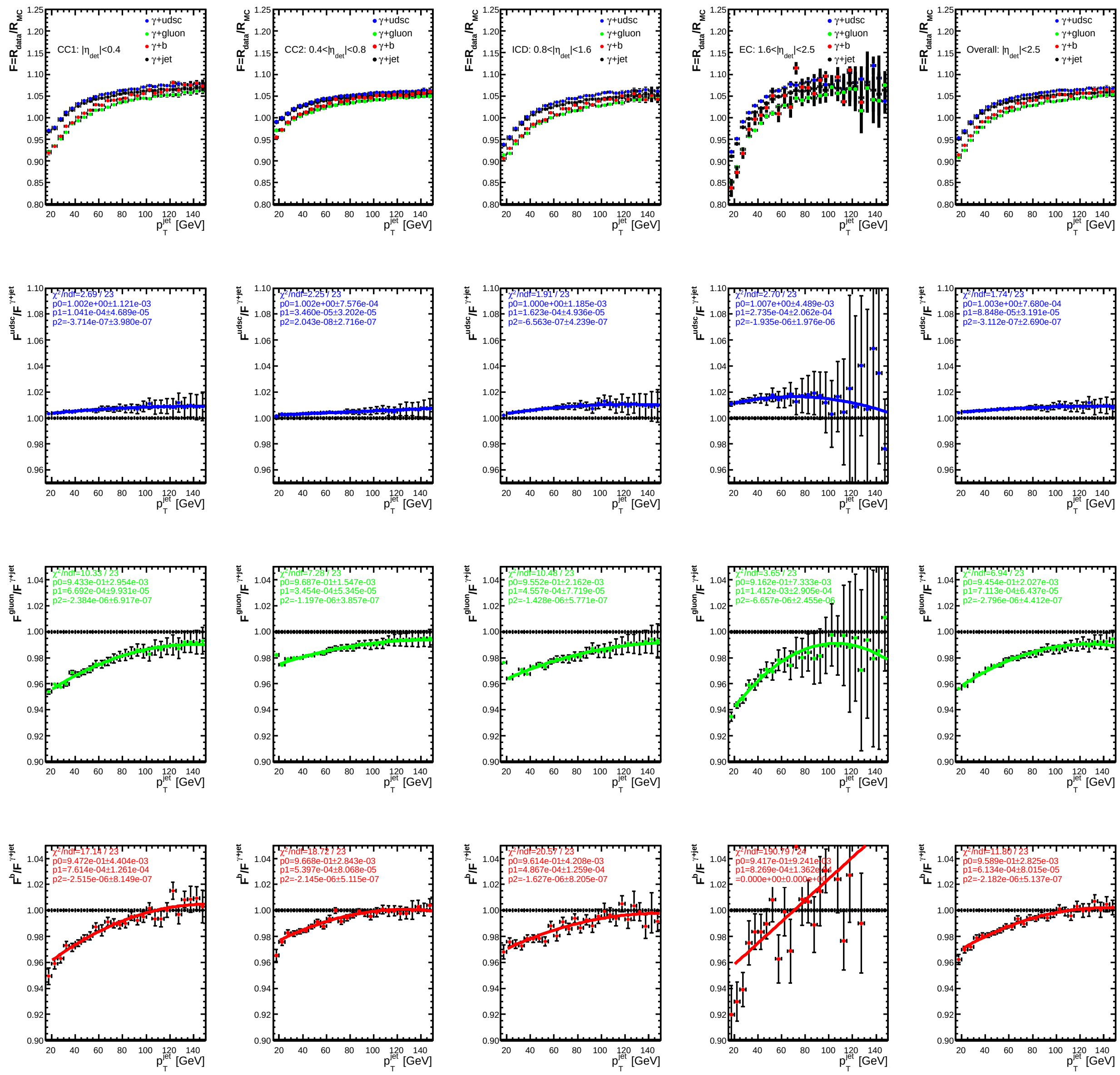

Figure 37: RunIIB1 MC-data correction factor F estimated for jets with different flavors in γ+jet MC samples. The MC single particle responses used here are extracted from the single particle MC samples with ZS turned off. Top: the correction factor F for light flavor quark jets (blue), gluon jets (green), b quark jets (red) and the averaged F for the γ+jets sample (black). The 2nd-4th rows show the ratio between F for different flavors of jets and the averaged F for the γ+jets sample.

5 Uncertainties

5.1 Residual of the MC Closure Test

As shown in section 2, there are residuals in the MC closure test for the MC single particle responses. The effect on the MC-data correction factor F_{corr} is assigned as a systematic uncertainty and is studied as the following. Instead of using the MC single particle responses extracted from the single particle MC samples produced with ZS turned off, we use the MC single particle responses from the single particle MC samples produced with ZS turned on. The MC closure test results from MC single particle responses with ZS turned on are shown in Fig. 54-58. The residuals for the former are larger than the ones for the latter.

Nevertheless, we obtain very similar MC-data correction factor F_{corr} using these MC single particle responses with ZS turned on as with ZS turned off. The difference on F_{corr} between both results is assigned

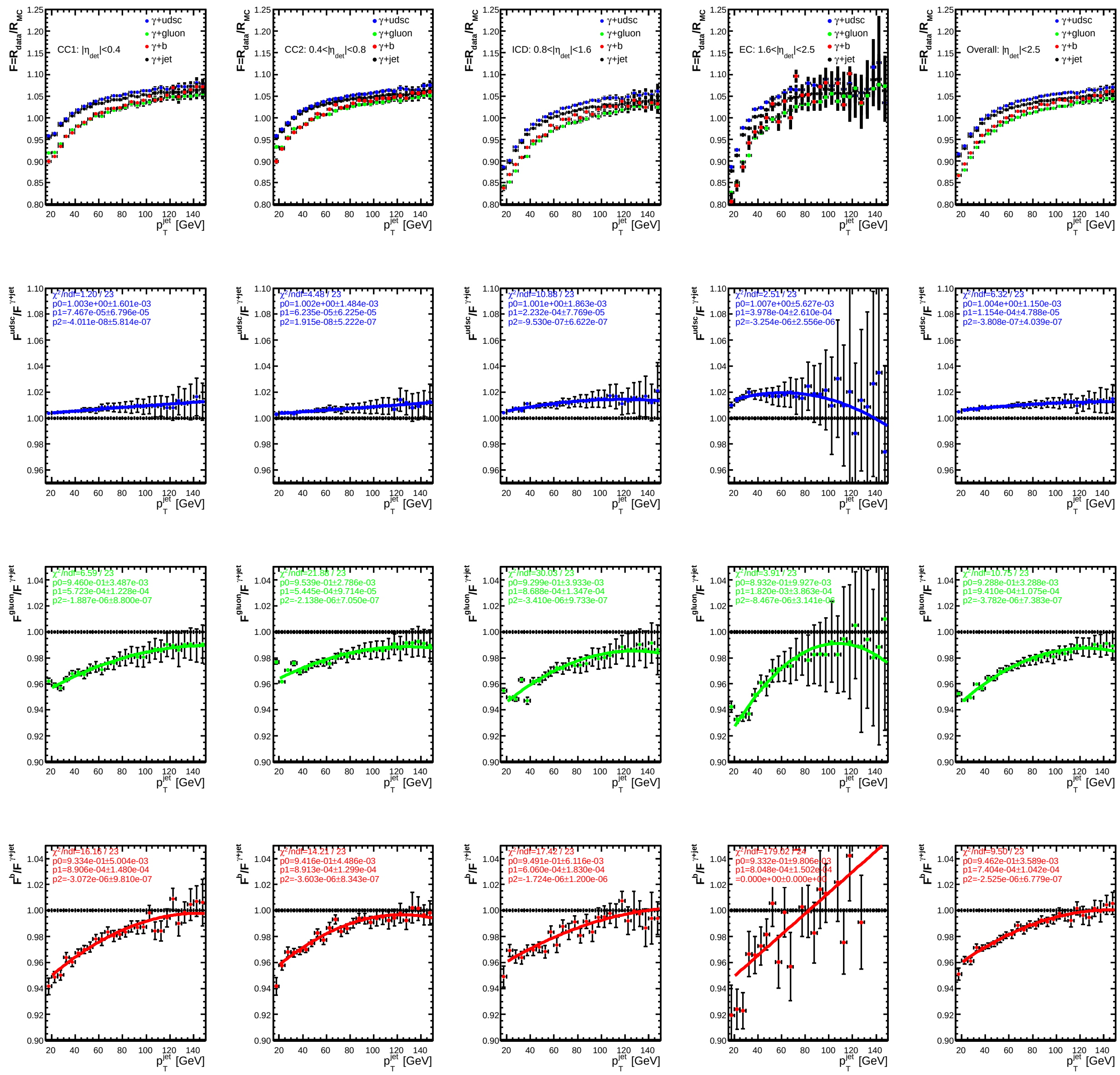

Figure 38: RunIIB2 MC-data correction factor F estimated for jets with different flavors in γ+jet MC samples. The MC single particle responses used here are extracted from the single particle MC samples with ZS turned off. Top: the correction factor F for light flavor quark jets (blue), gluon jets (green), b quark jets (red) and the averaged F for the γ+jets sample (black). The 2nd-4th rows show the ratio between F for different flavors of jets and the averaged F for the γ+jets sample.

as a systematic uncertainty due to the residual seen in the MC closure.

5.2 Electron and Photon Responses in Data

A systematic uncertainty is assigned due to the assumption in Eq. 9-10 as described in section 3, we assume that the MC simulation has the same electron, photon and muon responses as the ones in data. According to [5], the electron energy scale uncertainty is 0.3% by comparing the extracted Z mass in the two electron final state between the data and MC. Since electrons lose more energy in dead material than photons, the electron energy scale corrections effectively "over-correct" the photon energies, so another 0.5% photon-to-electron energy scale uncertainty is also taken into account according to [3]. We use the quadrature of the above two uncertainties as the photon energy scale uncertainty, 0.58%. We repeat the extraction of the single particle

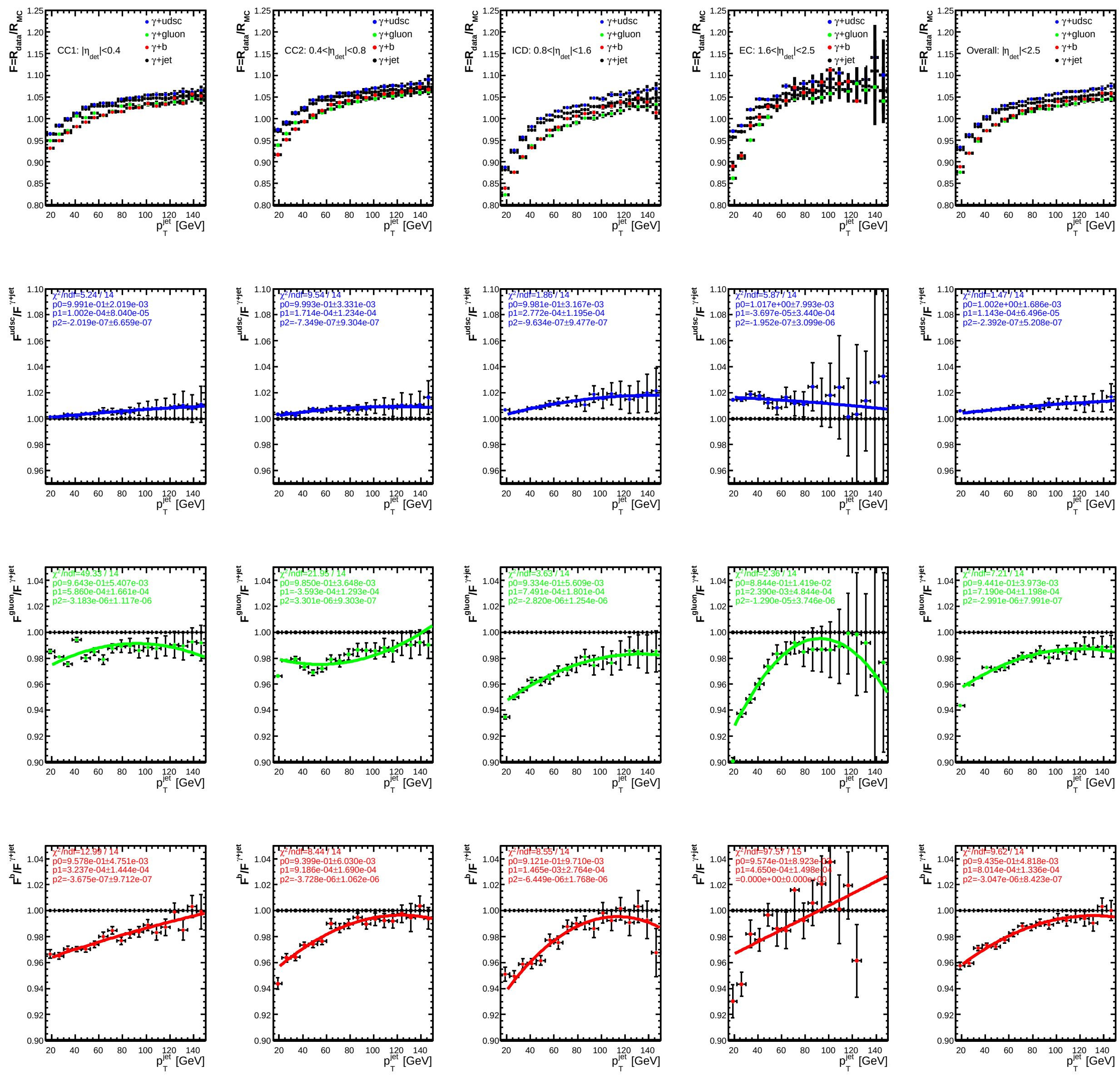

Figure 39: RunIIB34 MC-data correction factor F estimated for jets with different flavors in γ+jet MC samples. The MC single particle responses used here are extracted from the single particle MC samples with ZS turned off. Top: the correction factor F for light flavor quark jets (blue), gluon jets (green), b quark jets (red) and the averaged F for the γ+jets sample (black). The 2nd-4th rows show the ratio between F for different flavors of jets and the averaged F for the γ+jets sample.

data responses as described in section 3 but with:

$$R_{\gamma}^{data} = (1 \pm 0.0058) \cdot R_{\gamma}^{MC}, \quad (13)$$
$$R_{e^{\pm}}^{data} = (1 \pm 0.003) \cdot R_{e^{\pm}}^{MC}, \quad (14)$$

The change in the estimated MC-data correction factor F_{corr} is assigned as a systematic uncertainty.

5.3 Data Single Hadron Responses

The uncertainties on the parameters A, B and C shown in Fig. 7-12 are propagated to the MC-data correction factor F_{corr}.

5.4 Combined Systematic Uncertainty

The total systematic uncertainty is given by the quadrature sum of the above three contributions. The results for the F_{corr} ratios between F for different flavors of jets and the averaged F for the γ+jets sample are shown in Fig. 40-42.

Fig. 43 compare current RunIIB1 result with the previous one in [2]. A significant decrease in systematical uncertainties is observed. We also note that the values for F_{corr} differs in some regions. This may be caused by differences in data used for those plots. In [2], the results were obtained with RunIIB1 and RunIIB2 data, while current result only RunIIB1 data. The MC is RunIIB1 on both results.

6 FMCData processor

The correction factor F_{corr} as presented in Eq. 2 is intended to be used on-the-fly. For such application in analyses processor called FMCData was written. It computes F_{corr} using A, B, C parameters obtained in section 3 and the same algorithm as was used to produce Fig. 37-39. Parameterizations of the F in the γ+jet sample are included in the processor in order to provide the result described as in Eq. 2, which does not implie new MC JES. The processor is now part of the jetcorr package. The correction should be used as described in the text. For each MC jet, the processor runs over the particles in the particle jet and assigns multiplicative correction factor F_{corr} as was describes above. Note that this factor is independent from other multiplicative standard JES MC corrections. Similarly like other corrections this processor writes the result to TMBJet, where can be obtained for usage.

Currently supported algorithm by the processor is only JCCB jets. The processor includes results from [1] and from this note, so all DØ RunII epochs (A, B1, B2, B3, B4) are supported.

The systematical and statistical uncertainties as shown in Fig. 40-42 are also part of the processor and are assigned to the jet same way as the correction factor itself. The uncertainty is determined by jet energy and by flavor of the initial parton. To use the flavor of the jet one needs to run processor TagJetInitialParton first to provide information about the parton that initiated the jet. Config example can be found in `jes_tools/config/DumpJES.config` or in this note's Appendix D

7 Conclusion

Using the same method presented in [1] and [2], we extract final results on how to correct for the MC-data difference in the jet response for all available Run IIB MC and data JCCB jets. As an update to [2] we present improved results with significantly smaller uncertainties and results for all run epoch. Results for correction factor F_{corr} RunIIB1 - RunIIB3 MC and RunIIB1 - RunIIB4 data were presented, systematic and statistical uncertainties are taken into account. The processor, that computes the correction factor on-the-fly, is described in this note and is ready for use in analyses. It supports JCCB jets and all RunIIA and RunIIB (1-4) epochs.

Acknowledgments

We thank Georgy Golovanov, Peter Renkel, Jan Stark, Peter Svoisky and many others for their valuable suggestions and help.

References

[1] S. Atkins et al., Correction for the MC-Data Difference in the Jet response at DØ, DØ note 6143.

[2] S. Atkins et al., Correction for the MC-Data Difference in the Jet response at DØfor Run IIB, DØ note 6144.

[3] Jet Energy Scale Determination for DØ Run IIb, DØ note 6327.

[4] K. Peters, Calorimeter: performance and future plans, talk in the D0reco meeting on March 7, 2007. J. Stark, EM calorimeter: Eta-Equalisation and Absolute Scale, talk in the DØ collaboration meeting on December 6, 2006.

[5] X. Bu et al., DØ Note 5846.

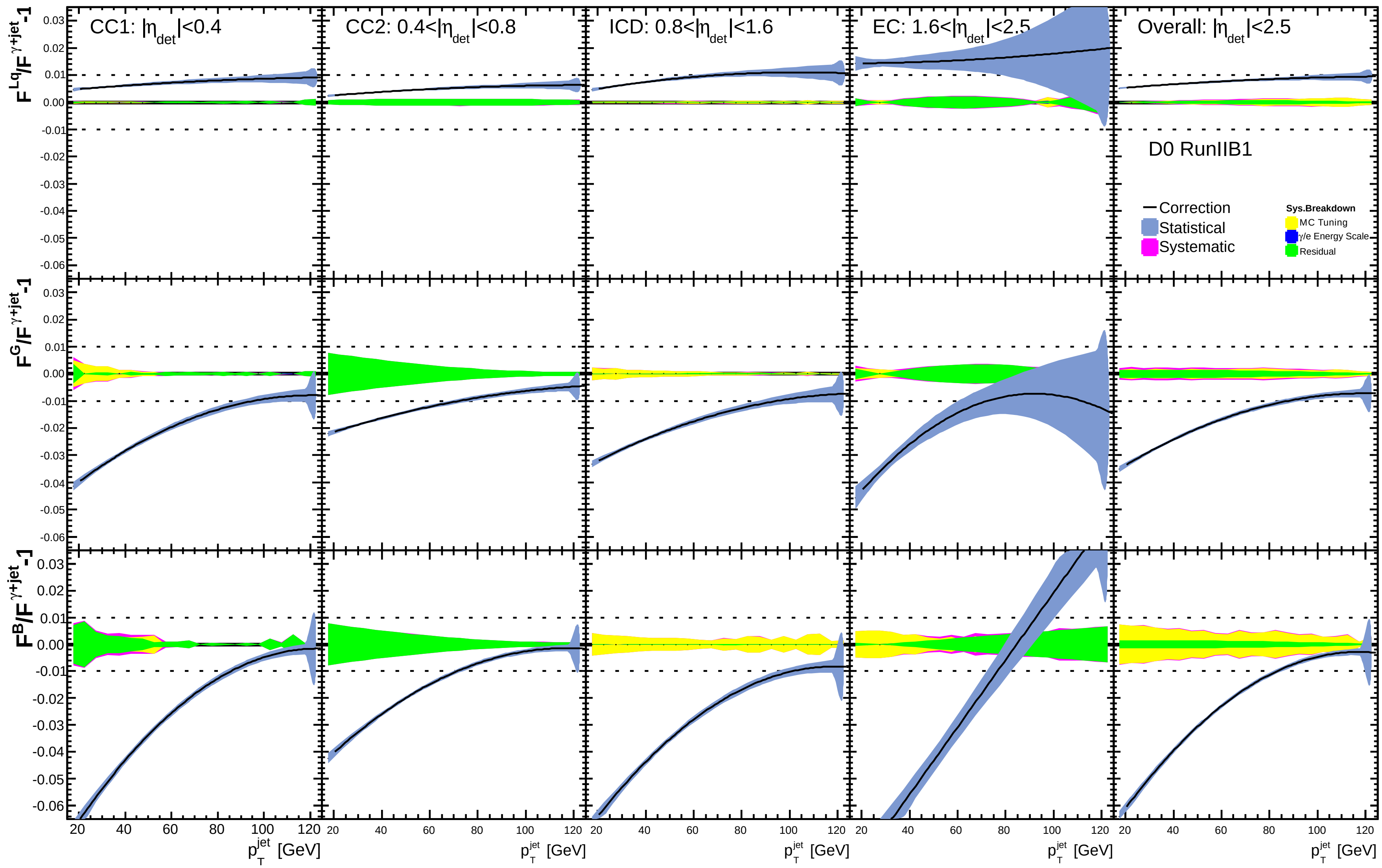

Figure 40: Correction factor for MC-data difference in the jet response for different flavors of jets for RunIIB1. They are given by the ratios between F for different flavors of jets and the averaged F for the γ+jets sample.

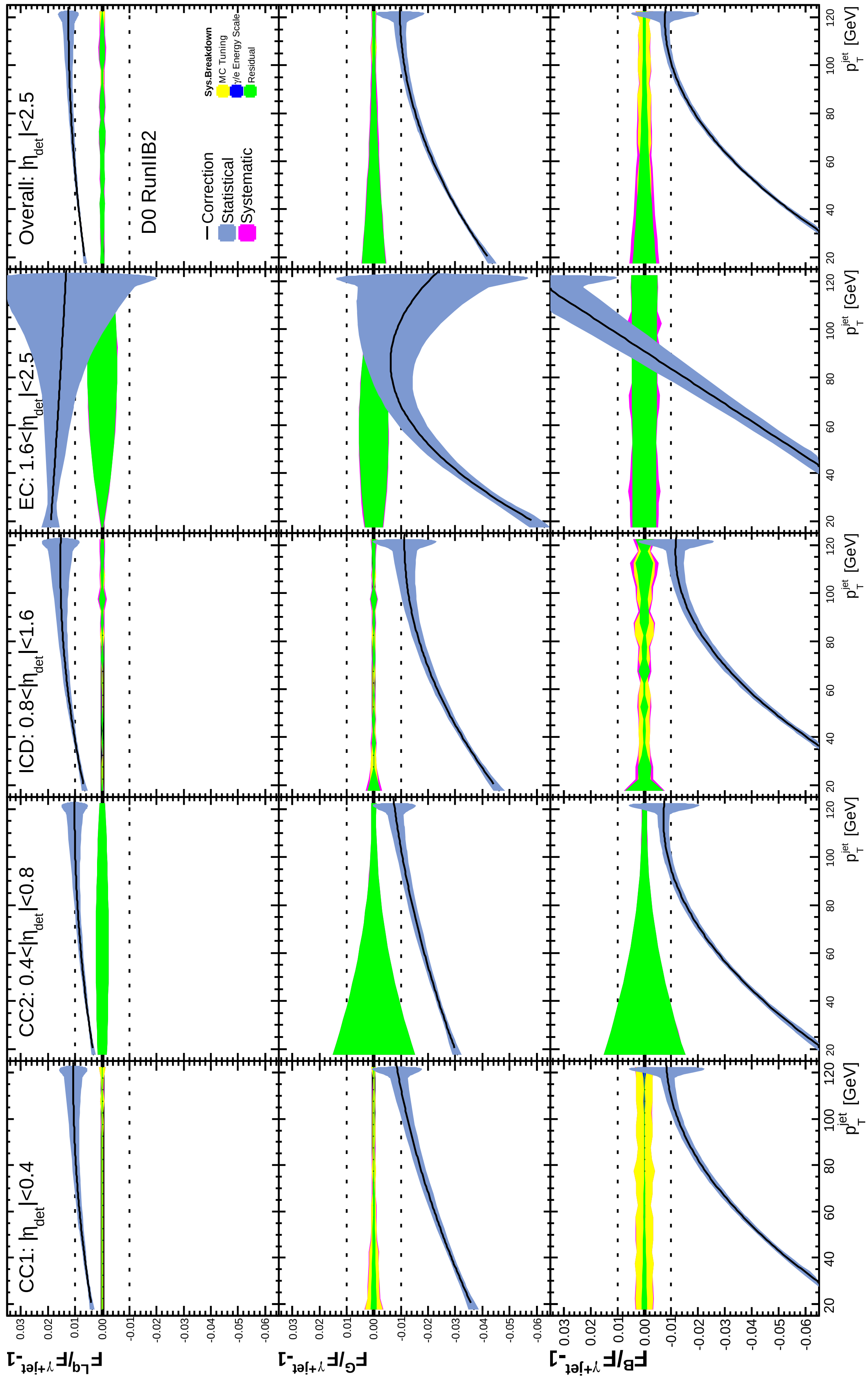

Figure 41: Correction factor for MC-data difference in the jet response for different flavors of jets for RunIIB2. They are given by the ratios between F for different flavors of jets and the averaged F for the γ+jets sample.

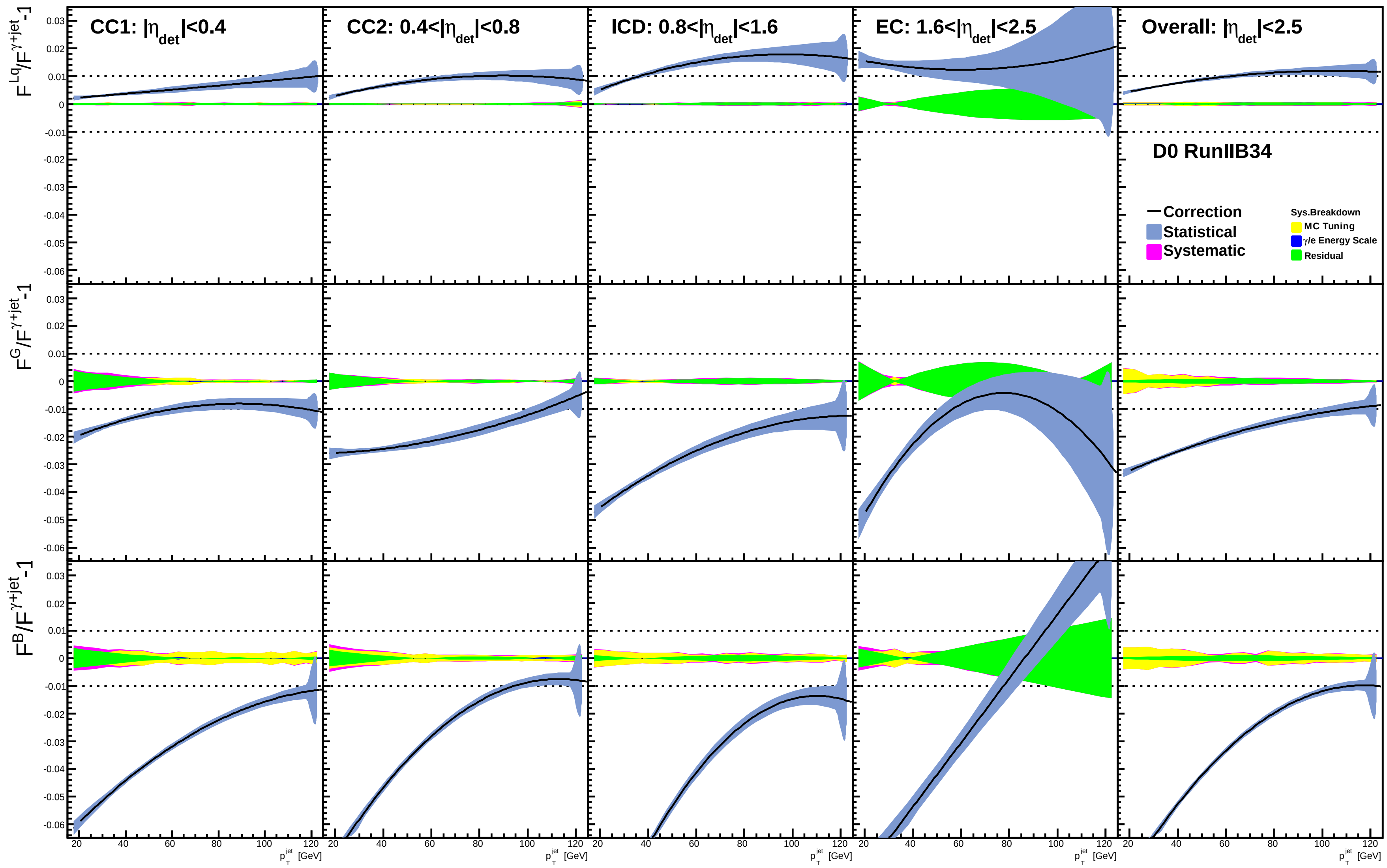

Figure 42: Correction factor for MC-data difference in the jet response for different flavors of jets for RunIIB34. They are given by the ratios between F for different flavors of jets and the averaged F for the γ+jets sample.

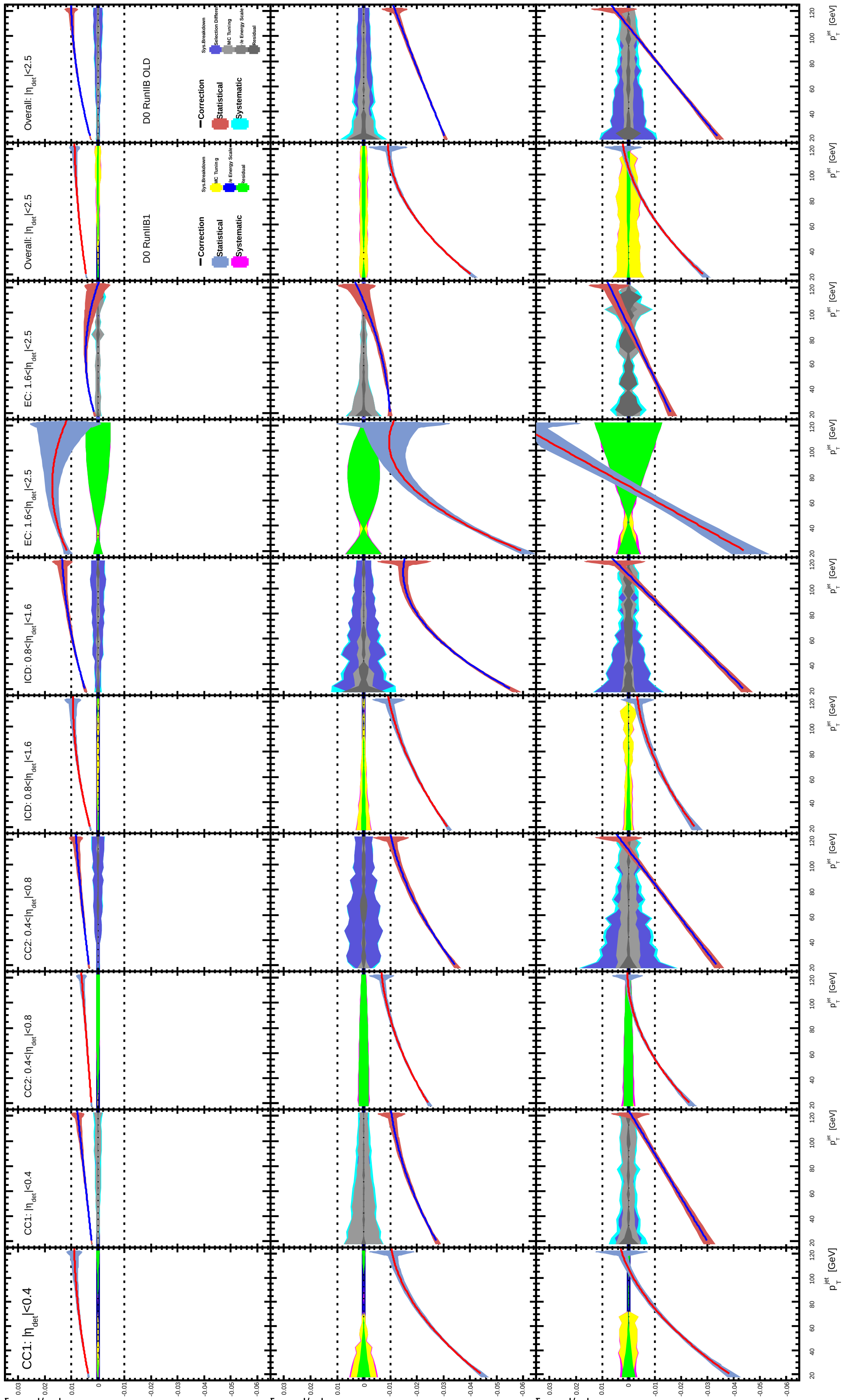

Figure 43: Comparison of the correction factor for MC-data difference in the jet response for different flavors of jets from [2] and from this note 40. Frame by frame left is from this note and right (OLD) is the previous result from [2].

A MC Single Particle Responses From Single Particle MC Samples Produced With Zero Suppression Turned Off

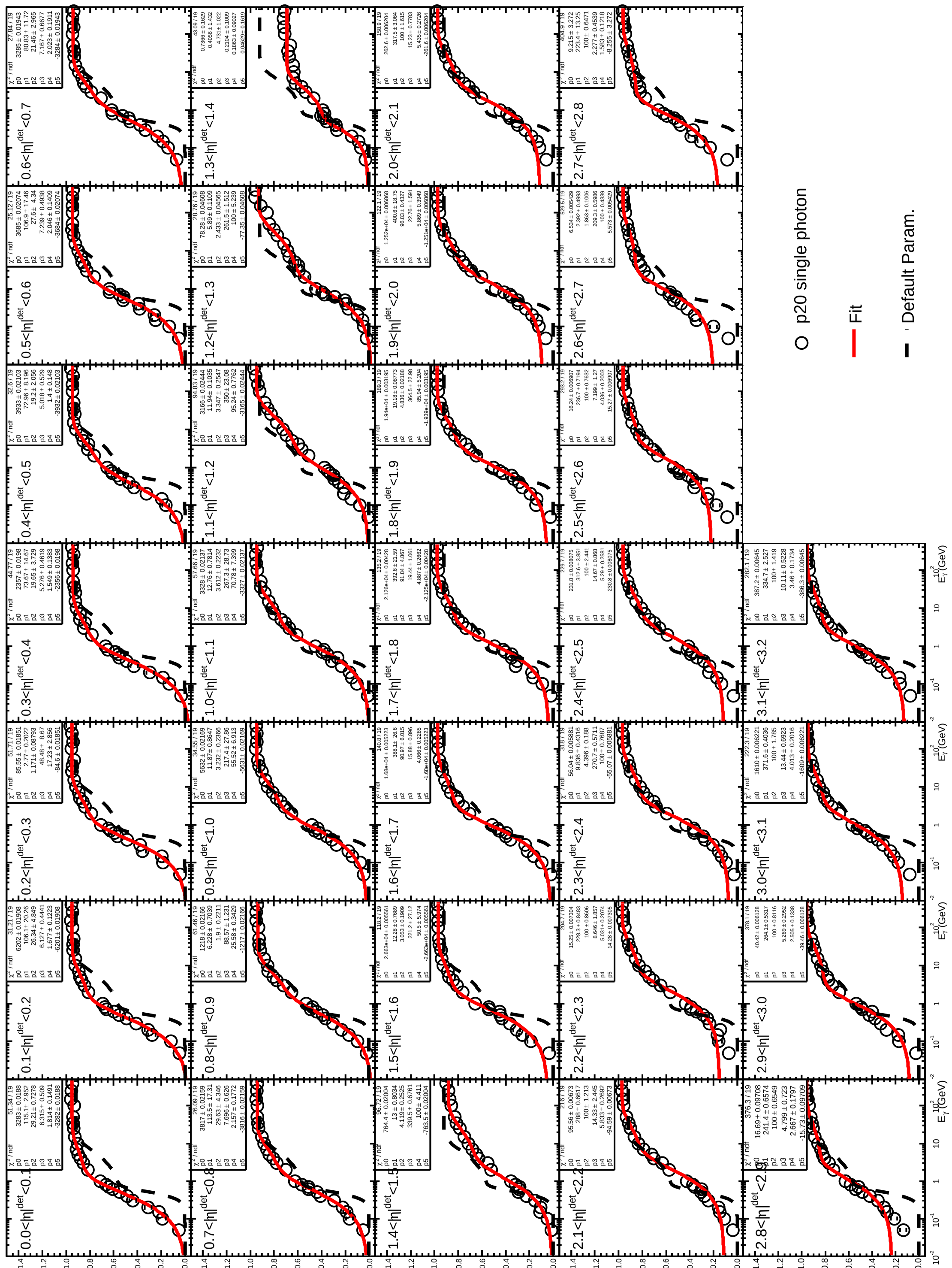

Figure 44: MC single photon response from Run IIB single γ MC sample, produced without ZS, calorimeter noise or ZB overlay. The black dashed line corresponds to the single photon response from Run IIA W mass studies. The red line is a fit to the MC points in black circles.

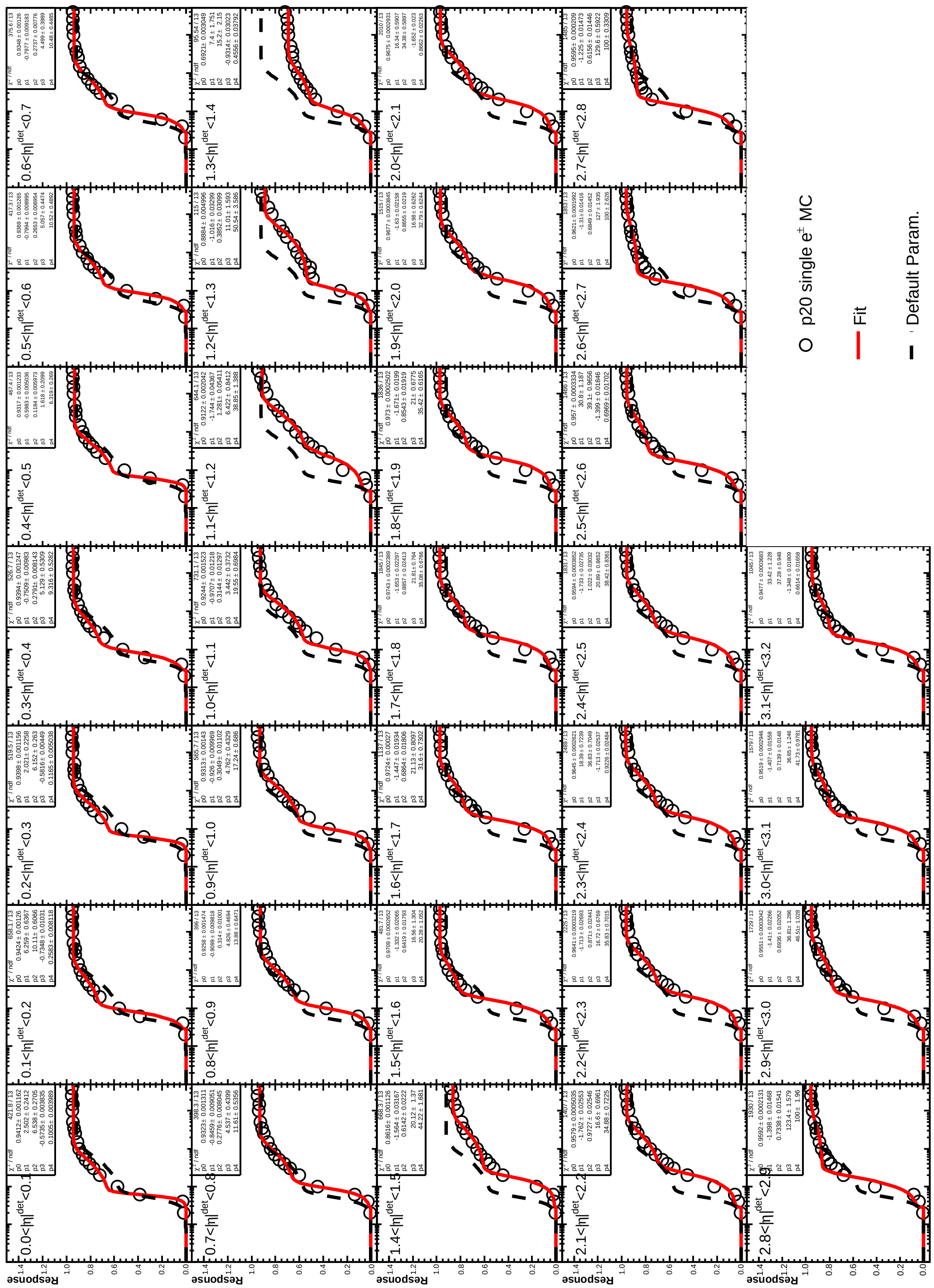

Figure 45: MC single electron response from Run IIB single $e^{\pm}$ MC sample, produced without ZS, calorimeter noise or ZB overlay. The black dashed line corresponds to the single electron response from Run IIA W mass studies. The red line is a fit to the MC points in black circles.

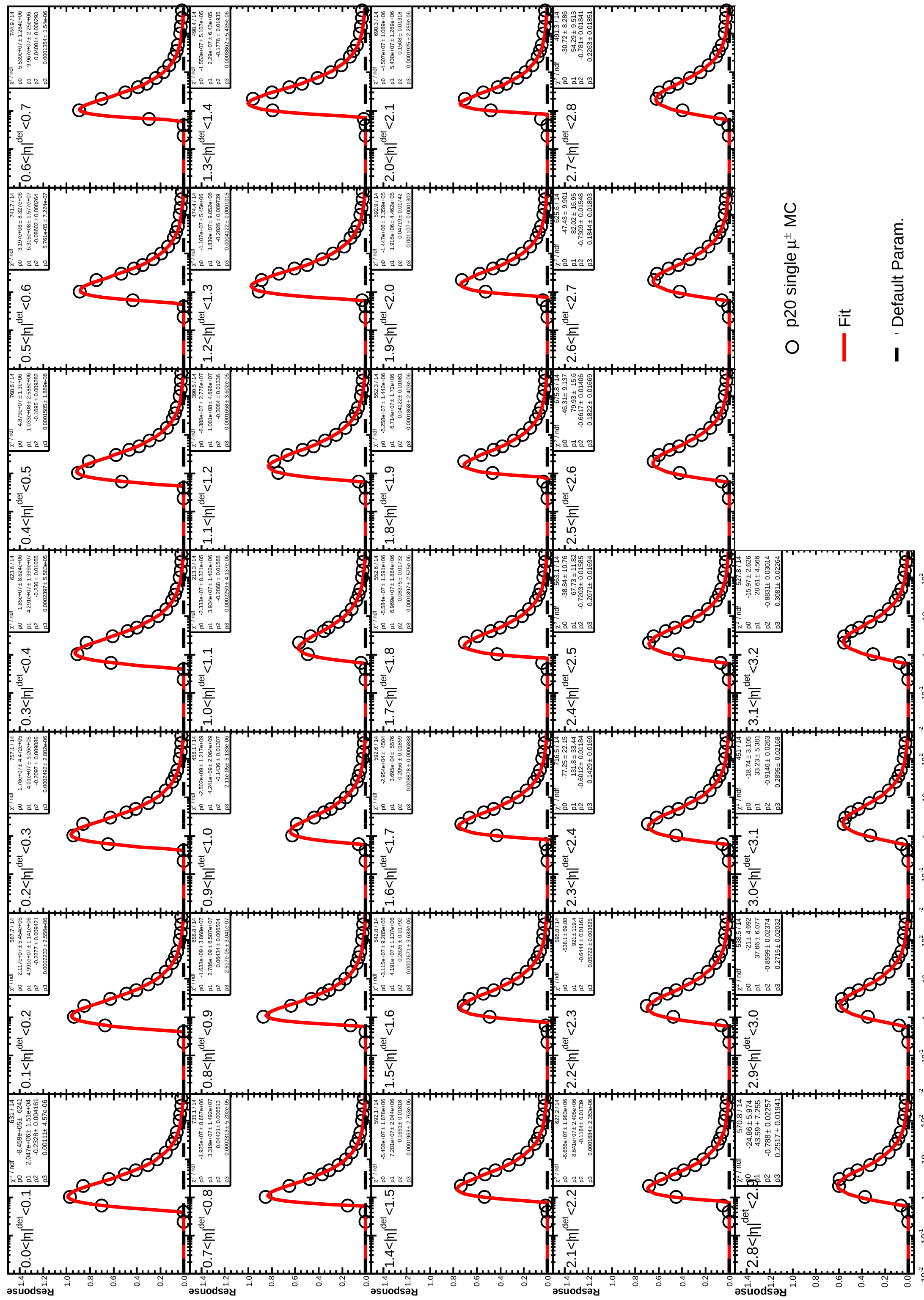

Figure 46: MC single electron response from Run IIB single $\mu^{\pm}$ MC sample, produced without ZS, calorimeter noise or ZB overlay. The black dashed line corresponds to 0. The red line is a fit to the MC points in black circles.

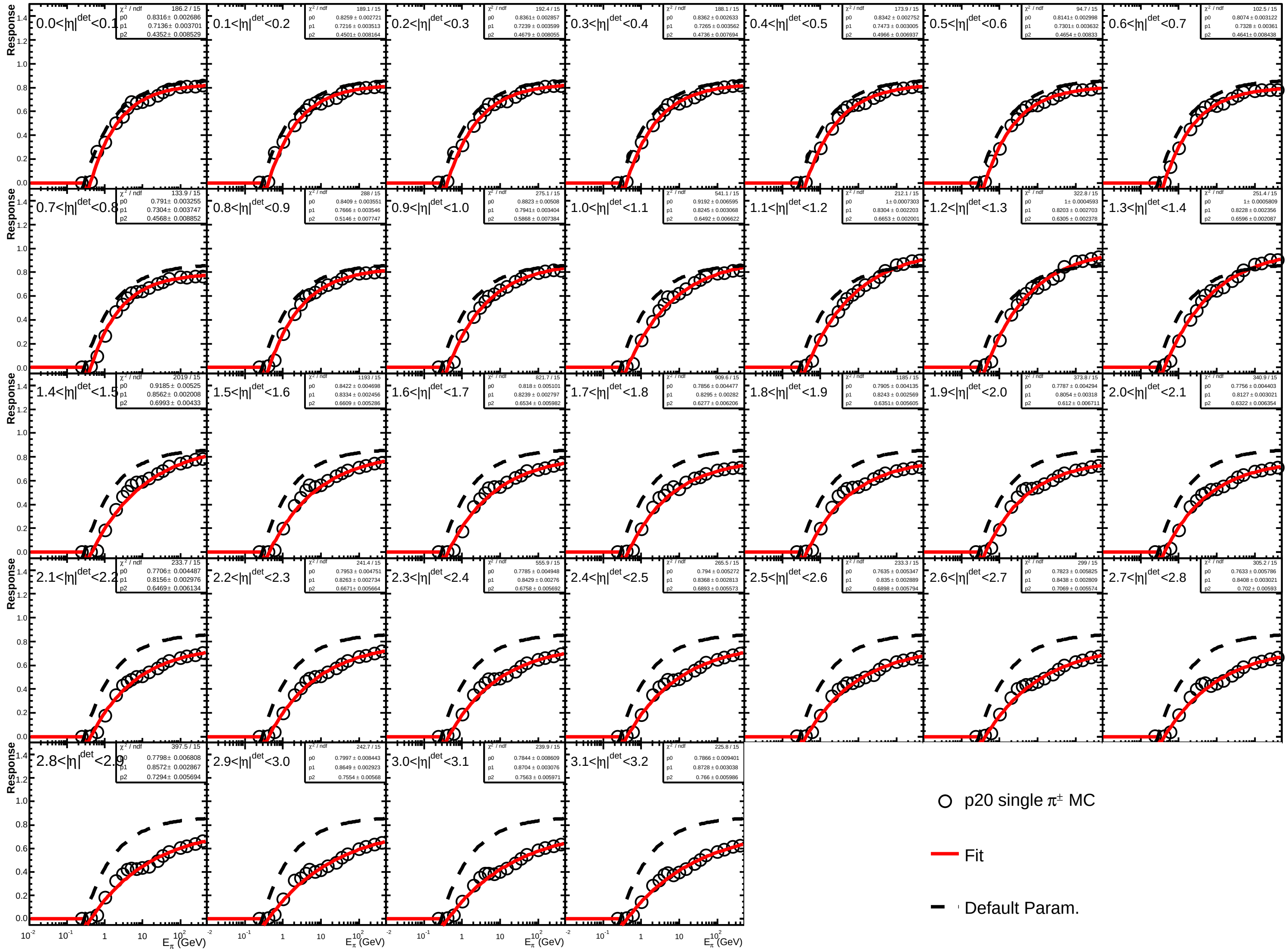

Figure 47: MC single pion response from Run IIB single $\pi^{\pm}$ MC sample, produced without ZS, calorimeter noise or ZB overlay. The black dashed line corresponds to the single pion response from Run IIA JES studies. The red line is a fit to the MC points in black circles.

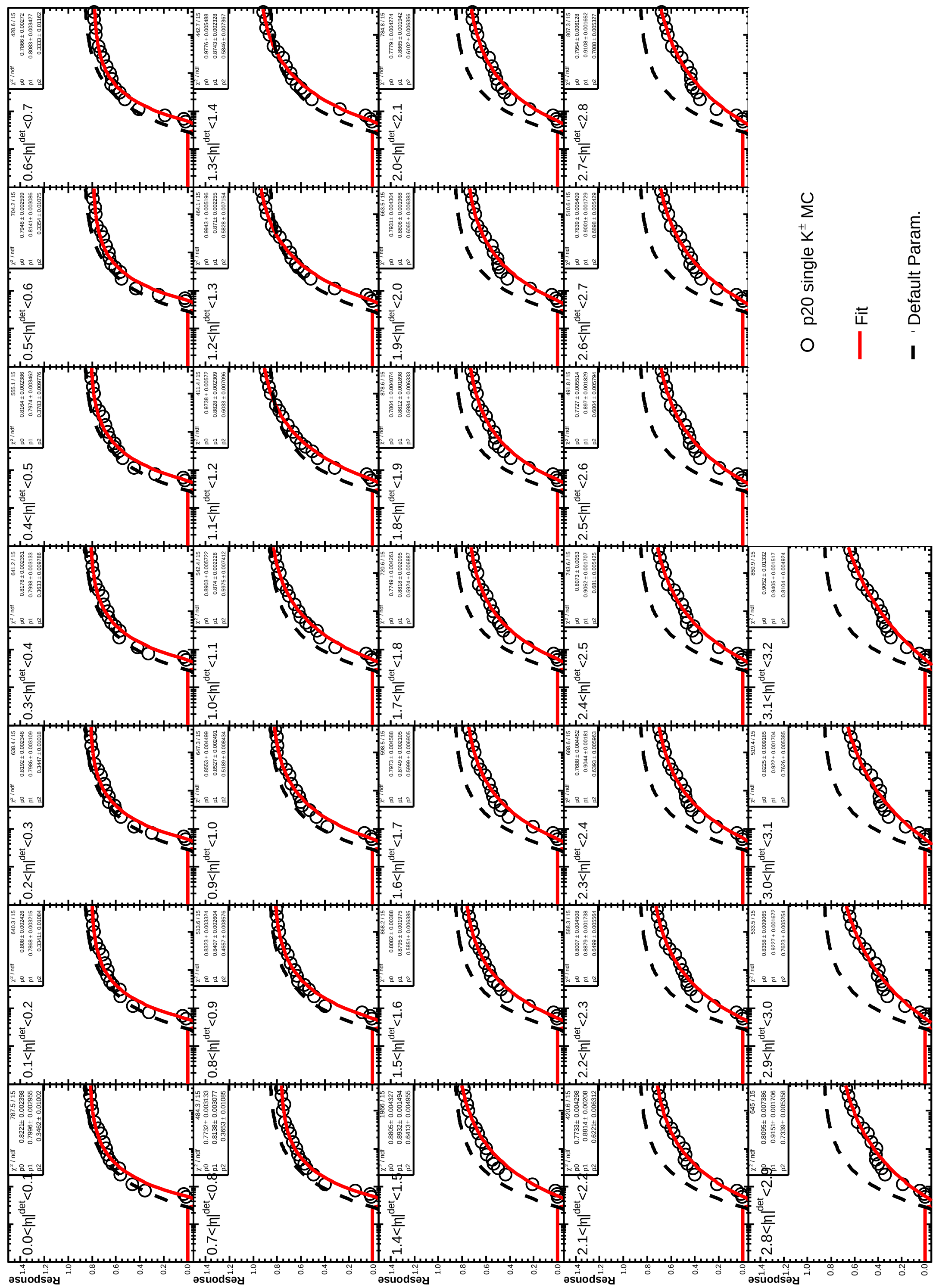

Figure 48: MC single kaon response from Run IIB single $K^{\pm}$ MC sample, produced without ZS, calorimeter noise or ZB overlay. The black dashed line corresponds to the single pion response from Run IIA JES studies. The red line is a fit to the MC points in black circles.

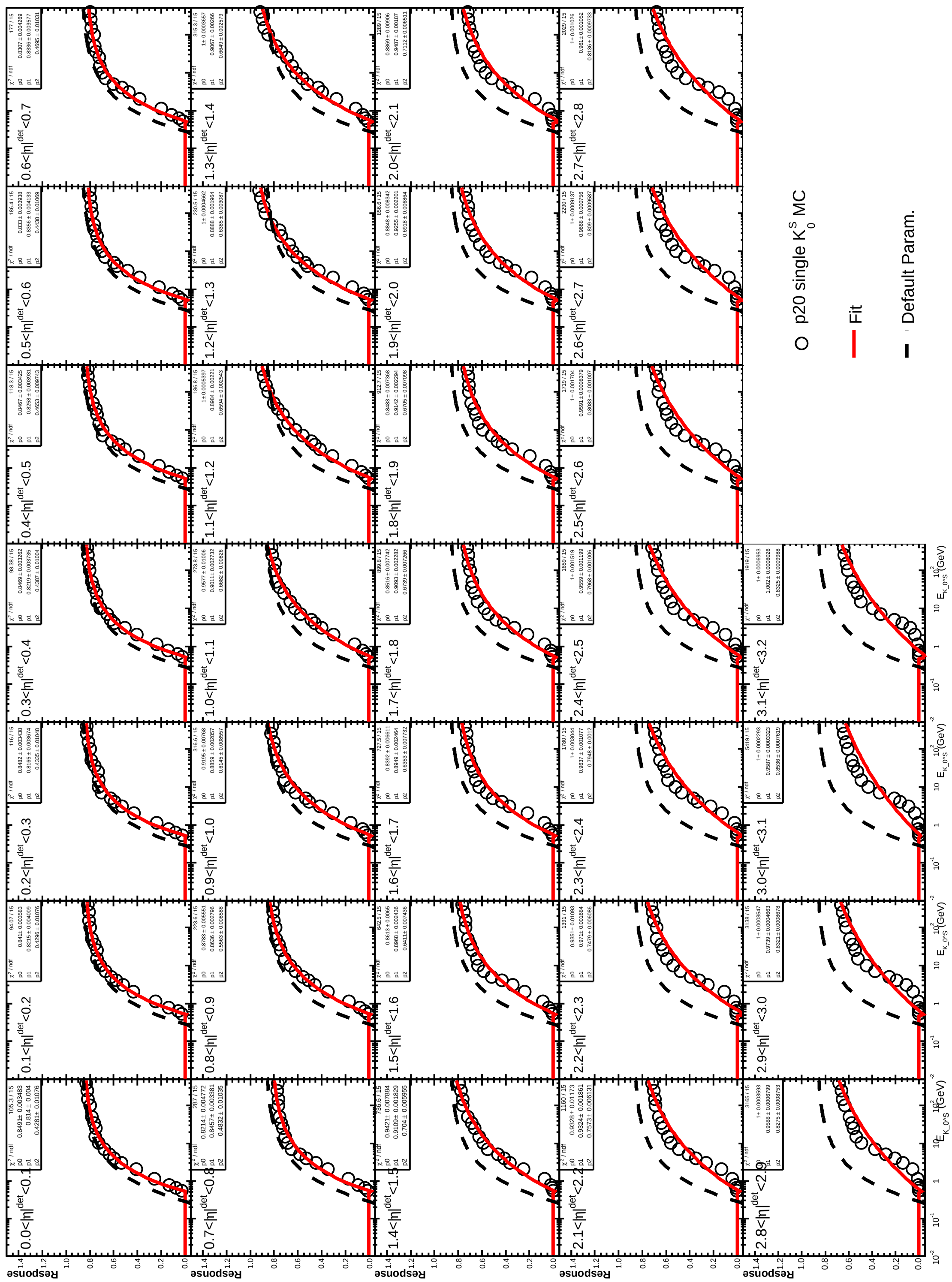

Figure 49: MC single kaon response from Run IIB single K_0^S MC sample, produced without ZS, calorimeter noise or ZB overlay. The black dashed line corresponds to the single pion response from Run IIA JES studies. The red line is a fit to the MC points in black circles.

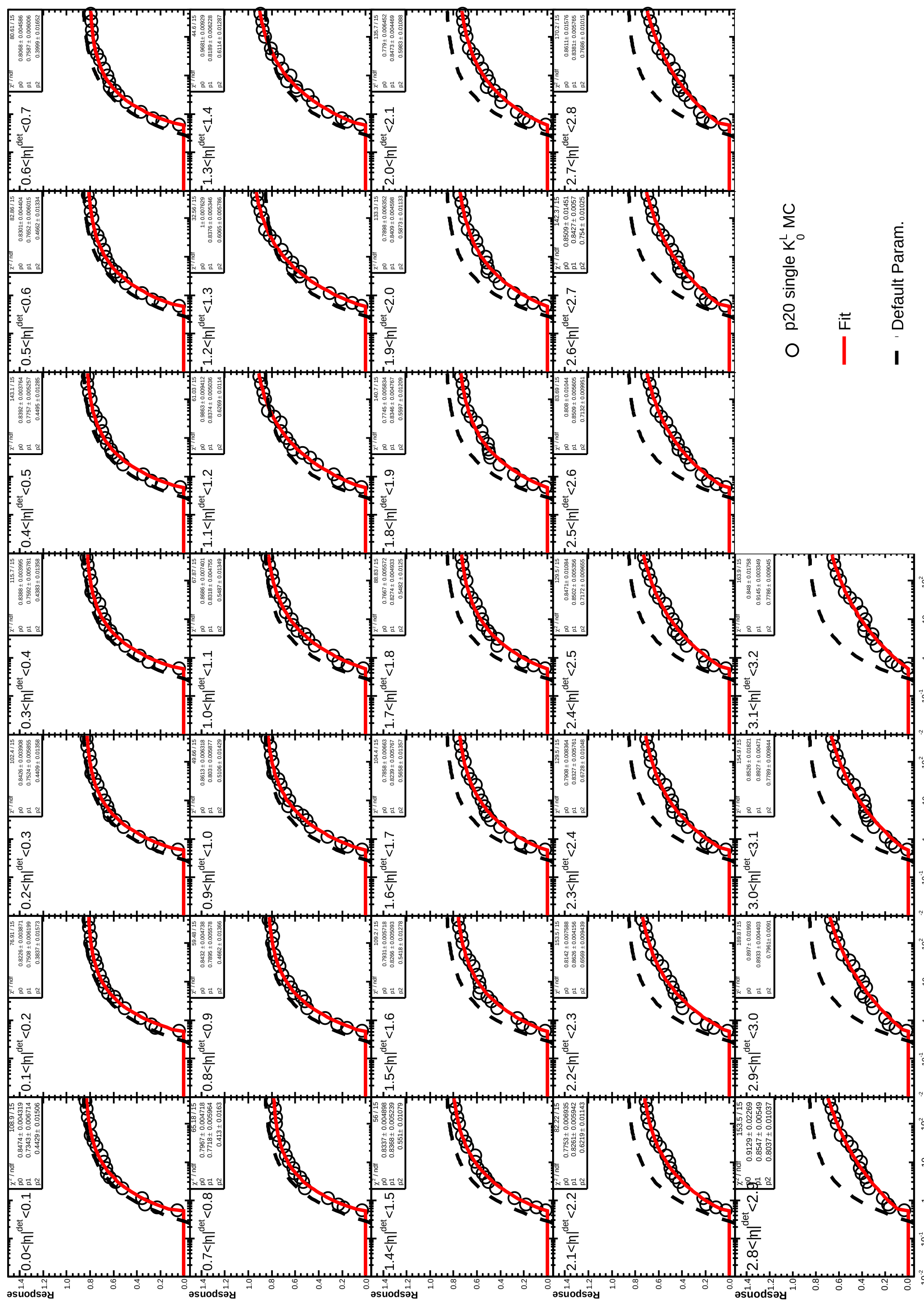

Figure 50: MC single kaon response from Run IIB single K_0^L MC sample, produced without ZS, calorimeter noise or ZB overlay. The black dashed line corresponds to the single pion response from Run IIA JES studies. The red line is a fit to the MC points in black circles.

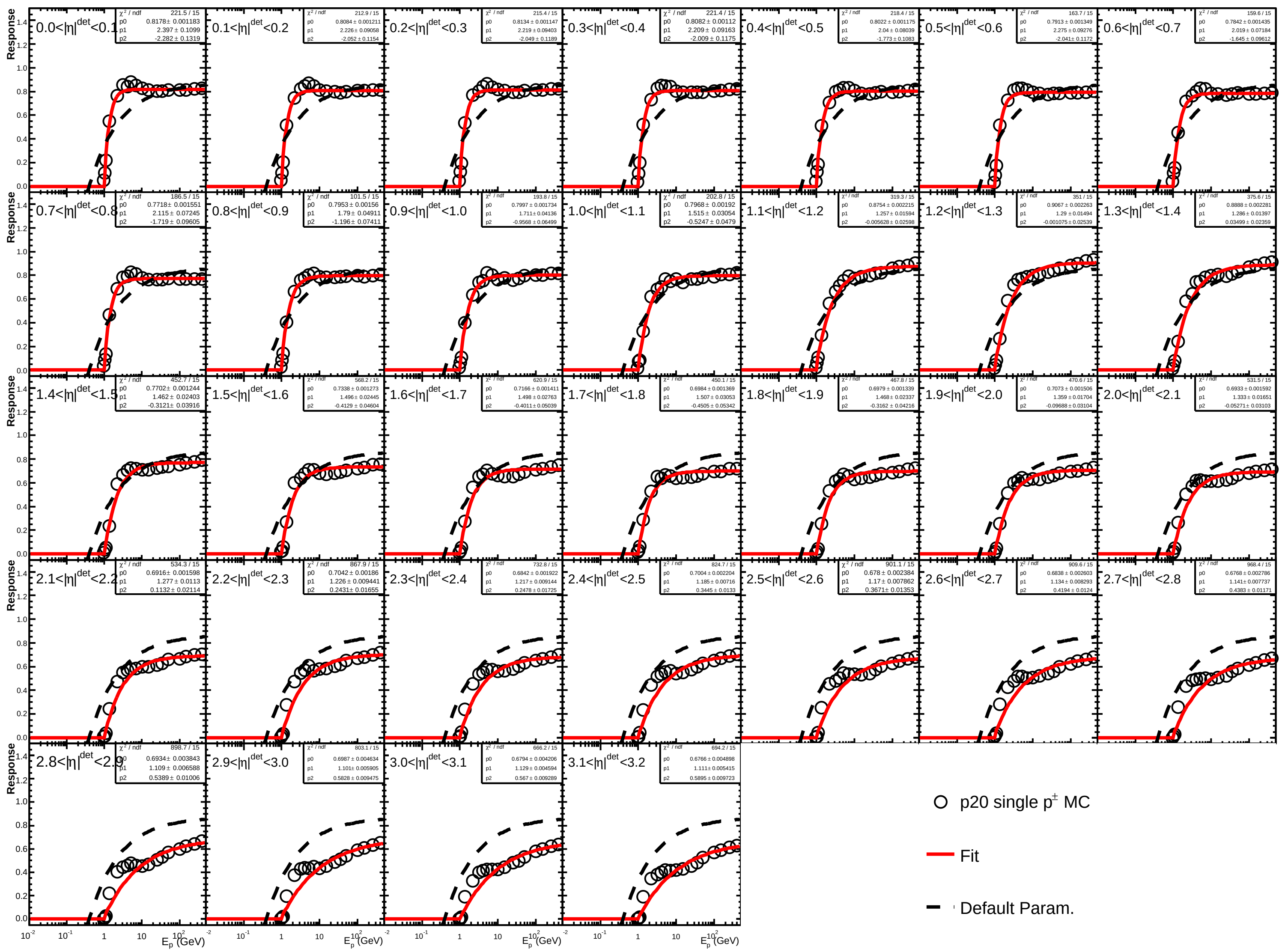

Figure 51: MC single proton response from Run IIB single $p^{\pm}$ MC sample, produced without ZS, calorimeter noise or ZB overlay. The black dashed line corresponds to the single proton response from Run IIA JES studies. The red line is a fit to the MC points in black circles.

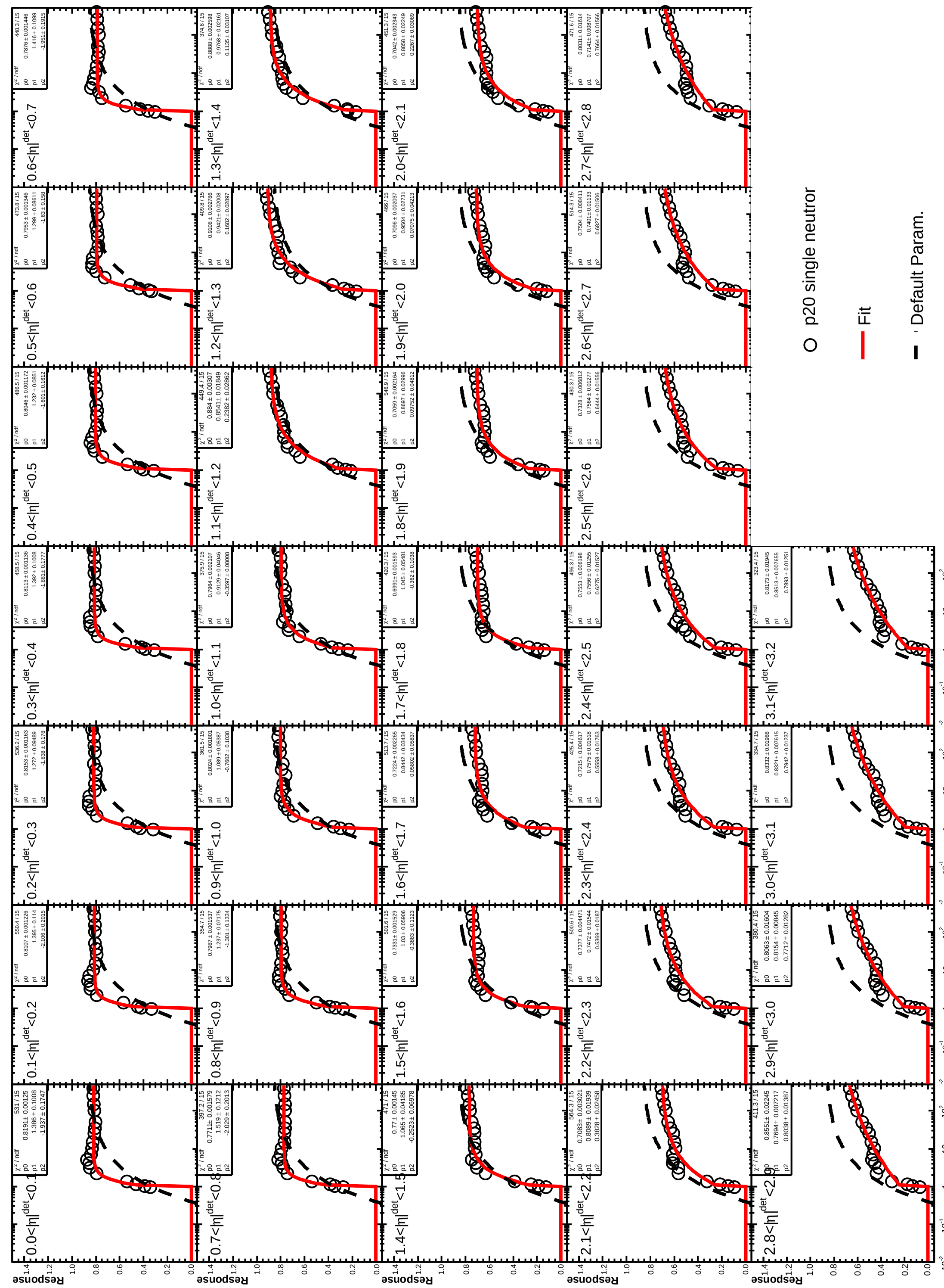

Figure 52: MC single proton response from Run IIB single n MC sample, produced without ZS, calorimeter noise or ZB overlay. The black dashed line corresponds to the single proton response from Run IIA JES studies. The red line is a fit to the MC points in black circles.

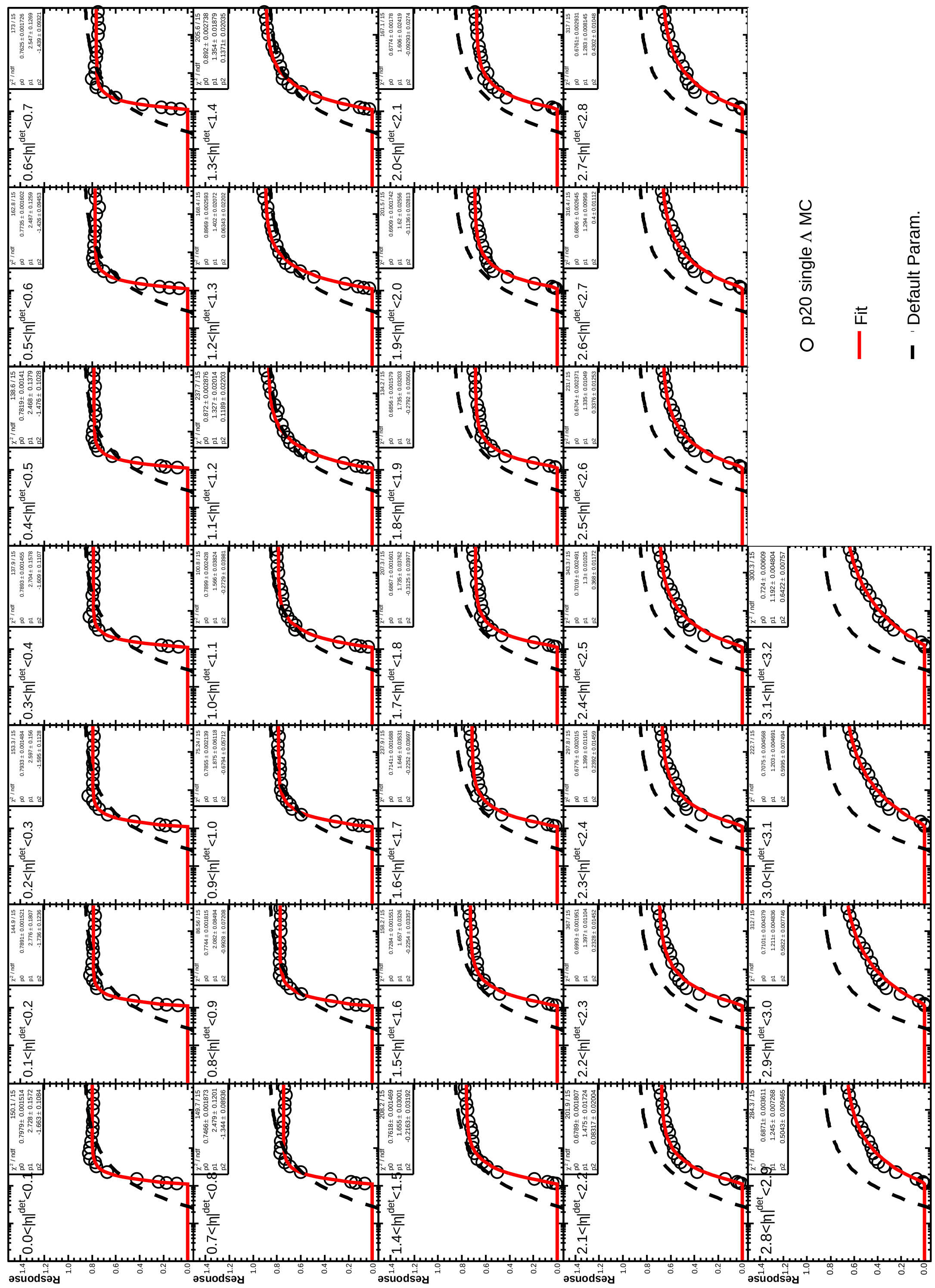

Figure 53: MC single proton response from Run IIB single Λ MC sample, produced without ZS, calorimeter noise or ZB overlay. The black dashed line corresponds to the single pion response from Run IIA JES studies. The red line is a fit to the MC points in black circles.

B MC single particle responses with ZS turned on

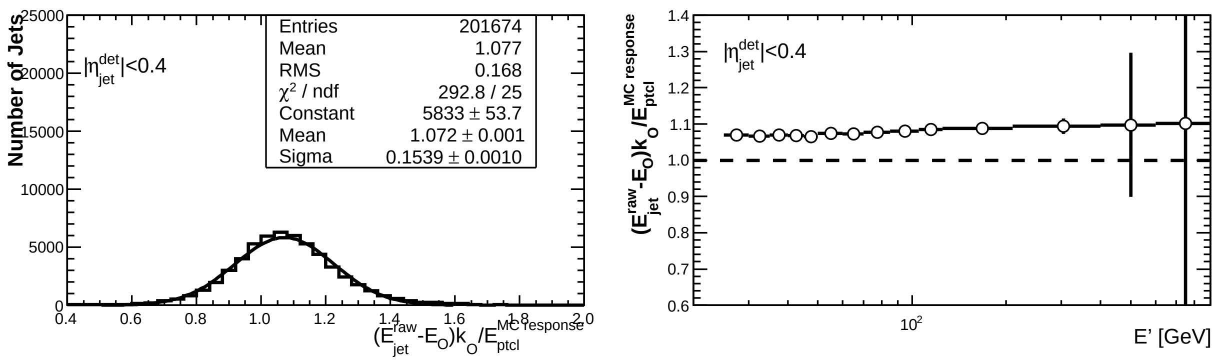

Figure 54: MC closure test for jets in p20 γ+jet MC sample produced without ZB overlay for $|\eta_{det}^{jet}| < 0.4$. The single particle MC responses are derived with ZS turned on. The x-axis E' is given by $p_T^{\gamma} \cdot cosh(\eta^{jet})$. The error bars on y corresponds to the standard deviation of $y = E_{jet}^{raw} / \sum_i E_i \cdot R_i^{MC}$ in each bin.

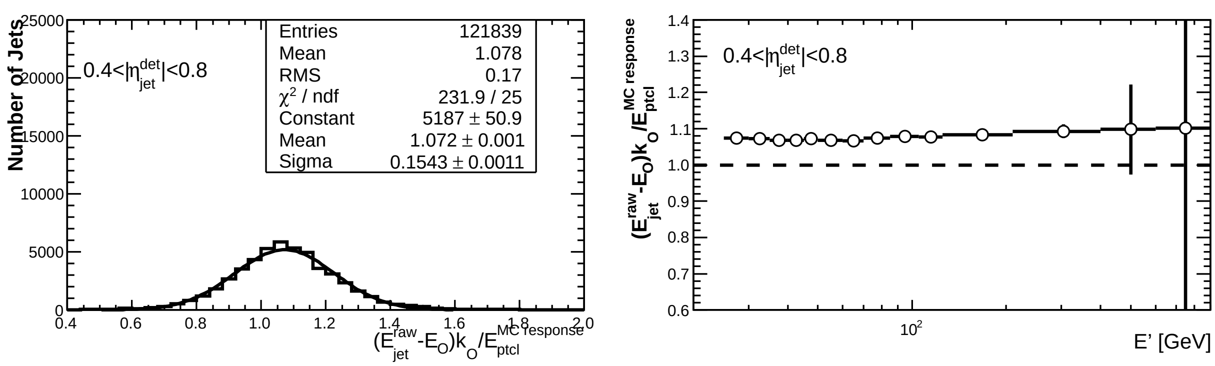

Figure 55: MC closure test for jets in p20 γ+jet MC sample produced without ZB overlay for $0.4 < |\eta_{det}^{jet}| < 0.8$. The single particle MC responses are derived with ZS turned on. The x-axis E' is given by $p_T^{\gamma} \cdot cosh(\eta^{jet})$. The error bars on y corresponds to the standard deviation of $y = E_{jet}^{raw} / \sum_i E_i \cdot R_i^{MC}$ in each bin.

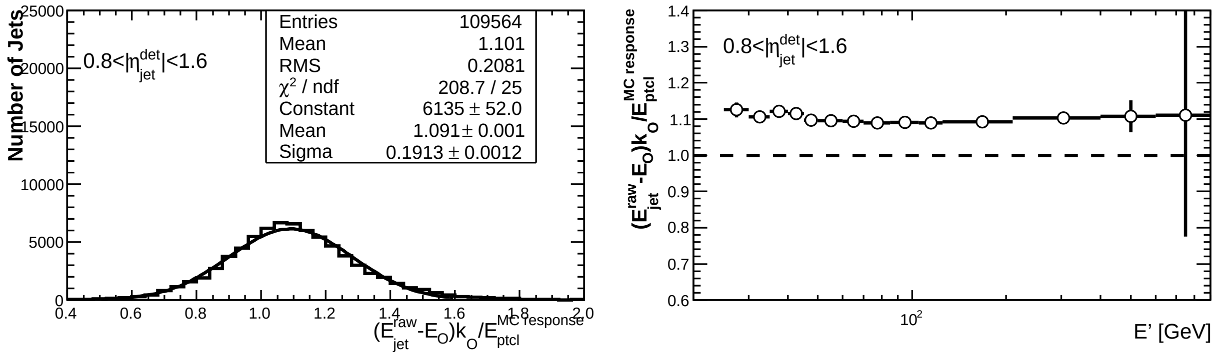

Figure 56: MC closure test for jets in p20 γ+jet MC sample produced without ZB overlay for $0.8 < |\eta_{det}^{jet}| < 1.6$. The single particle MC responses are derived with ZS turned on. The x-axis E' is given by $p_T^{\gamma} \cdot cosh(\eta^{jet})$. The error bars on y corresponds to the standard deviation of $y = E_{jet}^{raw} / \sum_i E_i \cdot R_i^{MC}$ in each bin.

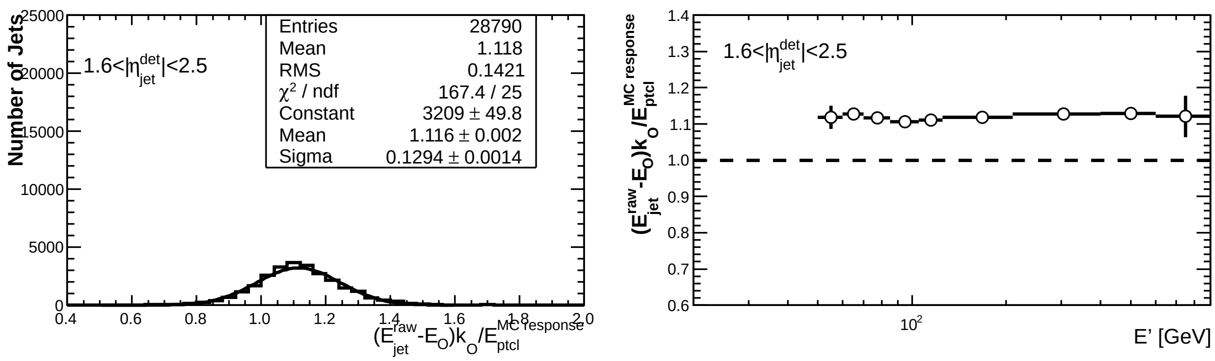

Figure 57: MC closure test for jets in p20 γ+jet MC sample produced without ZB overlay for $1.6 < |\eta_{det}^{jet}| < 2.5$. The single particle MC responses are derived with ZS turned on. The x-axis E' is given by $p_T^{\gamma} \cdot cosh(\eta^{jet})$. The error bars on y corresponds to the standard deviation of $y = E_{jet}^{raw} / \sum_i E_i \cdot R_i^{MC}$ in each bin.

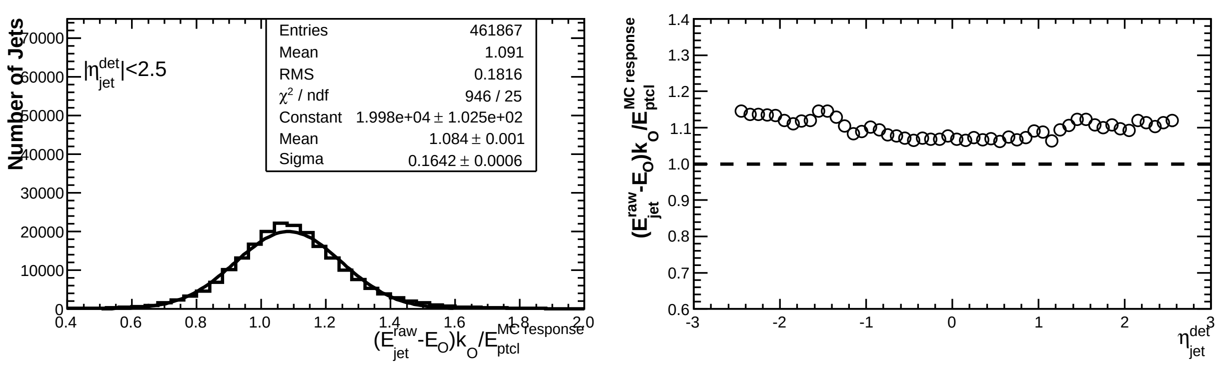

Figure 58: MC closure test for jets in p20 γ+jet MC sample produced without ZB overlay for $|\eta_{det}^{jet}| < 2.5$. The single particle MC responses are derived with ZS turned on. The x-axis E' is given by $p_T^{\gamma} \cdot cosh(\eta^{jet})$. The error bars on y corresponds to the standard deviation of $y = E_{jet}^{raw} / \sum_i E_i \cdot R_i^{MC}$ in each bin.

C Corrected MC Single Particle Responses From Single Particle MC Samples Produced With Zero Suppression Turned Off

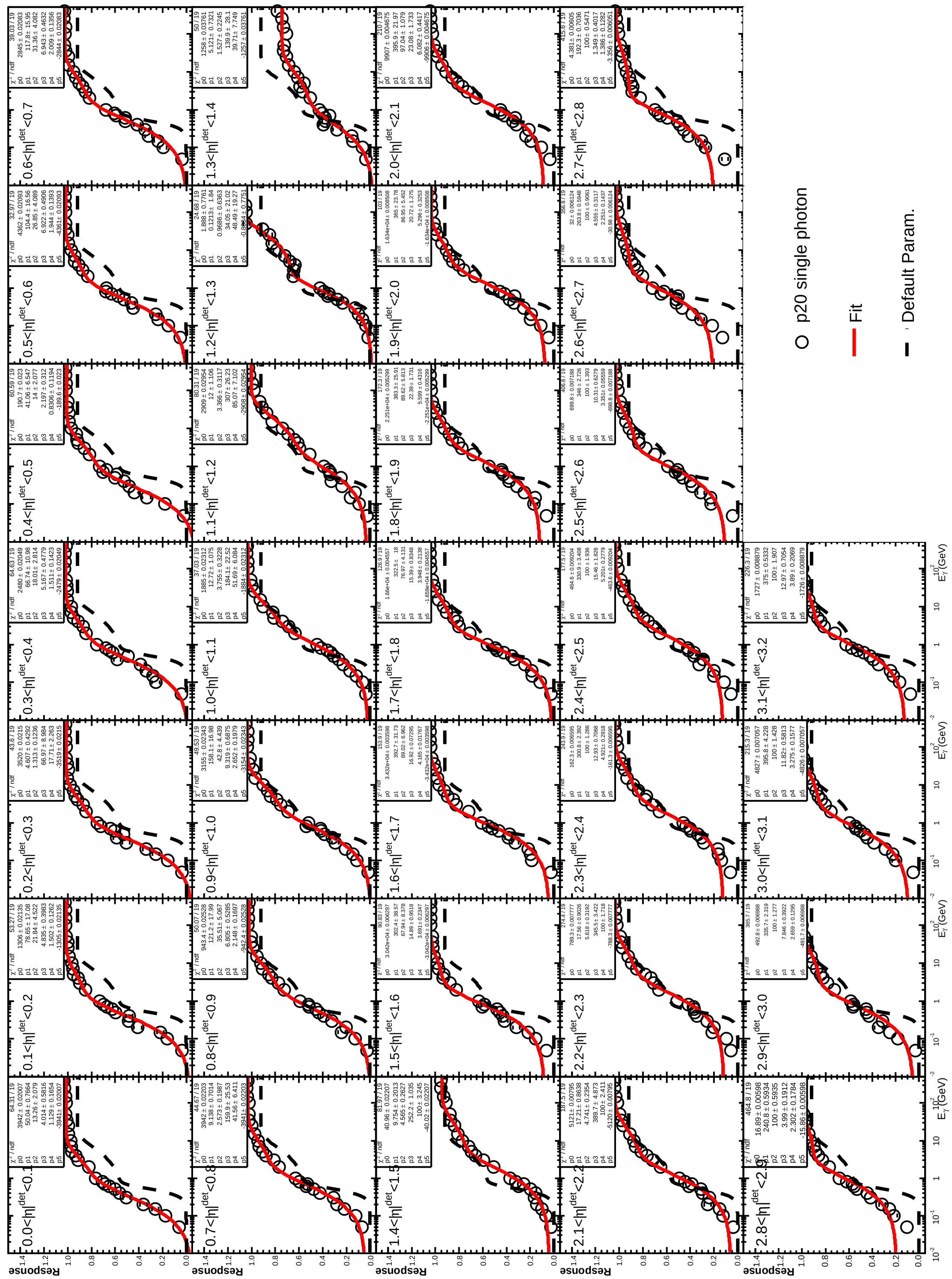

Figure 59: W-mass style MC single photon response from Run IIB single γ MC sample, produced without ZS, calorimeter noise or ZB overlay (see text for details). The black dashed line corresponds to the single photon response from Run IIA W mass studies. The red line is a fit to the MC points in black circles.

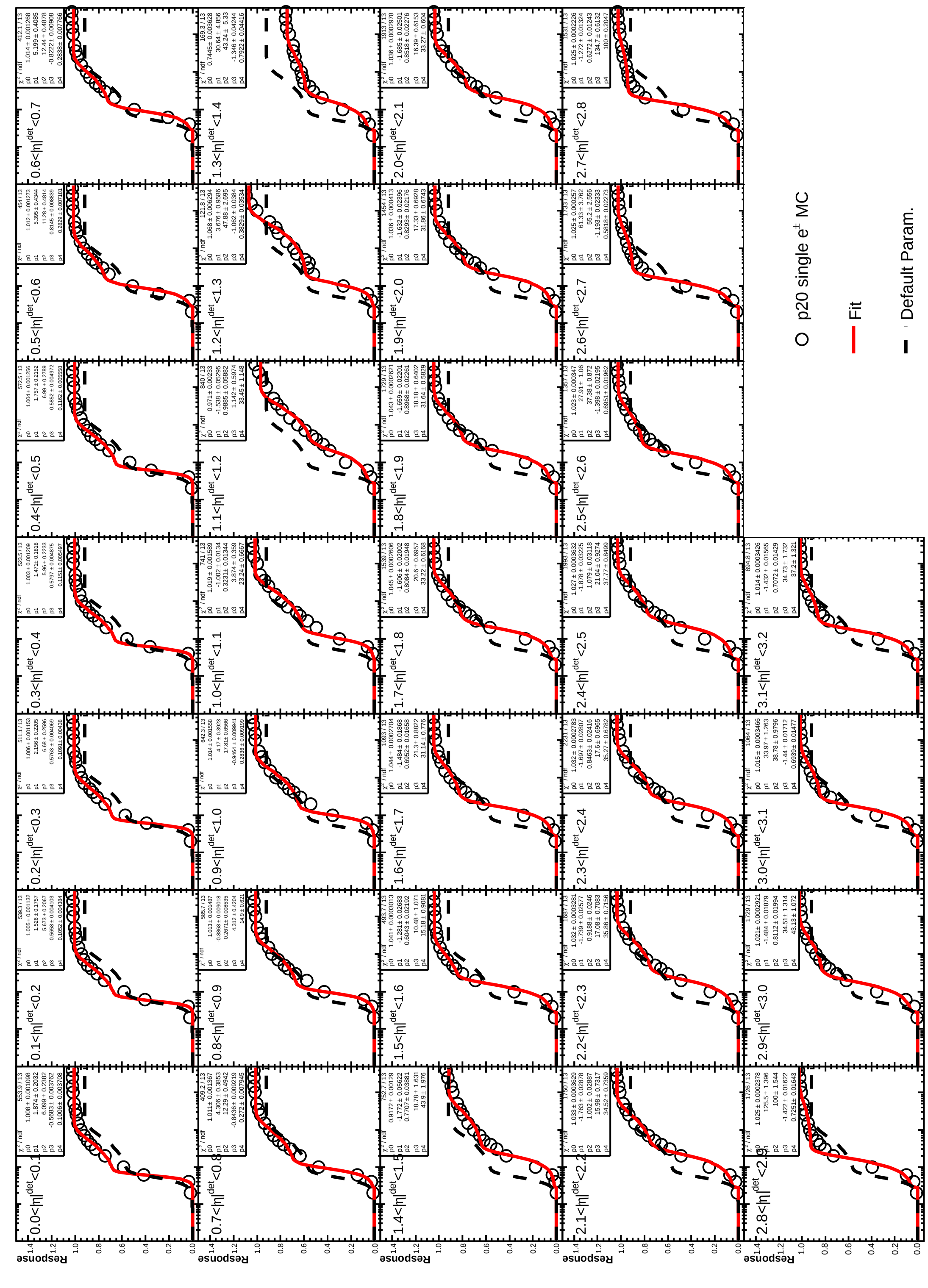

Figure 60: W-mass style MC single electron response from Run IIB single $e^{\pm}$ MC sample, produced without ZS, calorimeter noise or ZB overlay (see text for details). The black dashed line corresponds to the single electron response from Run IIA W mass studies. The red line is a fit to the MC points in black circles.

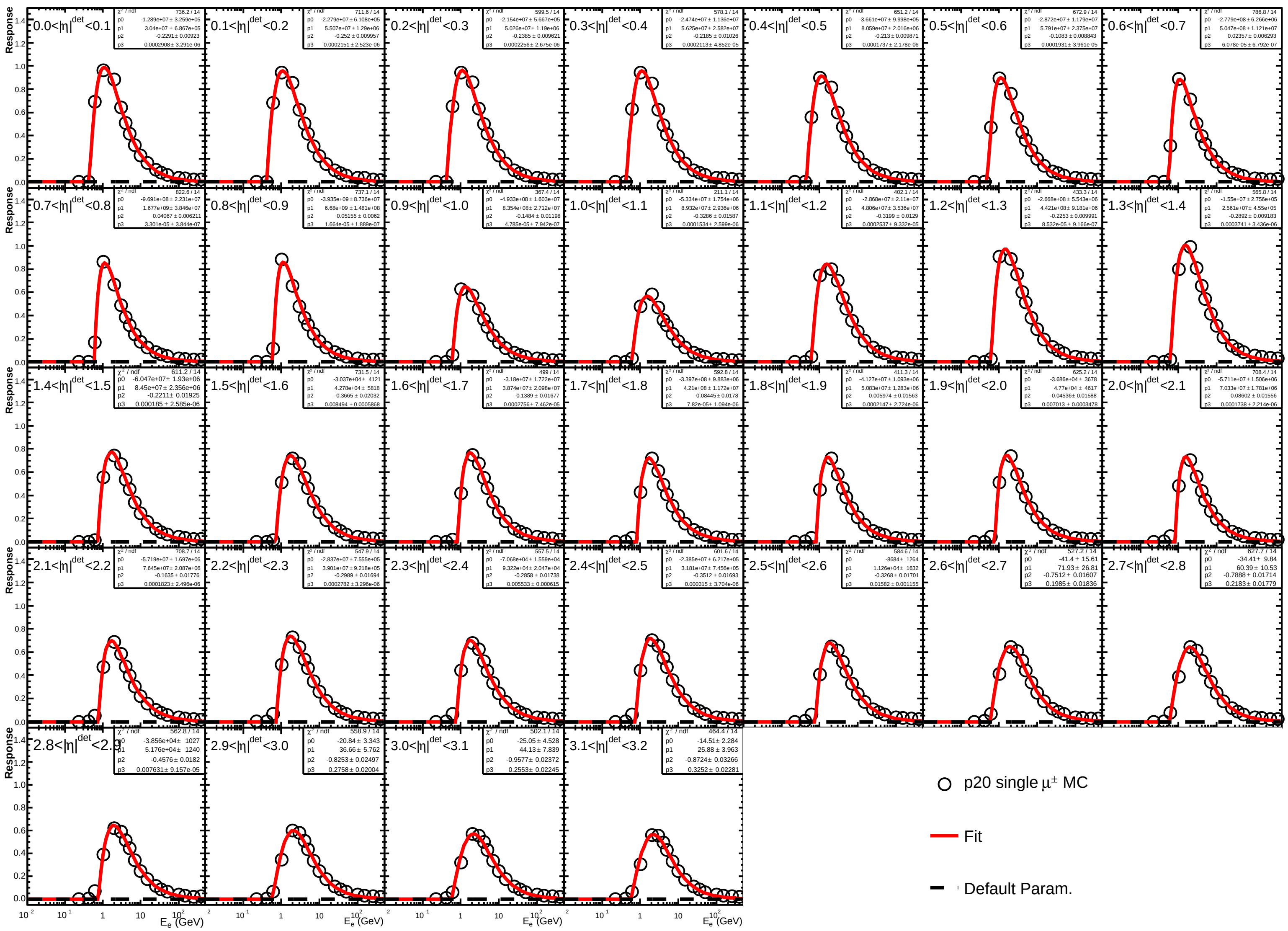

Figure 61: W-mass style MC single electron response from Run IIB single $\mu^{\pm}$ MC sample, produced without ZS, calorimeter noise or ZB overlay (see text for details). The black dashed line corresponds to 0. The red line is a fit to the MC points in black circles.

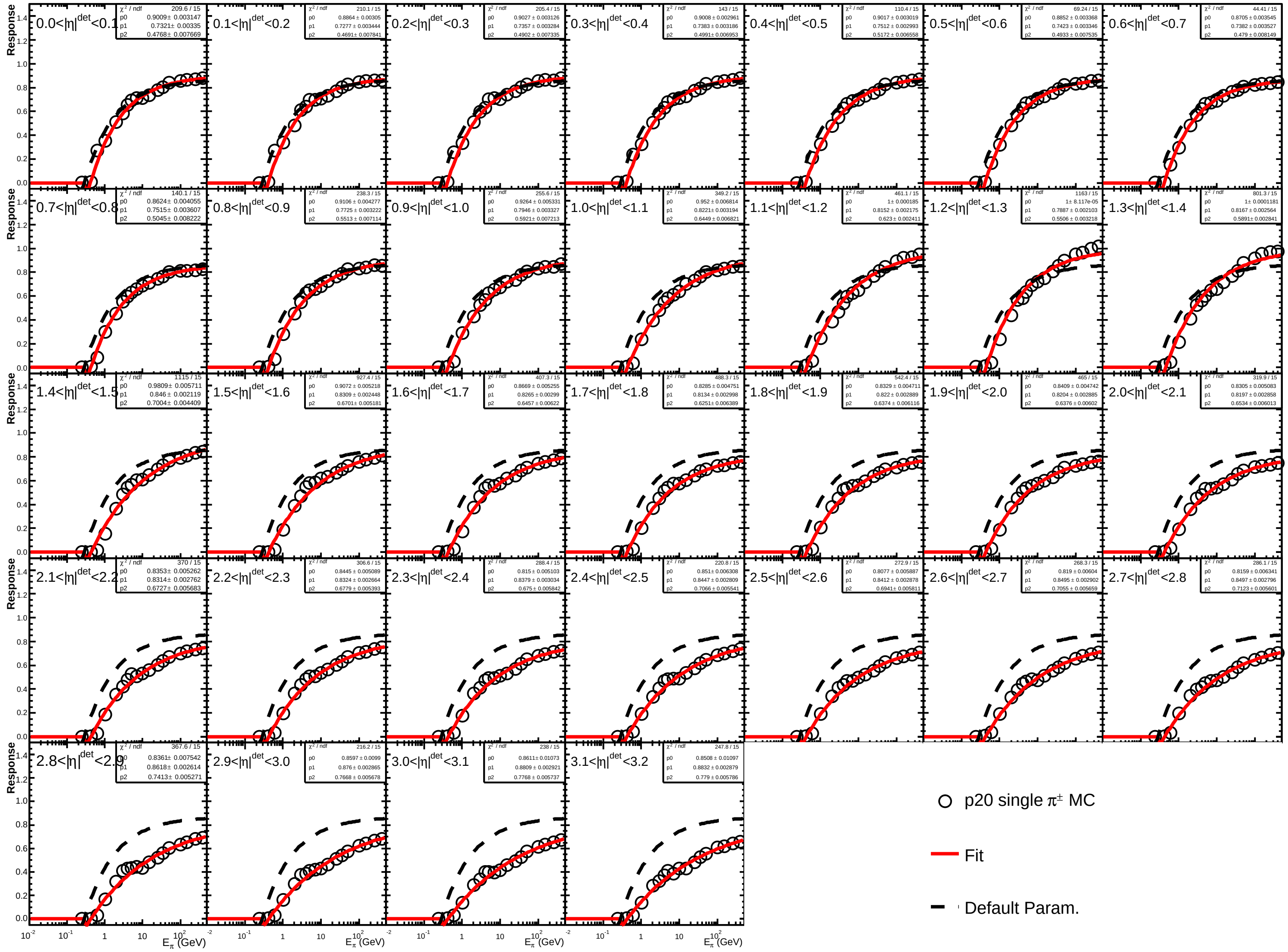

Figure 62: W-mass style MC single pion response from Run IIB single $\pi^{\pm}$ MC sample, produced without ZS, calorimeter noise or ZB overlay (see text for details). The black dashed line corresponds to the the single pion response from Run IIA JES studies. The red line is a fit to the MC points in black circles.

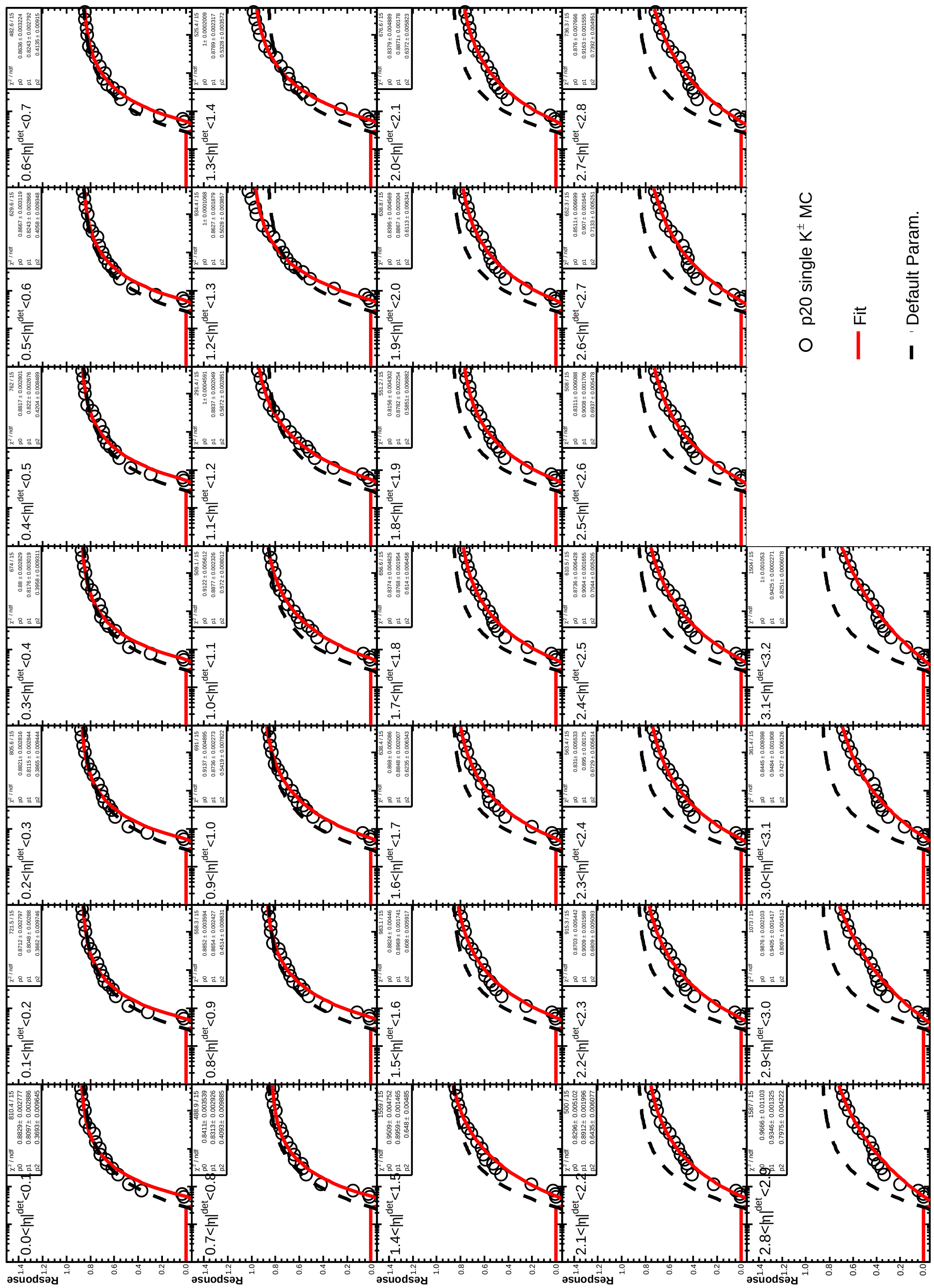

Figure 63: W-mass style MC single kaon response from Run IIB single $K^{\pm}$ MC sample, produced without ZS, calorimeter noise or ZB overlay (see text for details). The black dashed line corresponds to the single pion response from Run IIA JES studies. The red line is a fit to the MC points in black circles.

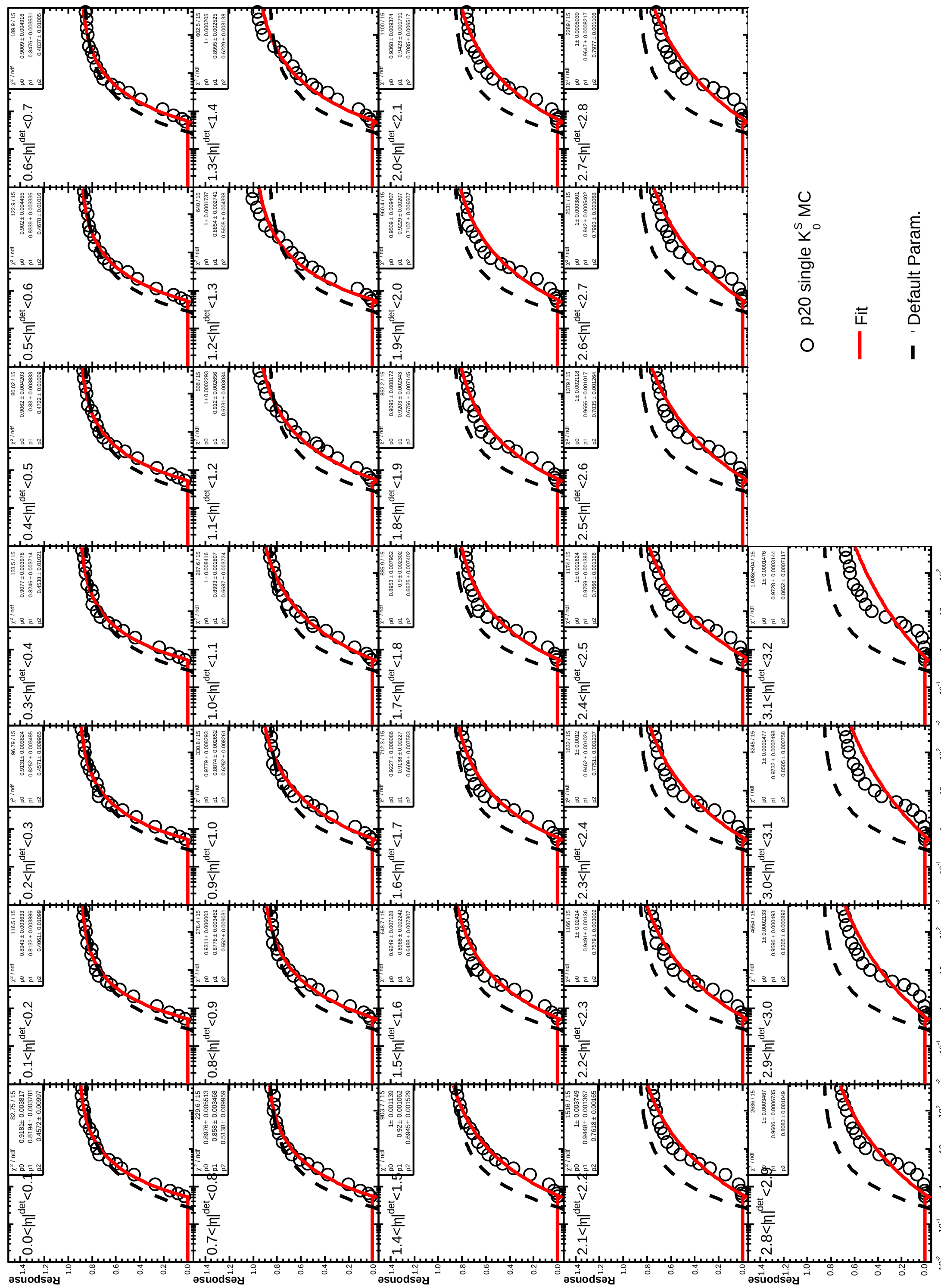

Figure 64: W-mass style MC single kaon response from Run IIB single K_0^S MC sample, produced without ZS, calorimeter noise or ZB overlay (see text for details). The black dashed line corresponds to the single pion response from Run IIA JES studies. The red line is a fit to the MC points in black circles.

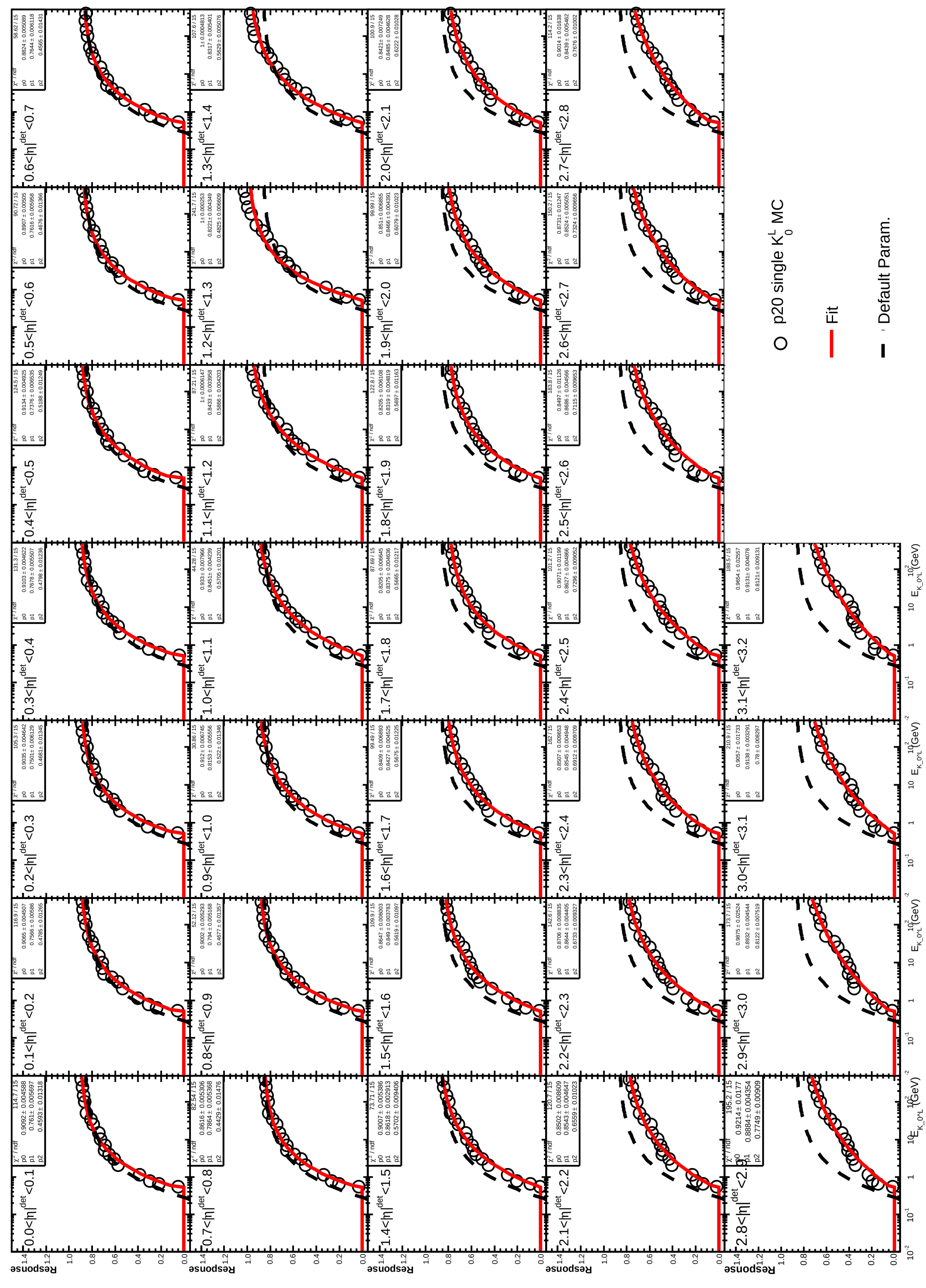

Figure 65: W-mass style MC single kaon response from Run IIB single K_0^L MC sample, produced without ZS, calorimeter noise or ZB overlay (see text for details). The black dashed line corresponds to the single pion response from Run IIA JES studies. The red line is a fit to the MC points in black circles.

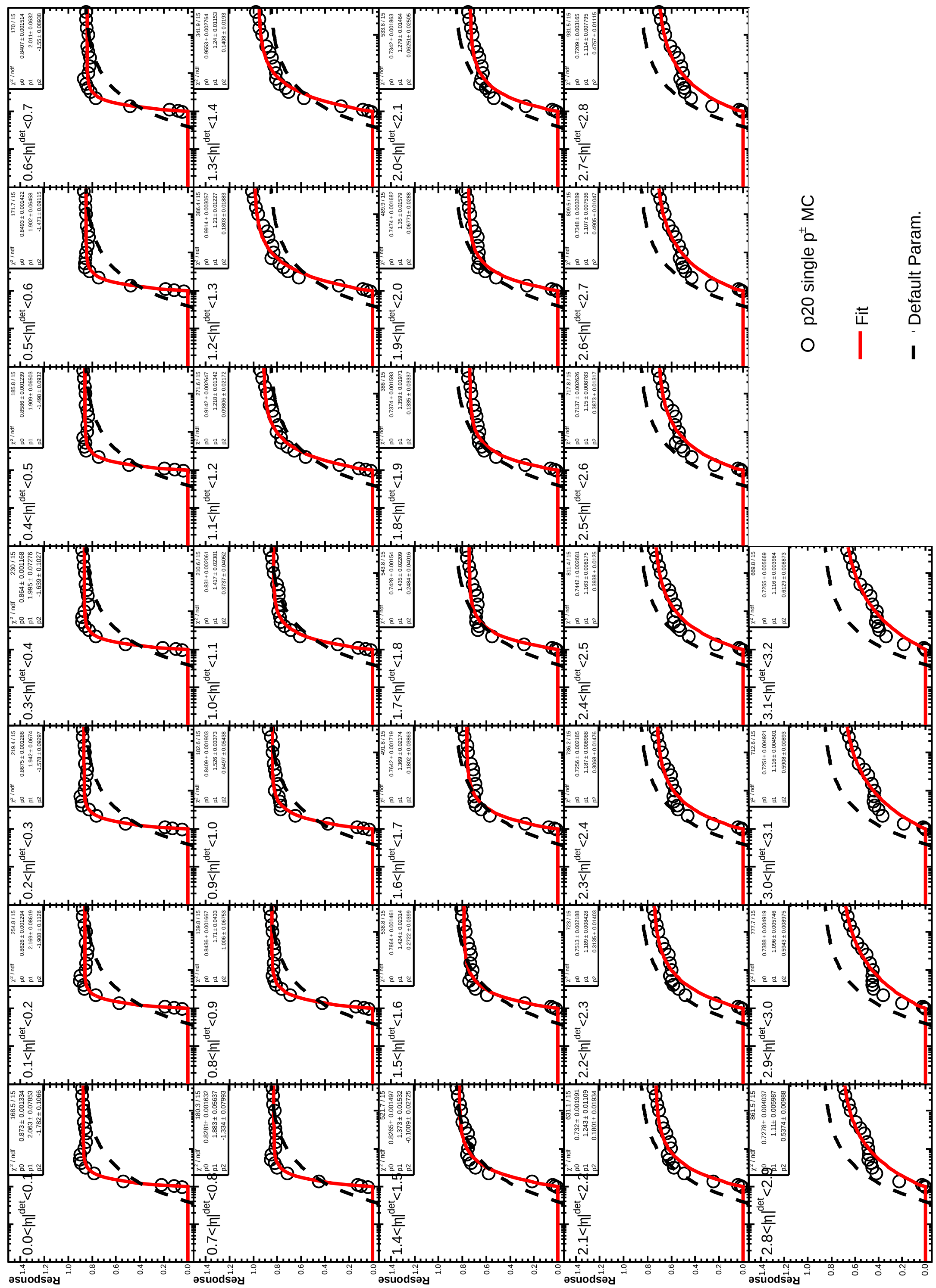

Figure 66: W-mass style MC single proton response from Run IIB single $p^{\pm}$ MC sample, produced without ZS, calorimeter noise or ZB overlay (see text for details). The black dashed line corresponds to the single proton response from Run IIA JES studies. The red line is a fit to the MC points in black circles.

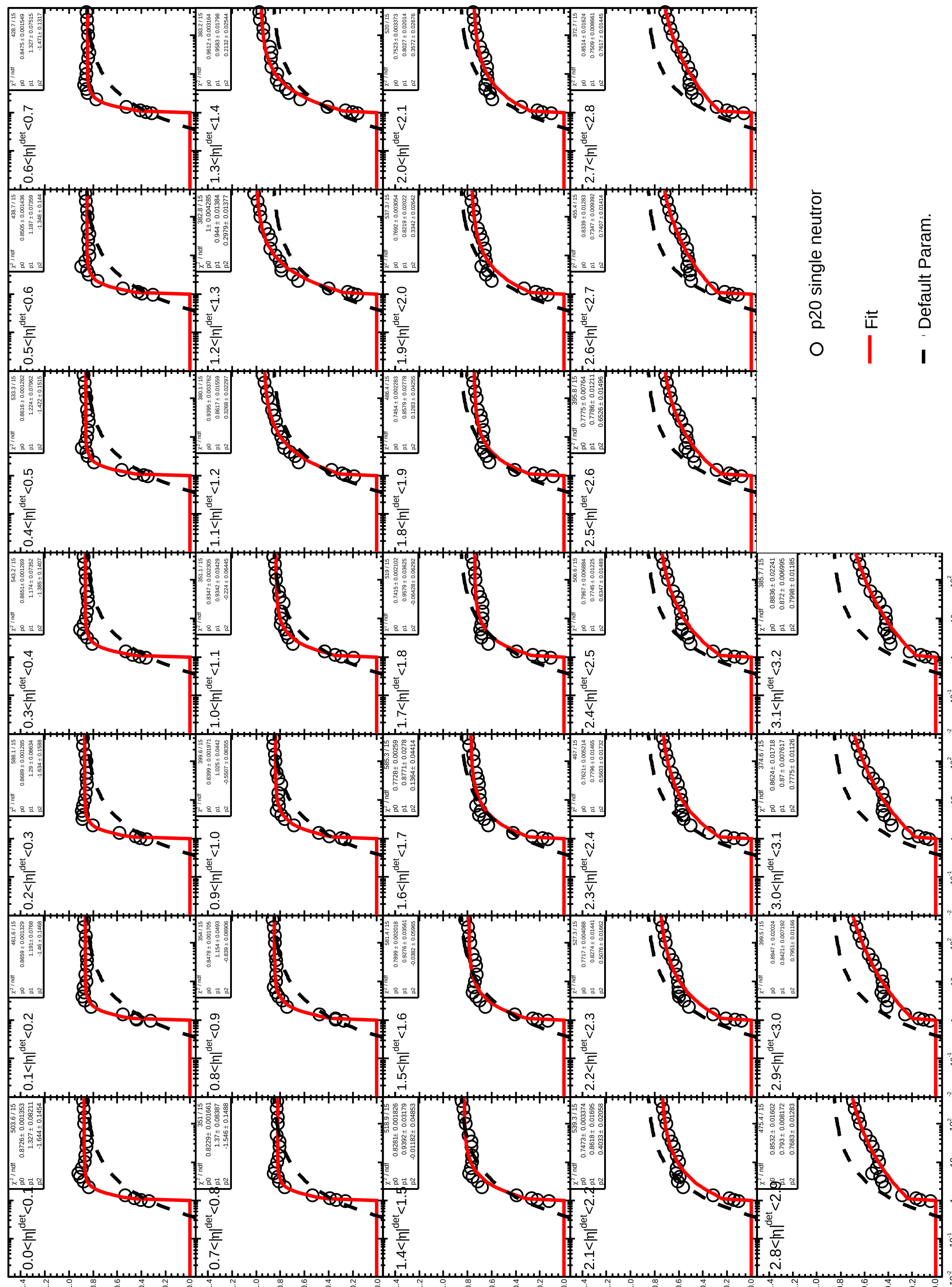

Figure 67: W-mass style MC single proton response from Run IIB single n MC sample, produced without ZS, calorimeter noise or ZB overlay (see text for details). The black dashed line corresponds to the single proton response from Run IIA JES studies. The red line is a fit to the MC points in black circles.

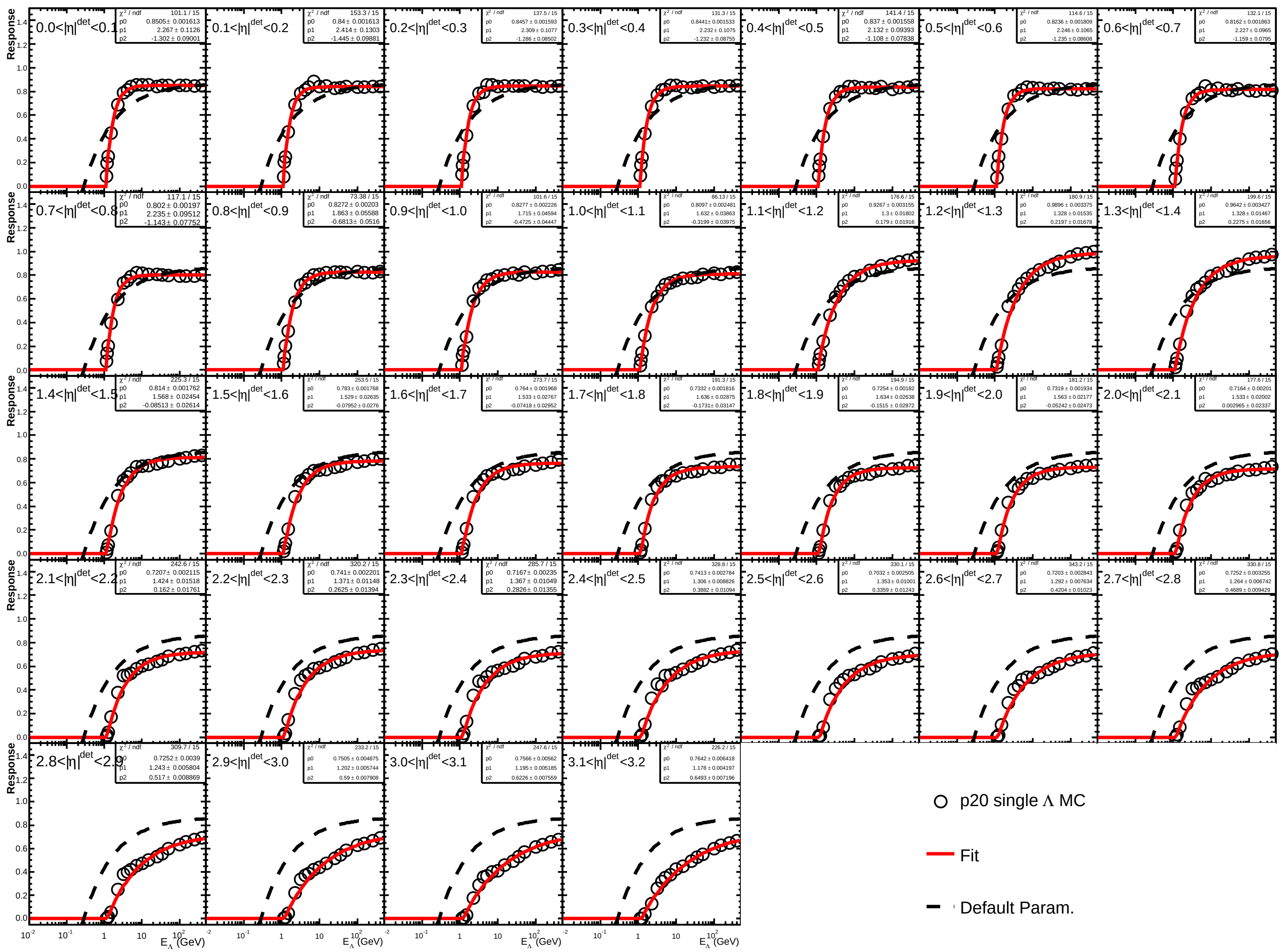

Figure 68: W-mass style MC single proton response from Run IIB single Λ MC sample, produced without ZS, calorimeter noise or ZB overlay (see text for details). The black dashed line corresponds to the single pion response from Run IIA JES studies. The red line is a fit to the MC points in black circles.

D Example of JES config with FMCData processor

```
#
# Extracts JES corrections and dumps them on screen
#
# Date:    $Date: 2011/09/07 22:33:14 $
# Version: $Revision: 1.2 $
# Author:  Gianluca Petrillo (petrillo@fnal.gov)
#
# Changes:
# 20120702 (petrillo@fnal.gov)
#   add support for MC-to-data correction (FMCData processor)
#

cafe.Packages:  tmb_tree, cafe
+cafe.Packages: g2c, jetcorr, jes_tools
+cafe.Packages: dq_util, caf_dq
+cafe.Packages: tau_tmb, tmb2ttau
+cafe.Packages: eff_utils, caf_mc_util, caf_util

# cafe.Events:       5000
# cafe.Skip:       500000


JESTOOLS.JetAlgo: JCCB
JESTOOLS.TestFMCdata: true


Constants.JetConeRadius_JCCB: 0.5
Constants.JetConeRadius_JCCA: 0.7


################################################################################
### Run chain
###
cafe.Run:  Group(FMCDataChain_%{JESTOOLS.TestFMCdata})
+cafe.Run: ApplyJES(JetCorr)
+cafe.Run: DumpJets(DumpJets)
+cafe.Run: ConfigDumper(ConfigDump)

FMCDataChain_true.Run: PartonFinder TagJetInitialParton FMCData(MCtoData)
FMCDataChain_false.Run: Passed(SkipFMCdata)

FMCDataChain_JetBranch_true:  %{MCtoData.To}
FMCDataChain_JetBranch_false: %{JESTOOLS.JetAlgo}

################################################################################
### MC-to-data correction [MCtoData]
###
# stable partons list is needed by FMCData processor
PartonFinder.Tree:              TMBTree
PartonFinder.DoStableParticles: true

TagJetInitialParton.From:       %{JESTOOLS.JetAlgo}
TagJetInitialParton.To:         Tagged%{JESTOOLS.JetAlgo}
TagJetInitialParton.TagLeptons: false
TagJetInitialParton.dR:         %{Constants.JetConeRadius_%{JESTOOLS.JetAlgo}}
```

```
MCtoData.Algo: %{JESTOOLS.JetAlgo}
MCtoData.Reco: RunIIb1
MCtoData.From: %{TagJetInitialParton.To}
MCtoData.To:   FMC_%{JESTOOLS.JetAlgo}


################################################################################
### ApplyJES[JetCorr]
###
JetCorr.From:                   %{JESTOOLS.JetAlgo}
JetCorr.To:                     Corr%{JESTOOLS.JetAlgo}
JetCorr.JetEnergyScale_jetalgo: %{JESTOOLS.JetAlgo}


################################################################################
### DumpJets[DumpJets]
###
DumpJets.Debug:    2
DumpJets.From:     %{JetCorr.To}
DumpJets.To:       DumpJetsDummy
DumpJets.JES:      JES
DumpJets.HeadLine: DUMPJET


################################################################################
### ConfigDumper[ConfigDump]
###
ConfigDump.DumpToROOTDir: 0


################################################################################
```